

General Disclaimer

One or more of the Following Statements may affect this Document

- This document has been reproduced from the best copy furnished by the organizational source. It is being released in the interest of making available as much information as possible.
- This document may contain data, which exceeds the sheet parameters. It was furnished in this condition by the organizational source and is the best copy available.
- This document may contain tone-on-tone or color graphs, charts and/or pictures, which have been reproduced in black and white.
- This document is paginated as submitted by the original source.
- Portions of this document are not fully legible due to the historical nature of some of the material. However, it is the best reproduction available from the original submission.

ORIGINAL PAGE IS
OF POOR QUALITY

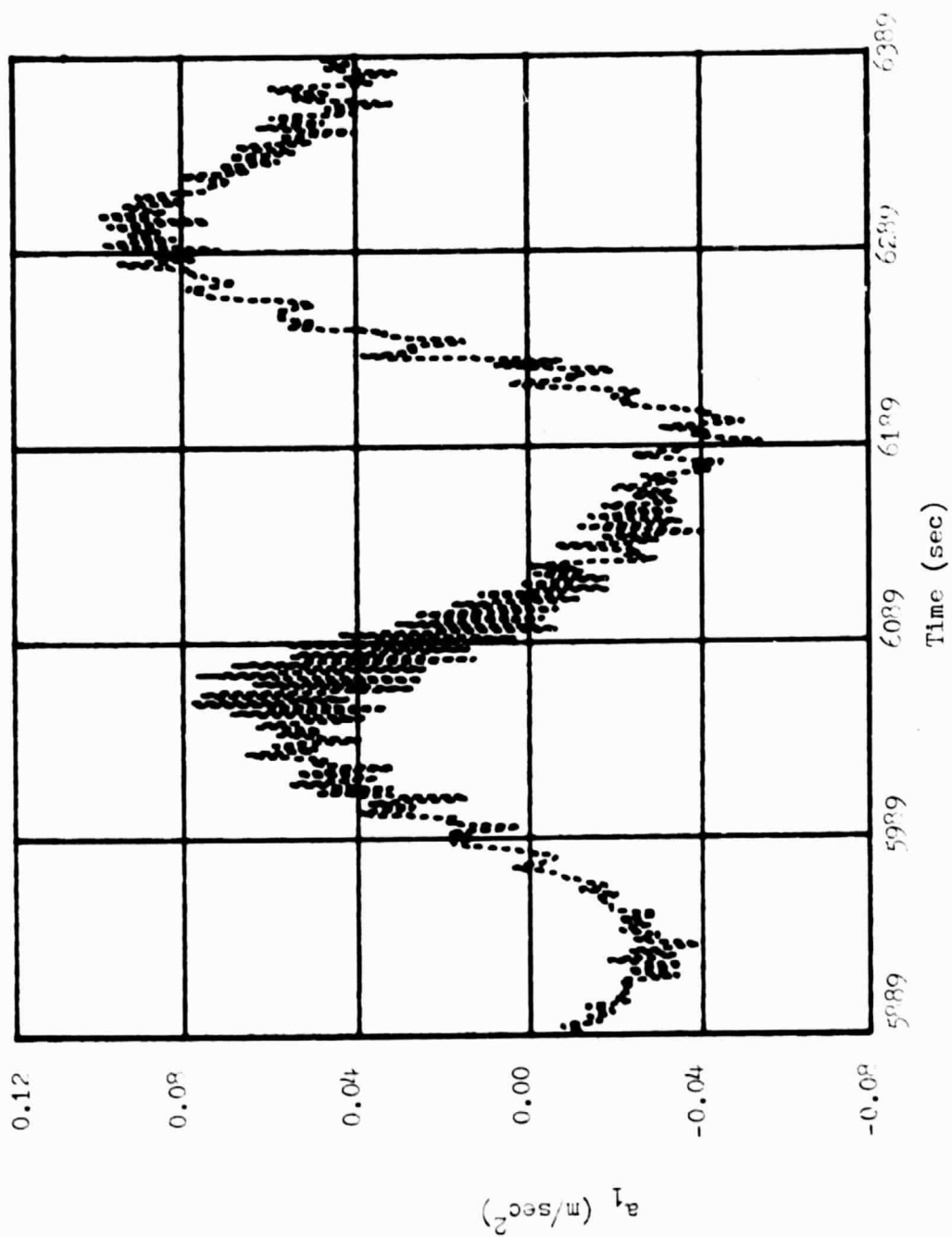
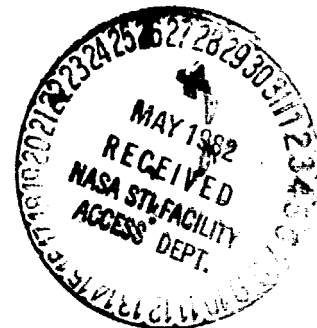
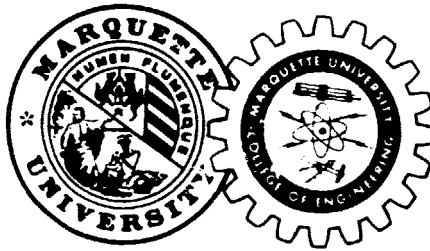


Fig. (4.1-5) Plot of Balloon's Translational Acceleration (a_1) (5989 to 6389)

(NASA-CA-100940) FEASIBILITY OF OBSERVER
SYSTEM FOR DETERMINING ORIENTATION OF
BALLOON BORNE OBSERVATIONAL PLATFORMS
(Marquette Univ.) 119 p. HC A00/AF A01

NO2-14170

JUN 11 1982
CSCL 01A 33/02 27855



COLLEGE OF ENGINEERING

MARQUETTE UNIVERSITY
MILWAUKEE, WISCONSIN 53233

**FEASIBILITY OF OBSERVER SYSTEM FOR
DETERMINING ORIENTATION OF BALLOON BORNE
OBSERVATIONAL PLATFORMS**

**N. J. NIGRO, PROFESSOR
MECHANICAL ENGINEERING DEPT.**

**J. C. GAGLIARDI, GRADUATE STUDENT
MECHANICAL ENGINEERING DEPT.**

1
/

TABLE OF CONTENTS

	<u>Page</u>
Chapter I Introduction	1
1.1 Motivation and Relevance of Thesis	1
1.2 Present Status of Problem	3
1.3 Object of Thesis	4
Chapter II Development of Balloon System Mathematical Model	5
2.1 Idealizations of System	5
2.2 Generalized Coordinates	8
2.3 Lagrange's Equation	10
2.4 Kinematics	12
2.5 System Lagrangian	15
2.6 System Math Model	16
2.7 State Variable Form of Math Model	19
Chapter III Development of Observer System Mathematical Models	22
3.1 Concept of Observability	22
3.2 Observability of Balloon Systems	24
3.3 Observability of Balloon System With Output Bias	25
3.4 Development of Full Order Identity Observer System for Balloon System Without Bias	27
3.5 Development of Identity Observer System For Balloon System With Bias	32

	<u>Page</u>
Chapter IV Results and Conclusions	34
4.1 Data for LACATE Mission	34
4.2 Results From Simulation Study	34
4.3 Discussion of Simulation Study Results	67
4.4 Observer Results For Determining Orientation of Balloon Platform	69
4.5 Discussion of Balloon Observer Results	96
4.6 Conclusions	98
Appendices	100
A. Balloon Translational Acceleration Components	100
B. Fortran Coding	104
1. Body Axis Accelerations	104
2. Balloon Fourth Order Observer	105
3. Balloon Fifth Order Observer	106
4. Hamming-Predictor Corrector	107
Bibliography	112

LIST OF FIGURES

Figure		Page
1.1-1	LACATE Balloon System	2
2.1-1	Idealized LACATE System	6
2.1-2	Idealized Balloon Subsystem	7
2.2-1	Eulerian Angles	9
2.2-2	Platform Angular Velocities	11
3.4-1	Block Diagram For Asymptotic State Estimator	29
4.1-1	Plot of Balloon's Translational Accel. ($0 \leq t \leq 500$)	38
4.1-2	Plot of Balloon's Trans. Accel. (a_1) ($0 \leq t \leq 500$)	39
4.1-3	Plot of Balloon's Trans. Accel. (a_2) ($0 \leq t \leq 500$)	40
4.1-4	Plot of Balloon's Trans. Accel. ($5889 \leq t \leq 6389$)	41
4.1-5	Plot of Balloon's Trans. Accel. (a_1) ($5889 \leq t \leq 6389$)	42
4.1-6	Plot of Balloon's Trans. Accel. (a_2) ($5889 \leq t \leq 6389$)	43
4.2-1	Simulation Results For Angular Displacement (4th Order Observer, $u=0$, $\lambda=-0.6$)	46
4.2-2	Simulation Results For Angular Velocity (4th Order Observer, $u=0$, $\lambda=-0.6$)	47
4.2-3	Simulation Results For Angular Displacement (4th Order Observer, $u=0.002t$, $\lambda=-0.6$)	48
4.2-4	Simulation Results For Angular Velocity (4th Order Observer, $u=0.002t$, $\lambda=-0.6$)	49
4.2-5	Simulation Results For Angular Displacement (4th Order Observer, $u=0$, $\lambda=-0.6$, Bias= 1.0×10^{-4})	50
4.2-6	Simulation Results For Angular Velocity (4th Order Observer, $u=0$, $\lambda=-0.6$, Bias= 1.0×10^{-4})	51
4.2-7	Simulation Results For Angular Displacement (4th Order Observer, $u=0$, $\lambda=-0.6$, Bias= $4.0 \times 10^{-6}t$)	52
4.2-8	Simulation Results For Angular Velocity (4th Order Observer, $u=0$, $\lambda=-0.6$, Bias= $4.0 \times 10^{-6}t$)	53
4.2-9	Simulation Results For Angular Displacement (4th Order Observer, $u=0$, $\lambda=-0.6$, Bias= $0.005 \cos 13t$)	54
4.2-10	Same as Fig.(4.2-9)	55
4.2-11	Simulation Results For Angular Velocity (4th Order Observer, $u=0$, $\lambda=-0.6$, Bias= $0.005 \cos 13t$)	56

Figure		Page
4.2-12	Same as Fig.(4.2-11)	57
4.2-13	Simulation Results For Output (Bias=0.005cos13t)	58
4.2-14	Simulation Results For Angular Displacement (5th Order Observer, $u=0$, $\lambda=-0.6$, Bias=0.002)	59
4.2-15	Simulation Results For Angular Velocity (5th Order Observer, $u=0$, $\lambda=-0.6$, Bias=0.002)	60
4.2-16	Simulation Results For Angular Displacement (5th Order Observer, $u=0$, $\lambda=-0.6$, Bias= $-1 \times 10^{-4}t + 0.002$)	61
4.2-17	Simulation Results For Angular Velocity (5th Order Observer, $u=0$, $\lambda=-0.6$, Bias= $-1 \times 10^{-4}t + 0.002$)	62
4.2-18	Simulation Results For Angular Displacement (5th Order Observer, $u=0$, $\lambda=-0.6$, Bias=0.005cos13t)	63
4.2-19	Same as Fig.(4.2-18)	64
4.2-20	Simulation Results For Angular Velocity (5th Order Observer, $u=0$, $\lambda=-0.6$, Bias=0.005cos13t)	65
4.2-21	Same as Fig.(4.2-20)	66
4.4-1	Actual Output For Cyroscope Mounted Along X_1 Body Axis	71
4.4-2	Actual Results For Angular Velocity (4th Order Observer, $u=0$, $\lambda=-0.5$)	72
4.4-3	Actual Results For Angular Displacement (4th Order Observer, $u=0$, $\lambda=-0.5$)	73
4.4-4	Actual Results For Angular Velocity (4th Order Observer, $u=a_1$, $\lambda=-0.5$)	74
4.4-5	Actual Results For Angular Displacement (4th Order Observer, $u=a_1$, $\lambda=-0.5$)	75
4.4-6	Actual Results For Angular Velocity (5th Order Observer, $u=0$, $\lambda=-0.2$)	76
4.4-7	Actual Results For Angular Displacement (5th Order Observer, $u=0$, $\lambda=-0.2$)	77
4.4-8	Same as Fig.(4.4-7)	78
4.4-9	Actual Results For Bias (5th Order Observer, $u=0$, $\lambda=-0.2$)	79
4.4-10	Actual Results For Angular Velocity (5th Order Observer, $u=0$, $\lambda=-0.5$)	80

Figure		Page
4.4-11	Actual Results For Angular Displacement (5th Order Observer, $u=0$, $\lambda=-0.5$)	81
4.4-12	Same as Fig.(4.4-11)	82
4.4-13	Actual Results For Bias (5th Order Observer, $u=0$, $\lambda=-0.5$)	83
4.4-14	Actual Results For Angular Velocity (5th Order Observer, $u=a_1$, $\lambda=-0.2$)	84
4.4-15	Actual Results For Angular Displacement (5th Order Observer, $u=a_1$, $\lambda=-0.2$)	85
4.4-16	Same as Fig.(4.4-15)	86
4.4-17	Actual Results For Bias (5th Order Observer, $u=a_1$, $\lambda=-0.5$)	87
4.4-18	Actual Results For Angular Velocity (5th Order Observer, $u=a_1$, $\lambda=-0.5$)	88
4.4-19	Actual Results For Angular Displacement (5th Order Observer, $u=a_1$, $\lambda=-0.5$)	89
4.4-20	Same as Fig.(4.4-19)	90
4.4-21	Actual Results For Bias (5th Order Observer, $u=a_1$, $\lambda=-0.5$)	91
4.4-22	Actual Results For Angular Velocity (5th Order Observer, $u=a_1$, $\lambda=-0.7$)	92
4.4-23	Actual Results For Angular Displacement (5th Order Observer, $u=a_1$, $\lambda=-0.7$)	93
4.4-24	Same as Fig.(4.4-23)	94
4.4-25	Actual Results For Bias (5th Order Observer, $u=a_1$, $\lambda=-0.7$)	95
A-1	Earth Fixed Axis	102
A-2	Body and Earth Fixed Coordinate Axes	103

LIST OF TABLES

Table		Page
4.1-1	Idealized LACATE System Properties	35
4.1-2	Coefficients of M and K Matrices	35
4.1-3	Coefficients of A Matrix	36
4.1-4	Coefficients of P Matrix	36
4.1-5	Balloon System Eigenvalues and Corresponding Eigenvectors	37
4.1-6	Balloon Modal Shape Functions and Periods	37

CHAPTER I

INTRODUCTION

1.1 Motivation and Relevance of Thesis

The LACATE (Lower Atmosphere Composition and Temperature Experiment) mission was a high altitude balloon platform test which employed an infrared radiometer to sense vertical profiles of the concentrations of selected atmospheric trace constituents and temperatures. The constituents were measured by inverting infrared radiance profiles of the earth's horizon. The radiometer line-of-sight was scanned vertically across the horizon at approximately 0.25° /second. The relative vertical positions of the data points making up the profile had to be determined to approximately 20 arc seconds.

The balloon system for accomplishing the mission is shown in Fig. 1.1-1. It consisted of: (a) a 39 million cubic feet (zero pressure) balloon, (b) a load bar containing the balloon control equipment, (c) a package containing additional balloon control electronics with gondola recovery parachute, and (d) a gondola containing the research equipment. The balloon was designed to lift the payload to a float altitude of approximately 150,000 feet.

Instrumentation to determine the attitude of the balloon platform consisted of a magnetometer and 3 orthogonally oriented precision rate gyros. The three rate gyros were employed to obtain an accurate time history of the angular velocity components of the research platform for subsequent data reduction and attitude determination.

The main problem in the LACATE experiment is to determine the instantaneous orientation (i.e., the attitude) of the instrumentation platform with respect to a local vertical. Moreover, this orientation

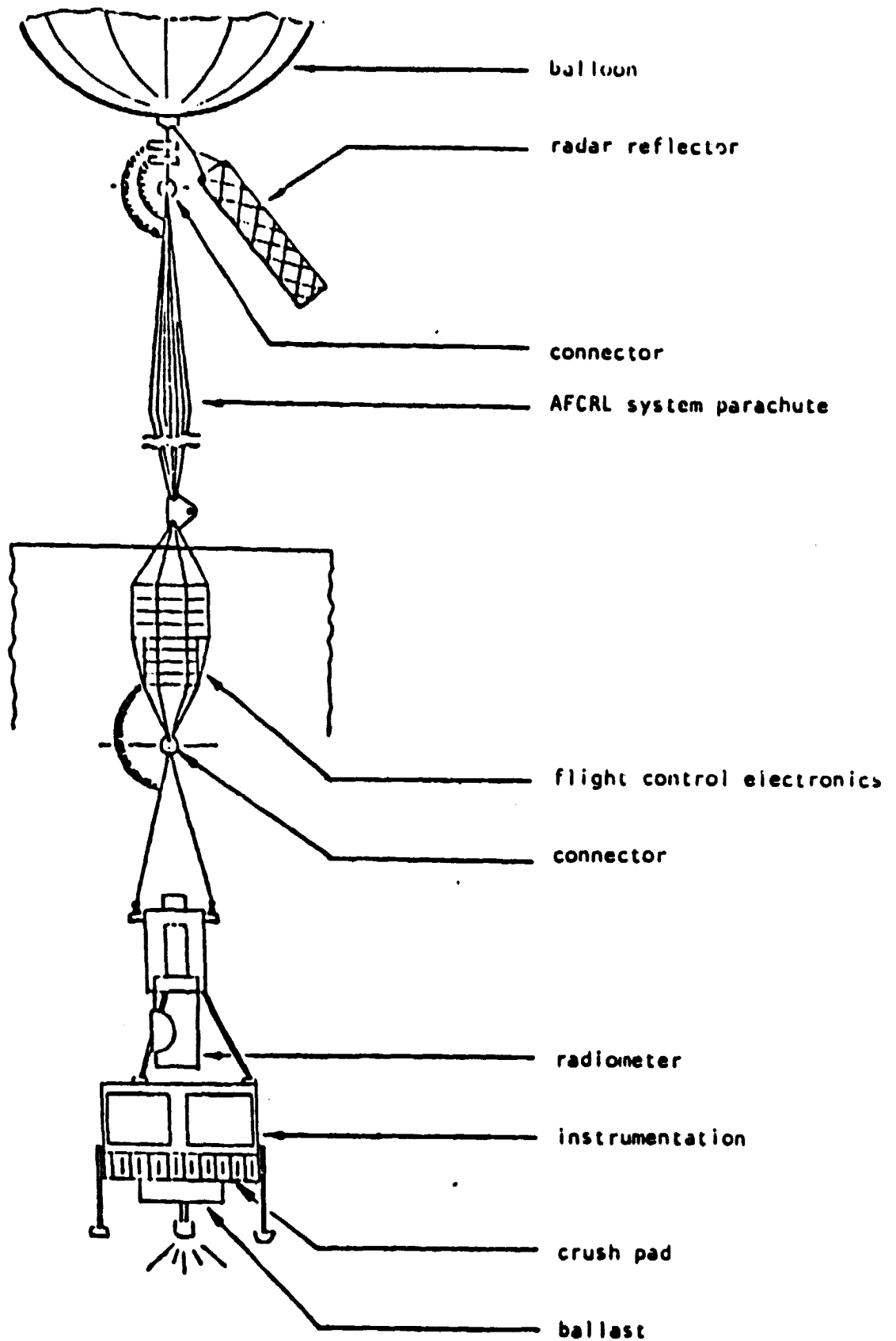


Fig.(1.1-1) LACATE BALLOON SYSTEM

must be determined to an accuracy of 1° . Once this is known, the orientation of the line-of-sight of the radiometer can be determined since its relative motion with respect to the platform is prescribed.

1.2 Present Status of the Problem

Stablizing the balloon research platform or predicting its orientation is a major problem which must be solved in all balloon borne experiments requiring line-of-sight instrumentation. Feedback control systems have been used to stabilize the balloon platform with respect to an inertial reference frame⁽¹⁾. Stability is obtained by suspending the platform at its center of gravity and employing some control system. Control system instrumentation includes sensors (rate gyros, digital star trackers, etc.) and reaction wheels for torquing the platform. Systems of this type, however, are usually extremely complex and costly.

An alternate approach to this problem is to allow the balloon platform to swing freely from its suspension point and then employ some method to determine its attitude (orientation). The orientation parameters for the platform are determined by fitting the results obtained from a mathematical model (which simulates the balloon system) to those results obtained from the platform's sensors (i.e., gyroscopes).

Several numerical parameter estimation methods have been developed to determine the attitude (orientation) parameters. The problem is normally solved by employing an optimization process which minimizes the error between predicted and known output results. In the case of balloon research platforms the optimization problem involves the minimization of the sum of the squares of the differences between the angular velocity components obtained from the rate gyroscopes and those

predicted from the mathematical model⁽²⁾. However, with this approach, the problem of determining the optimal decision variables, (i.e., initial condition parameters) can require considerable computer running time.

A promising, new approach for determining attitude of balloon research platforms involves observer state space reconstruction. For totally observable systems, state estimators can be constructed. The state estimator, which is driven by all plant inputs and outputs, can be used to determine the system state⁽³⁾.

Observer systems are state estimators constructed such that the error in the estimated state decays to zero over a finite time interval. By subtracting the plant model from the observer model, the error model for the reconstructed state can be determined. This model consists of a system of homogeneous, first order differential equations. The eigenvalues of the resulting eigenvalue problem can be chosen such that the error decays to zero in a small interval of time. In this case, then, the estimates response approaches the actual states exponentially.

1.3 Object of Thesis

The two main objectives of this thesis are given as follows:

1. Develop an observer model for predicting the orientation of balloon borne research platforms.
2. Employ this observer model in conjunction with actual data obtained from NASA'S LACATE mission in order to determine the platform orientation as a function of time.

In order to achieve the above objectives it will be necessary to first develop a general three dimensional mathematical model for simulating the motion of the balloon platform. This will be discussed next.

CHAPTER II

DEVELOPMENT OF BALLOON SYSTEM MATHEMATICAL MODEL

2.1 Idealizations of System

The general balloon system to be studied in this report is shown in Fig. 1.1-1. The actual motion of this system is very complex and involves various types of oscillations including bounce (vertical oscillation), pendulations (inplane motion) and spin (rotation). In general, it is necessary to first idealize this system before developing the mathematical model. For purposes of this study, the following idealizations will be made:

1. The mass of the balloon, subsystems and interconnecting subsystems, will be "lumped" at the locations shown in Fig. 2.1-1.
2. The balloon will be treated as an "equivalent" rigid body.
3. The altitude of the balloon static equilibrium position (float altitude) will be assumed to be a constant during the entire period of observation; i.e., changes in this altitude due to losses or changes in the properties of helium will be neglected.
4. The interconnecting cables will be considered to be inflexible.

The above idealizations were applied to the general balloon system shown in Fig. 1.1-1. The resulting idealized system is shown in Fig. 2.1-1.

There are two alternate approaches which can be followed for purposes of modeling the balloon system; these are summarized below.

1. The mathematical model for the entire balloon system (Fig. 2.1-1) can be developed. The major disadvantage of this approach is that it requires knowledge of the aerodynamic forces acting on the balloon itself. Moreover, with this model, a

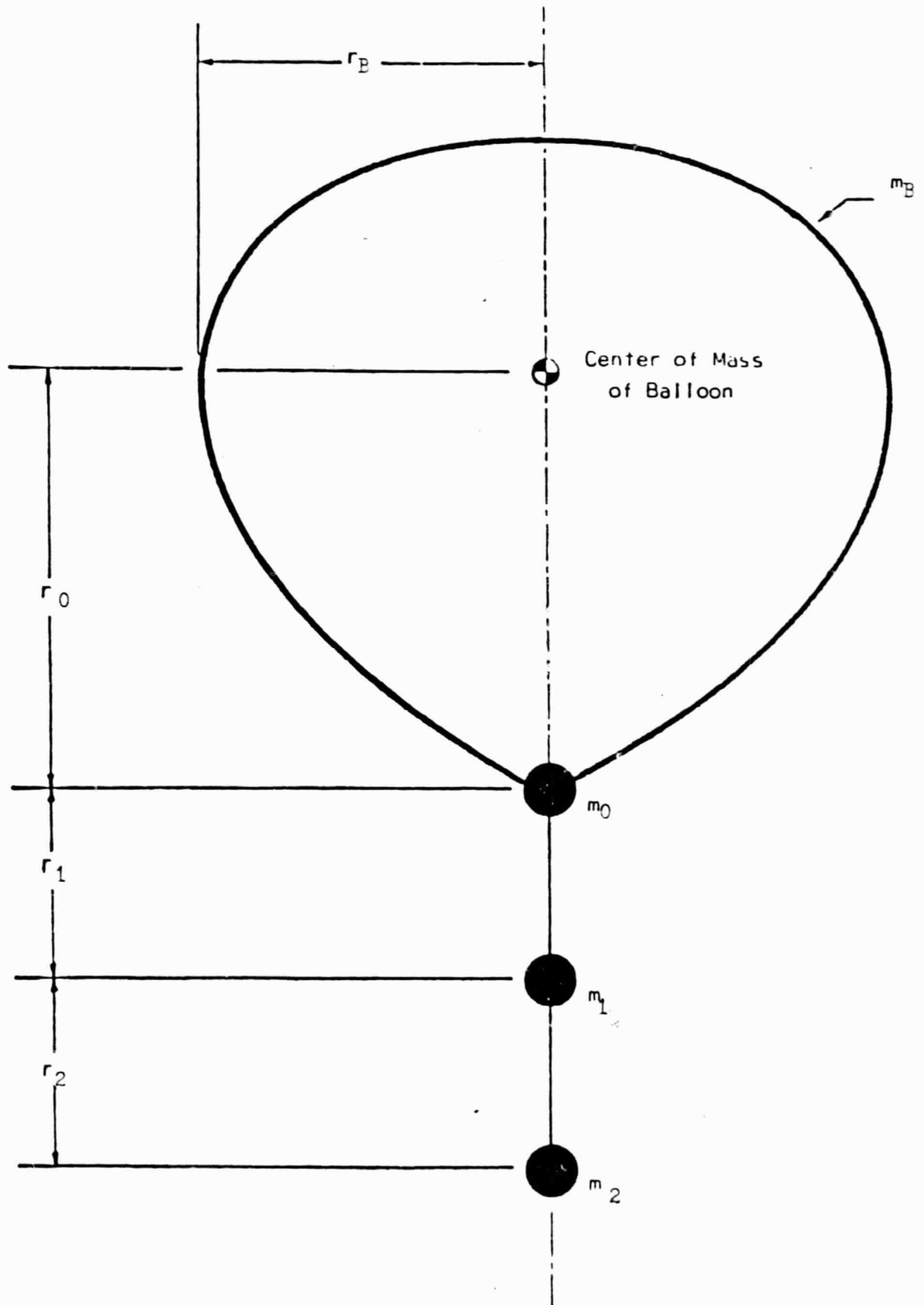


Fig.(2.1-1) Idealized LACAPL System

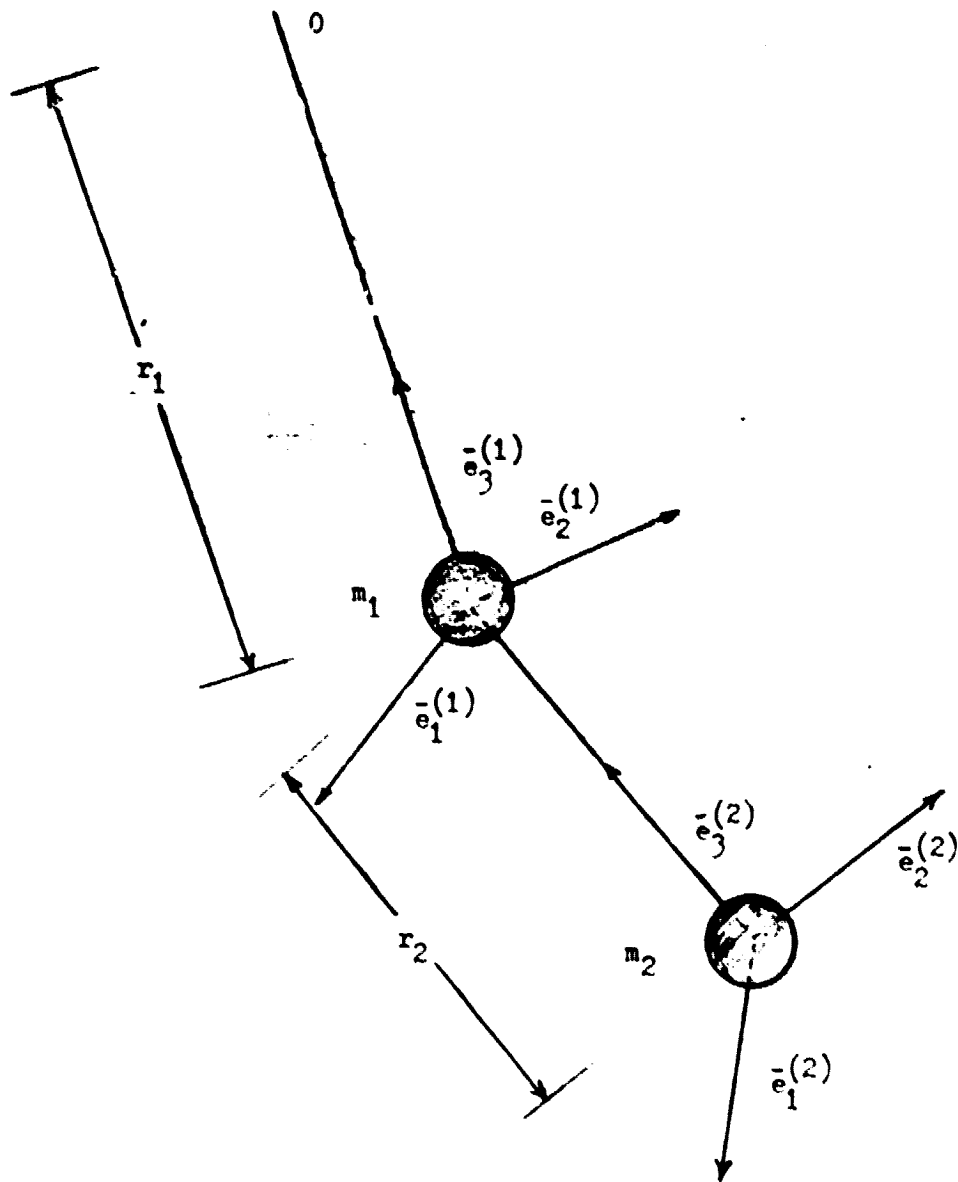


Fig.(2.1-2) Idealized Balloon Subsystem

large number of generalized coordinates are needed to specify the configuration of the system.

2. An alternate approach is to develop the mathematical model for predicting the motion of subsystems one and two (Fig. 2.1-2). This model does not include the aerodynamic forces acting on the balloon; however, it does require information on the motion of the radar reflector support point 0 (Fig. 2.1-2). The advantage of this model is that the number of degrees of freedom is decreased, and the aerodynamic force effects are automatically included if the motion of the support point is known. This is the model which will be used for carrying out the research discussed in this thesis.

2.2 Generalized Coordinates

The generalized coordinates for a given system are those coordinates which are employed to specify the configuration of the system at any instant of time. In any mechanical system there will be as many generalized coordinates as there are degrees of freedom. In the case of the idealized lumped system shown in Fig. 2.1-2, six generalized coordinates are required to specify the balloon configuration. These are comprised of six Euler angles which specify the orientation of the two subsystems. The three translational coordinates located at the radar reflector support point 0 are not considered to be generalized coordinates, since these are known (prescribed) from data obtained from the radar tracking installation.

In general, the Euler angles give the orientation of the body coordinate axes (X_i''') relative to a fixed coordinate system (X_i). A

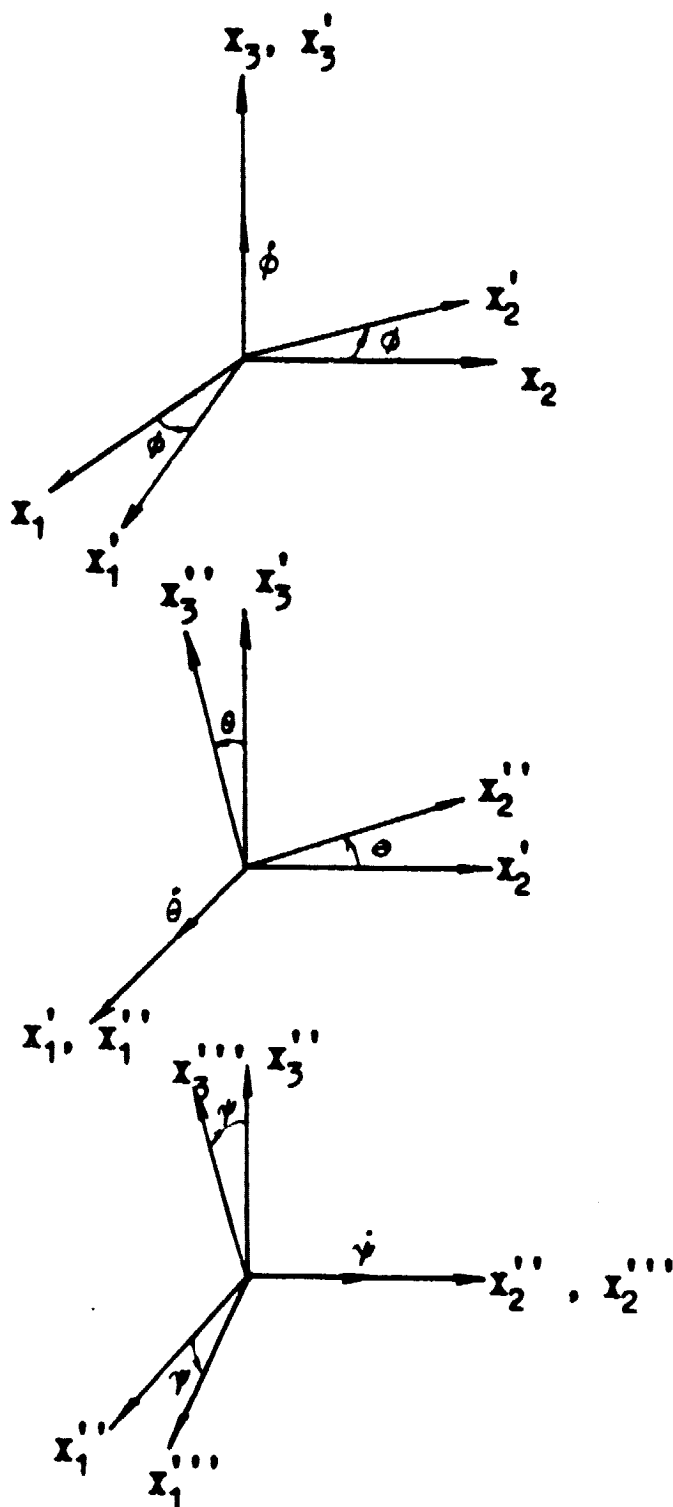


Fig.(2.2-1) Euler Angles for Balloon Orientation (Set III)

series of three rotations about the body axis is sufficient to allow the body axes to attain any desired orientation.

Several sets of Euler angles are possible for fixing the orientation of the subsystems. One set of Euler angles (Set III) was employed in this work and is shown in Fig. 2.2-1. The sequence of the three rotations which define this set is described below.

- a. a positive rotation ϕ about the X_3 axis resulting in the X_1' body system,
- b. a positive rotation θ about the X_1' axis resulting in the X_1'' body system, and
- c. a positive rotation ψ about the X_2'' axis resulting in the X_1''' body system.

The transformation equation for the above sequence of rotations is given as follows; i.e.,

$$\bar{X}''' = A\bar{X}$$

where

$$A = \begin{bmatrix} (C(\psi)C(\phi) - S(\phi)S(\psi)) & (C(\psi)S(\phi) + S(\theta)C(\phi)S(\psi)) & (-S(\psi)C(\theta)) \\ (-C(\theta)S(\phi)) & (C(\theta)C(\phi)) & (S(\theta)) \\ (S(\psi)C(\phi) + S(\theta)S(\phi)C(\psi)) & (S(\phi)S(\psi) - S(\theta)C(\phi)C(\psi)) & (C(\theta)C(\psi)) \end{bmatrix}$$

\bar{X} denotes the fixed system axes, and

\bar{X}''' denotes the fixed body system axes.

2.3 Lagrange's Equation

The mathematical model for simulating the motion of the research platform will be developed by employing Lagrange's equation. The general

ORIGINAL PAGE IS
OF POOR QUALITY

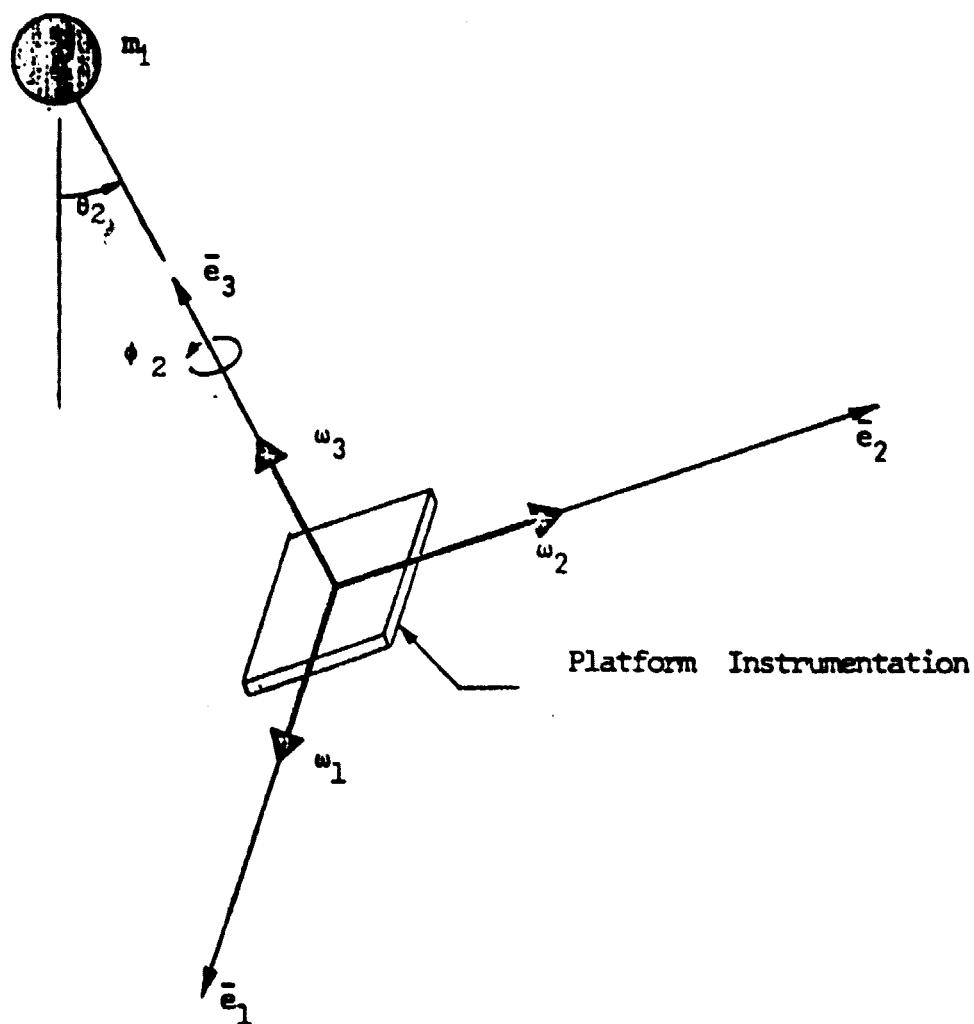


FIG. (2.2-2) Platform Angular Velocities

form of this equation is given as follows; i.e.,

$$\frac{d}{dt} \frac{\partial L}{\partial \dot{q}_i} - \frac{\partial L}{\partial q_i} = Q_i \quad (i = 1, \dots, n) \quad (2.3-1)$$

where

$L = T - V = \text{Lagrangian},$

$T = \text{kinetic energy of the system},$

$V = \text{potential energy of the system},$

$q_i = \text{generalized coordinates},$

$\dot{q}_i = \text{generalized velocities},$

$n = \text{the number of generalized coordinates, and}$

$Q_i = \text{the nonconservative generalized forces}.$

For purposes of this work the friction at the support points 0 and 1 will be neglected. In addition, the aerodynamic drag forces acting on subsystems 1 and 2 will also be neglected. Hence, the generalized forces Q_i are equal to zero and Eq. 2.3-1 reduces to

$$\frac{d}{dt} \frac{\partial L}{\partial \dot{q}_i} - \frac{\partial L}{\partial q_i} = 0. \quad (2.3-2)$$

2.4 Kinematics

In order to obtain the kinetic energy of the system, it is first necessary to develop the kinematic expressions for the velocity (angular and linear) of the subsystems. By employing the Euler angles, the angular velocities for subsystem (1) are given as follows; i.e.,

$$\begin{aligned} \omega_1^{(1)} &= (\dot{\phi}_1 \sin(\psi_1) \cos(\theta_1) + \dot{\theta}_1 \cos(\psi_1), \\ \omega_2^{(1)} &= (\dot{\phi}_1 \sin(\theta_1) + \dot{\psi}_1), \text{ and} \\ \omega_3^{(1)} &= (\dot{\phi}_1 \cos(\theta_1) \cos(\psi_1) + \dot{\theta}_1 \sin(\psi_1), \end{aligned} \quad (2.4-1)$$

where

$w_i^{(1)}$ = component of the angular velocity of subsystem (1)
along the i th body axis ($i = 1, 2, 3$), and

θ_1, ψ_1, ϕ_1 = Euler angles of rotation for subsystem (1).

Similarly, the angular velocities for subsystem (2) are:

$$\begin{aligned} w_1^{(2)} &= (-\dot{\phi}_2 S(\psi_2)C(\theta_2) + \dot{\theta}_2 C(\psi_2)), \\ w_2^{(2)} &= (\dot{\phi}_2 S(\theta_2) + \dot{\psi}_2, \text{ and} \\ w_3^{(2)} &= (\dot{\phi}_2 C(\theta_2)C(\psi_2) + \dot{\theta}_2 S(\psi_2), \end{aligned} \quad (2.4-2)$$

where

$w_i^{(2)}$ = component of the angular velocity of subsystem (2)
along the i th body axis ($i = 1, 2, 3$), and
 θ_2, ψ_2, ϕ_2 = Euler angles of rotation for subsystem (2).

By employing small angle approximations (i.e., $S(\theta) = \theta$, $C(\theta) = 1$),
and by neglecting second order terms in θ and ψ , Eq.(2.4-1) and (2.4-2)
can be written as follows:

$$\begin{aligned} w_1^{(1)} &= \dot{\theta}_1, \\ w_2^{(1)} &= \dot{\psi}_1, \\ w_3^{(1)} &= \dot{\phi}_1, \end{aligned} \quad (2.4-3)$$

and

$$\begin{aligned} w_1^{(2)} &= \dot{\theta}_2, \\ w_2^{(2)} &= \dot{\psi}_2, \\ w_3^{(2)} &= \dot{\phi}_2. \end{aligned} \quad (2.4-4)$$

The translational motion of the support point 0 (Fig. 2.1-2) is referred to an axis which is fixed in space. The translational velocity expression for this point is given as follows; i.e.,

$$\begin{aligned} v_1^{(0)} &= \dot{x}_1, \\ v_2^{(0)} &= \dot{x}_2 \\ v_3^{(0)} &= \dot{x}_3, \end{aligned} \quad (2.4-5)$$

where

$$\begin{aligned} v_i^{(0)} &= \text{absolute velocity components of support point 0} \\ &\quad (i = 1, 2, 3) \text{ along the } x_i \text{ body axis of subsystem (2).} \end{aligned}$$

The velocity expressions for support point (1) (Fig. 2.1-2) are given as follows; i.e.,

$$\begin{aligned} v_1^{(1)} &= (\dot{x}_1 - r_1 \dot{\psi}_1), \\ v_2^{(1)} &= (\dot{x}_2 + r_1 \dot{\theta}_1), \text{ and} \\ v_3^{(1)} &= (\dot{x}_3), \end{aligned} \quad (2.4-6)$$

where

$$\begin{aligned} v_i^{(1)} &= \text{absolute velocity components of point (1) along the} \\ &\quad \text{body axis of subsystem (2), and} \\ r_1 &= \text{distance between point (0) and point (1).} \end{aligned}$$

The velocity expressions for point (2) are given as follows; i.e.,

$$\begin{aligned} v_1^{(2)} &= (\dot{x}_1 - r_1 \dot{\psi}_1 - r_2 \dot{\psi}_2), \\ v_2^{(2)} &= (\dot{x}_2 + r_1 \dot{\theta}_1 + r_2 \dot{\theta}_2), \text{ and} \\ v_3^{(2)} &= \dot{x}_3 \end{aligned} \quad (2.4-7)$$

where

$$\begin{aligned} v_i^{(2)} &= \text{absolute velocity components of point (2) along the} \\ &\quad \text{body axis of subsystem (2), and} \end{aligned}$$

r_i = distance between point (i-1) and point (i).

The above equations were developed by employing small angle approximations (i.e., $S(\theta) = \theta$, $C(\theta) = 1$), and neglecting second order terms in θ and ψ . Moreover, it also assumes that the nature of the ring and clevis support at point (1) is such that the difference between the spin angles ϕ_1 and ϕ_2 is small.

2.5 System Lagrangian

The general kinetic expression for subsystems (1) and (2) is given as follows:

$$T^{(i)} = \frac{1}{2} m_i \bar{V}^{(i)} \cdot \bar{V}^{(i)} + \frac{I_{i1}}{2} (w_1^{(i)})^2 + \frac{I_{i2}}{2} (w_2^{(i)})^2 + \frac{I_{i3}}{2} (w_3^{(i)})^2 \quad (i=1,2) \quad (2.5-1)$$

where

$T^{(i)}$ = kinetic energy of subsystem (i),

m_i = mass of subsystem (i),

I_{i1}, I_{i2}, I_{i3} = moments of inertia of subsystems (i) along the (2) body axis, and

$w_j^{(i)}$ = components of the angular velocity of subsystem (i) along the (2) body axis.

The total kinetic energy T of the balloon system is obtained by summing Eq. (2.5-1) and substituting from Eqs. (2.4-3), (2.4-4), (2.4-6) and (2.4-7); this gives:

$$\begin{aligned} T &= T^{(1)} + T^{(2)} \\ &= \frac{m_1}{2} (\dot{x}_1 - r_1 \dot{\psi}_1)^2 + (\dot{x}_2 + r_1 \dot{\theta}_1)^2 + (\dot{x}_3)^2 \\ &\quad + \frac{I_{13}}{2} (\dot{\phi}_1)^2 + \frac{m_2}{2} (\dot{x}_1 - r_1 \dot{\psi}_1 - r_2 \dot{\psi}_2)^2 \\ &\quad + (\dot{x}_2 + r_1 \dot{\theta}_1 + r_2 \dot{\theta}_2)^2 + (\dot{x}_3)^2 + \frac{I_{23}}{2} (\dot{\phi}_2)^2. \end{aligned} \quad (2.5-2)$$

For purposes of developing Eq. (2.5-2) the moments of inertia I_{12}, I_{11} , and I_{22} were neglected and m_1 and m_2 were treated as point masses.

The system potential energy is due to the presence of the conservative gravitational forces and is given as follows:

$$V = V^{(1)} + V^{(2)} \quad (2.5-3)$$

where

$$\begin{aligned} V^{(1)} &= -m_1 g r_1 C(\theta_1) C(\psi_1), \text{ and} \\ V^{(2)} &= -m_2 g (r_1 C(\theta_1) C(\psi_1) + r_2 C(\theta_2) C(\psi_2)). \end{aligned}$$

The system Lagrangian (L), which is defined in Eq. (2.3-1), is obtained by subtracting the total potential energy (Eq. (2.5-3)) from the total kinetic energy (Eq. (2.5-2)) and is given as follows:

$$\begin{aligned} L &= T - V \\ &= \frac{1}{2} m_1 (\dot{X}_1 - r_1 \dot{\psi}_1)^2 + (\dot{X}_2 + r_1 \dot{\theta}_1)^2 + (\dot{X}_3)^2 \\ &\quad + \frac{I_{13}}{2} (\dot{\phi}_1)^2 + \frac{1}{2} m_2 (\dot{X}_1 - r_1 \dot{\psi}_1 - r_2 \dot{\psi}_2)^2 \\ &\quad + (\dot{X}_2 + r_1 \dot{\theta}_1 + r_2 \dot{\theta}_2)^2 + (\dot{X}_3)^2 + \frac{I_{23}}{2} (\dot{\phi}_2)^2 \\ &\quad + m_1 g r_1 C(\theta_1) C(\psi_1) \\ &\quad + m_2 g (r_1 C(\theta_1) C(\psi_1) + r_2 C(\theta_2) C(\psi_2)). \end{aligned} \quad (2.5-4)$$

2.6 System Math Model

The equations for the motion of the balloon platform are obtained by substituting the Lagrangian from Eq. (2.5-4) into Eq. (2.3-2). The resulting equations are given below.

$$\begin{aligned} m_{11}\ddot{\theta}_1 + m_{12}\ddot{\theta}_2 + k_{11}\theta_1 &= -f_1 a_1, \\ m_{21}\ddot{\theta}_1 + m_{22}\ddot{\theta}_2 + k_{22}\theta_2 &= -f_2 a_1, \end{aligned} \quad (2.6-1)$$

$$\begin{aligned} m_{11}\ddot{\psi}_1 + m_{12}\ddot{\psi}_2 + k_{11}\psi_1 &= f_1 a_2, \\ m_{21}\ddot{\psi}_1 + m_{22}\ddot{\psi}_2 + k_{22}\psi_2 &= f_2 a_2, \end{aligned} \quad (2.6-2)$$

$$\begin{aligned} \ddot{\phi}_1 &= 0, \text{ and} \\ \ddot{\phi}_2 &= 0, \end{aligned} \quad (2.6-3)$$

where

$$m_{11} = (m_1 + m_2)r_1^2,$$

$$m_{12} = m_2 r_1 r_2,$$

$$m_{21} = m_2 r_1 r_2,$$

$$m_{22} = m_2 r_2^2,$$

$$k_{11} = (m_1 + m_2)g r_1,$$

$$k_{22} = m_2 g r_2,$$

$$f_1 = (m_1 + m_2)r_1,$$

$$f_2 = m_2 r_2,$$

a_1 = acceleration component of point (0) along the $e_2^{(2)}$ body axis, and

a_2 = acceleration component of point (0) along the $e_1^{(2)}$ body axis.

Eqs. (2.6-1) and (2.6-2) were developed by assuming small displacements;

i.e., $C(\theta_i) = C(\psi_i) = 1$, $S(\theta_i) = \theta_i$, $S(\psi_i) = \psi_i$.

Eq. (2.6-3) yields that $\dot{\phi}_i$ is a constant. In this study the pre-

cision of this model was improved by employing the transformation equation for the angular velocity $w_3^{(1)}$. As stated earlier, it will be assumed that $\phi_1 = \phi_2$. Thus, Eq. (2.6-3) will be replaced with the following:

$$\dot{\phi}_1 = \dot{\phi}_2 = w_3^{(2)} \quad (2.6-4)$$

where

$w_3^{(2)}$ is the angular velocity obtained from the rate gyro mounted along the $e_3^{(2)}$ body axis.

Eqs. (2.6-1) and (2.6-2) can be written in matrix form as follows:

$$M\ddot{\eta}_i + K\eta_i = R_i a_i \quad (i=1,2) \quad (2.6-5)$$

$$E_i = C\dot{\eta}_i \quad (i=1,2) \quad (2.6-6)$$

where

$$\eta_1 = \begin{bmatrix} \theta_1 \\ \theta_2 \end{bmatrix},$$

$$\eta_2 = \begin{bmatrix} \psi_1 \\ \psi_2 \end{bmatrix},$$

$$M = \begin{bmatrix} m_{11} & m_{12} \\ m_{21} & m_{22} \end{bmatrix},$$

$$K = \begin{bmatrix} k_{11} & 0 \\ 0 & k_{22} \end{bmatrix},$$

$$F_1 = \begin{bmatrix} -f_1 \\ -f_2 \end{bmatrix},$$

$$F_2 = \begin{bmatrix} f_1 \\ f_2 \end{bmatrix},$$

$$E_1 = w_1^{(2)},$$

$w_1^{(2)} = \dot{\theta}_2$ = the component of the angular velocity of subsystem
(2) along the $e_1^{(2)}$ body axis,

$$E_2 = w_2^{(2)},$$

$w_2^{(2)} = \dot{\psi}_2$ = the component of the angular velocity of subsystem
(2) along the $e_2^{(2)}$ body axis,

$$C = (0 \ 1),$$

$$\dot{\eta}_1 = \begin{bmatrix} \dot{\theta}_1 \\ \dot{\theta}_2 \end{bmatrix}, \text{ and}$$

$$\dot{\eta}_2 = \begin{bmatrix} \dot{\psi}_1 \\ \dot{\psi}_2 \end{bmatrix}.$$

The numerical values for the m_{ij} and k_{ij} coefficients were computed by employing the properties of the balloon system which are given in Table 4.1-1. These resulting values are given in Table 4.1-2.

2.7 State Variable Form of Math Model

Eqs. (2.6-5) and (2.6-6) can be expressed in general state variable form as follows:

$$L \dot{q} = Nq + Ru, \text{ and} \quad (2.7-1)$$

$$y = Cq \quad (2.7-2)$$

where

$$q = \begin{bmatrix} \eta_1 \\ \eta_2 \\ \dot{\eta}_1 \\ \dot{\eta}_2 \end{bmatrix},$$

$$L = \begin{bmatrix} 1 & 0 & 0 & 0 \\ 0 & 1 & 0 & 0 \\ 0 & 0 & m_{11} & m_{12} \\ 0 & 0 & m_{21} & m_{22} \end{bmatrix},$$

$$N = \begin{bmatrix} 0 & 0 & 1 & 0 \\ 0 & 0 & 1 & 1 \\ -k_{11} & 0 & 0 & 0 \\ 0 & -k_{22} & 0 & 0 \end{bmatrix},$$

$$R = \text{control matrix} = \begin{bmatrix} 0 \\ 0 \\ f_1 \\ f_2 \end{bmatrix},$$

u = control variable,

$$y = W^{(2)},$$

$W^{(2)}$ = the component of platform angular velocity along the system (2) body axis, and

$$C = (0 \ 0 \ 0 \ 1).$$

Eqs. (2.7-1) and (2.7-2) can be further expressed as follows:

$$\dot{q} = Aq + Bu, \text{ and} \tag{2.7-3}$$

$$y = C q$$

(2.7-4)

where

$$A = L^{-1} N = \begin{bmatrix} 0 & 0 & 1 & 0 \\ 0 & 0 & 0 & 1 \\ a_{31} & a_{32} & 0 & 0 \\ a_{41} & a_{42} & 0 & 0 \end{bmatrix} ,$$

$$B = L^{-1} R = \begin{bmatrix} 0 \\ 0 \\ b_3 \\ b_4 \end{bmatrix} .$$

The elements of the A and B matrices are given below; i.e.,

$$a_{31} = \frac{-m_{22} k_{11}}{j} ,$$

$$a_{32} = \frac{m_{12} k_{22}}{j} ,$$

$$a_{41} = \frac{m_{21} k_{11}}{j} ,$$

$$a_{42} = \frac{-m_{11} k_{22}}{j} ,$$

$$b_3 = \frac{m_{22} f_1 - m_{12} f_2}{j} ,$$

$$b_4 = \frac{-m_{21} f_1 + m_{11} f_2}{j} ,$$

where

$$j = m_{11} m_{22} - m_{21} m_{12} .$$

The numerical values for the a_{ij} and b_i coefficients were computed by employing the values of k_{ij} and m_{ij} which are given in Table 4.1-2. These resulting values are given in Tables 4.1-3 and 4.1-4.

CHAPTER III

DEVELOPMENT OF OBSERVER SYSTEM MATHEMATICAL MODELS

3.1 Concept of Observability

The observability of a system implies the determinability of the system state from an observation of the output over a finite time interval starting from the instant at which the state is desired⁽⁴⁾. It is assumed that the system inputs, outputs and mathematical model are known.

For purposes of referencing the work in this chapter, the state variable form of the balloon's model (Eqs. (2.7-3) and 2.7-4)) will be rewritten below; i.e.,

$$\dot{q} = A q + B u, \quad (3.1-1)$$

$$q(t_0) = q_0, \text{ and}$$

$$y = Cq. \quad (3.1-2)$$

where

q is the n th order state vector,

q_0 is the unknown initial state vector,

u is the single (scalar) input,

y is the single (scalar) output,

n is the order of the system,

A is a $n \times n$ matrix,

B is a $n \times 1$ matrix, and

C is a $1 \times n$ matrix.

Eq. (3.1-1) determines the plant dynamics and indicates how the input (or control) u affects the state vector q . The matrix A characterizes the plant dynamics when u is not present; this is the so-called free-response case. The matrix B determines how the plant response is affected by the input (or control) vector u . Eq. (3.1-2) defines the relationship between state vector q and the system output y .

For system observability, the basic question is as follows: "Is it possible to identify the initial state q_0 by observing the output (y) over a finite time interval?" Precise definitions of system observability are given as follows:

1. Definition 3.1a. A state q_1 , i.e. $q(t_1)$ of a system is said to be observable at time t_0 , if knowledge of the input $u(t)$ and output $y(t)$ over a finite time $t_0 < t < t_1$, completely determines the state q_0 . Otherwise, the state is said to be unobservable at t_0 .
2. Definition 3.1b. If all system states $q(t)$ are observable, then the system is said to be completely observable or just observable.
3. Definition 3.1c. If the state q_1 is observable and if the knowledge of the input and the output over an arbitrarily small interval of time suffices to determine q_0 (independent of t_0), then the state is said to be totally observable.
4. Definition 3.1d. If all the states $q(t)$ are totally observable, then the system is said to be totally observable⁽⁵⁾.

The necessary condition for observability of the balloon system is given in the following section.

3.2 Observability of Balloon Systems

The following theorem (Ref. 3) can be employed to determine the observability for general time - invariant systems.

Theorem 3.2a. The time-invariant system described by Eqs. (3.1-1) and (3.1-2) is totally observable if and only if the composite matrix M has rank n, where

$$M = \begin{bmatrix} C \\ CA \\ C(A^2) \\ \vdots \\ C(A^{n-1}) \end{bmatrix}, \text{ and}$$

n, C and A are defined in Eqs. (3.1-1) and 3.1-2).

The observability of the balloon system described by Eqs. (2.7-3) and (2.7-4) can now be determined by showing that the composite matrix M has rank 4. For this purpose, the matrices C, CA, $C(A^2)$ and $C(A^3)$ are given as follows:

$$C = (0 \ 0 \ 0 \ 1),$$

$$CA = (a_{41} \ a_{42} \ 0 \ 0),$$

$$C(A^2) = (0 \ 0 \ a_{41} \ a_{42}), \text{ and}$$

$$C(A^3) = ((a_{41}a_{31} + a_{42}a_{41}) \ (a_{32}a_{41} + a_{42}^2) \ 0 \ 0).$$

The specific form of the composite matrix M for the balloon system model is given as follows, i.e.

$$M = \begin{bmatrix} C \\ CA \\ C(A^2) \\ C(A^3) \end{bmatrix} ; \text{ i.e., } M = \begin{bmatrix} 0 & 0 & 0 & 1 \\ a_{41} & a_{42} & 0 & 0 \\ 0 & 0 & a_{41} & a_{42} \\ (a_{41}a_{31} + a_{41}a_{42}) & (a_{32}a_{41} + a_{42}^2) & 0 & 0 \end{bmatrix} .$$

In order to show that the rank of $M =$ four, it is necessary to prove that the determinant is non zero. It can be shown that the determinant for M is non zero if the following expression is non zero, i.e., if

$$m_1 m_2 r_1^2 r_2^2 \neq 0.$$

Thus, the balloon system is completely observable since the composite matrix M has rank = 4.

3.3 Observability of Balloon System With Output Bias

Previous studies have been conducted for the LACATE system in order to determine the nature of the balloon's platform motion⁽⁶⁾. The time history of the platform pendulation angles ($\theta(t)$ and $\psi(t)$) was determined by integrating the output from the rate gyros. The study indicated that the platform motion consisted of small oscillations superimposed on a line with (nearly) constant slope. These results suggested that the gyroscopes contain a constant bias error.

In order to take into account the error in the output (y) due to bias in the gyroscopes, the matrices in Eqs. (3.1-1) and (3.1-2) are defined as follows; i.e.,

$$A = \begin{bmatrix} 0 & 0 & 1 & 0 & 0 \\ 0 & 0 & 0 & 1 & 0 \\ a_{31} & a_{32} & 0 & 0 & 0 \\ a_{41} & a_{42} & 0 & 0 & 0 \\ 0 & 0 & 0 & 0 & 0 \end{bmatrix},$$

$$B = \begin{bmatrix} 0 \\ 0 \\ b_3 \\ b_4 \\ 0 \end{bmatrix},$$

$$u = a,$$

$$y = w^{(2)} + q_5,$$

$w^{(2)}$ = the component of the angular velocity of the platform along the specified body axis,

q_5 = corresponding gyroscope bias, and

$$C = (0 \ 0 \ 0 \ 1 \ 1).$$

The observability of the system model described by Eqs. (3.1-1) and (3.1-2) can be ascertained by showing that the corresponding composite matrix M has rank 5. It can be shown that the composite matrix M for this system is given as follows; i.e.,

$$M = \begin{bmatrix} C \\ CA \\ C(A^2) \\ C(A^3) \\ C(A^4) \end{bmatrix}$$

$$M = \begin{bmatrix} 0 & 0 & 0 & 1 & 1 \\ a_{41} & a_{42} & 0 & 0 & 0 \\ 0 & 0 & a_{41} & a_{42} & 0 \\ (a_{41}a_{31}+a_{42}a_{41}) & (a_{41}a_{32}+a_{42}^2) & 0 & 0 & 0 \\ 0 & 0 & (a_{41}a_{31}+a_{42}a_{41}) & (a_{41}a_{32}+a_{42}^2) & 0 \end{bmatrix}$$

It can be shown that the determinant of the above matrix is non-zero if the resulting expression is non zero; i.e., if

$$m_1 m_2 (r_2 + r_1) \neq 0.$$

Thus, the system described by Eqs. (3.1-1) and (3.1-2) is completely observable since the composite matrix M has rank = 5.

3.4 Development of Full Order Identity Observer for Balloon System

Without Bias

An n th order identity observer (or asymptotic-state estimator) can be constructed for the completely observable n th order plant described by Eqs. (3.1-1) and (3.1-2). The observer is described by the following equations; i.e.,

$$\dot{Z} = FZ + B u + G y, \text{ and} \quad (3.4-1)$$

$$Z(t_0) = Z_0.$$

where

Z is an n +th order estimate of the state vector q ,

Z_0 is an estimate of the unknown initial state vector q_0 ,

G is an $n \times 1$ matrix,

$F = (A - GC)$, and

Y , u , B and C are as described in Eqs. (3.1-1) and (3.1-2).

An inspection of Eq. (3.4-1) reveals that the state estimators response (Z) will be determined from a consideration of the observer dynamics, external inputs and plant outputs. The observer dynamics are controlled by the F matrix. The external input u contributes to the state estimator's response via the control matrix B . From Eq. (3.1-1), it can be seen that this control matrix B and the external inputs u are identical for both the plant and observer.

For accurate state space reconstruction the plant output y must be fed into the observer model. By coupling the plant output y to the observer via the G matrix, the observer becomes a closed loop estimator. This is illustrated in Fig. (3.4-1).

The F matrix in Eq. (3.4-1) is constructed such that the difference between the output of the observer model and the plant model is zero over some finite time interval. This error (E) is given as follows; i.e.,

$$E = Z - q. \quad (3.4-2)$$

Subtracting Eq. (3.1-1) from (3.4-1) yields the following:

$$\dot{E} = FE. \quad (3.4-3)$$

The solution of Eq. (3.4-3) yields:

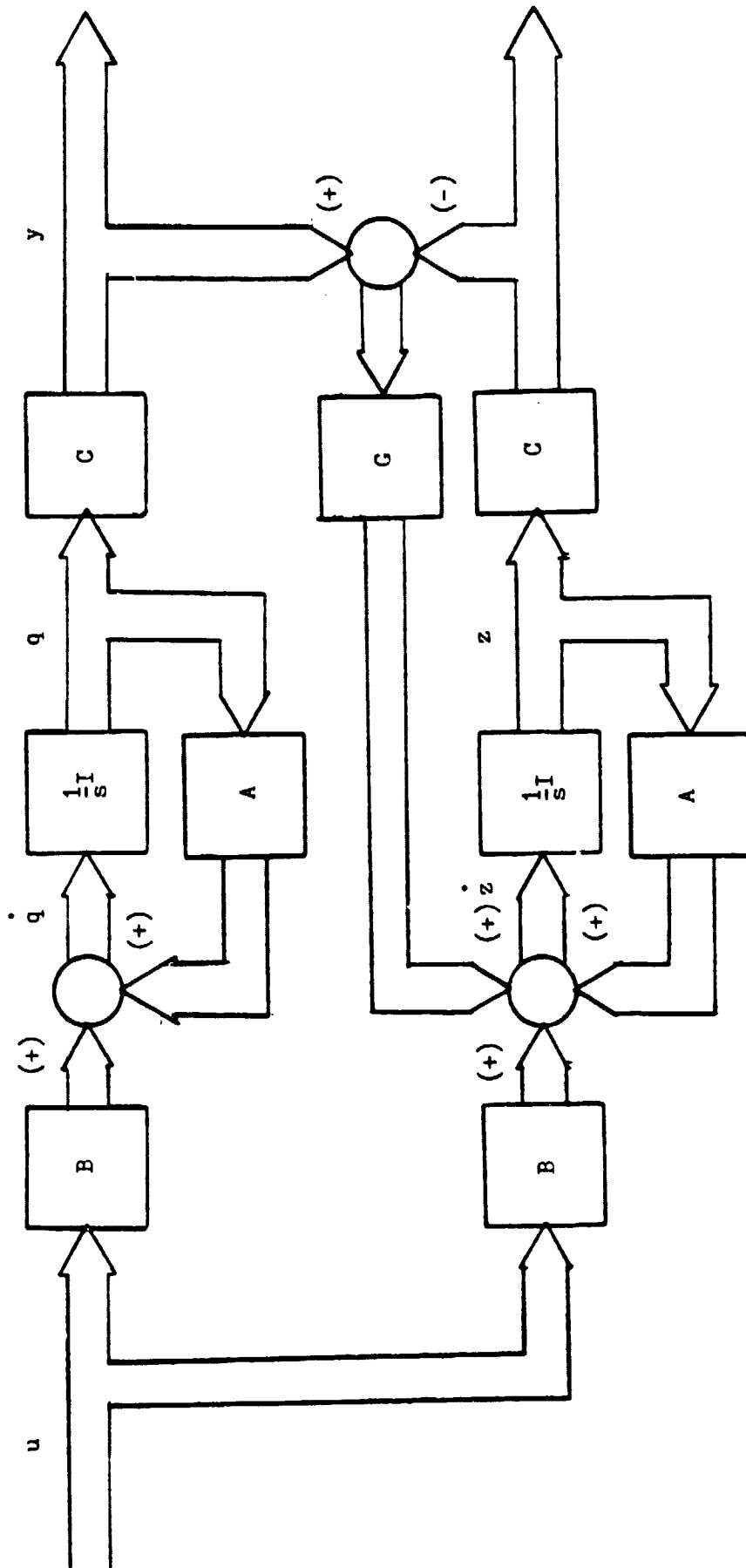


Fig.(3.4-1) Block Diagram For Asymptotic State Estimator

$$E = E_0 e^{F(t-t_0)} \quad (3.4-4)$$

where

$$E_0 = Z_0 - Q_0.$$

It is clear from Eq. (3.4-4) that the error, E , decays exponentially to zero if G is chosen such that all of the eigenvalues of F are negative or have negative real parts. Also, these eigenvalues must be more negative than the eigenvalues of A to insure accurate response.

The detailed form of the F matrix in Eq. (3.4-3) can be obtained by substituting the form of the A and C matrices which are defined in Eq. (2.7-3) and (2.7-4). This yields the following; i.e.,

$$F = (A - GC), \text{ i.e.,}$$

$$F = \begin{bmatrix} 0 & 0 & 1 & -g_1 \\ 0 & 0 & 0 & (1-g_2) \\ a_{31} & a_{32} & 0 & -g_3 \\ a_{41} & a_{42} & 0 & -g_4 \end{bmatrix},$$

where

$$G = \begin{bmatrix} g_1 \\ g_2 \\ g_3 \\ g_4 \end{bmatrix}.$$

The form of the solution for E in Eq. (3.4-3) is given as follows

$$E = X e^{\lambda t}.$$

Substitution of this into Eq. (3.4-3) yields the following eigenvalue problem:

$$(F - \lambda I)X = 0$$

where

I = the identity matrix, and

F = matrix defined in Eq. (3.4-1).

The necessary and sufficient condition for determining the eigenvalues of the matrix F is that

$$| F - \lambda I |; \text{ i.e.,} \quad \begin{vmatrix} -\lambda & 0 & 1 & -g_1 \\ 0 & -\lambda & 0 & (1-g_2) \\ a_{31} & a_{32} & -\lambda & -g_3 \\ a_{41} & a_{42} & 0 & (-g_4-\lambda) \end{vmatrix} = 0. \quad (3.4-5)$$

The characteristic polynomial obtained by expanding Eq. (3.4-5) is given below; i.e.,

$$\begin{aligned} & (\lambda^4) + (g_4\lambda^3) + ((g_1a_{41} - a_{31} - a_{42} + g_2a_{42})\lambda^2) \\ & + ((-g_4a_{31} + g_3a_{41})\lambda) + (-a_{32}a_{41} + a_{42}a_{31} \\ & + g_2a_{32}a_{41} - g_2a_{42}a_{31}) = 0. \end{aligned} \quad (3.4-6)$$

Critical damping of the error E is obtained by determining the G matrix such that all of the eigenvalues are negative and equal. This yields the following values for the G matrix: i.e.,

$$g_1 = ((-6\lambda^2 - a_{31} - a_{42} + g_2 a_{42}) / (-a_{41})),$$

$$g_2 = ((-\lambda^4 - a_{32} a_{41} + a_{42} a_{31}) / (-a_{32} a_{41} + a_{42} a_{31})),$$

$$g_3 = ((-4\lambda^3 + g_4 a_{31}) / a_{41}), \text{ and}$$

$$g_4 = (-4\lambda).$$

3.5 Development of Identity Observer Systems for Balloon System With

Bias

In the case of the fifth order identity observer system the matrices in Eq. (3.4-1) have the following form; i.e.,

$$F = \begin{bmatrix} 0 & 0 & 1 & -g_1 & -g_1 \\ 0 & 0 & 0 & (1-g_2) & -g_2 \\ a_{31} & a_{32} & 0 & -g_3 & -g_3 \\ a_{41} & a_{42} & 0 & -g_4 & -g_4 \\ 0 & 0 & 0 & -g_5 & -g_5 \end{bmatrix},$$

$$G = \begin{bmatrix} g_1 \\ g_2 \\ g_3 \\ g_4 \\ g_5 \end{bmatrix},$$

and y , u , B and C are as described in Eqs. (3.1-1) and (3.1-2).

The eigenvalues for the F matrix corresponding to the bias model are obtained from the following condition; i.e.,

$$\begin{vmatrix} -\lambda & 0 & 1 & -g_1 & -g_1 \\ 0 & -\lambda & 0 & (1-g_2) & -g_2 \\ a_{31} & a_{32} & -\lambda & -g_3 & -g_3 \\ a_{41} & a_{41} & 0 & (-\lambda-g_4) & -g_4 \\ 0 & 0 & 0 & -g_5 & (-\lambda-g_5) \end{vmatrix} = 0. \quad (3.5-1)$$

The characteristic polynomial of Eq. (3.5-1) is given as follows;

i.e.,

$$\begin{aligned} & (\lambda^5) + ((g_4 + g_5)\lambda^4) + ((g_1 a_{41} + g_2 a_{42} - a_{31} - a_{42})\lambda^3) \\ & + ((g_3 a_{41} - g_4 a_{31} - g_5 a_{31} - g_5 a_{42})\lambda^2) \\ & + ((-g_2 a_{41} a_{31} + g_2 a_{41} a_{32} + a_{42} a_{31} - a_{41} a_{32})\lambda) \\ & + (g_5 a_{42} a_{31} - g_5 a_{41} a_{32}) = 0. \end{aligned} \quad (3.5-2)$$

The final form of the G matrix elements (obtained from the condition for critical damping) are given as follows;

$$\begin{aligned} g_1 &= ((10\lambda^2 - g_2 a_{42} + a_{31} + a_{42})/a_{41}), \\ g_2 &= ((5\lambda^4 - a_{42} a_{31} + a_{41} a_{32})/(-a_{42} a_{31} + a_{41} a_{32})), \\ g_3 &= ((-10\lambda^3 + g_4 a_{31} + g_5 (a_{31} + a_{42}))/a_{41}), \\ g_4 &= (-5\lambda - g_5), \text{ and} \\ g_5 &= ((-\lambda^5)/a_{42} a_{31} - a_{31} - a_{41} a_{32}). \end{aligned}$$

CHAPTER IV

RESULTS AND CONCLUSIONS

4.1 Data for LACATE Mission

Figure (1.1-1) illustrates the actual LACATE balloon system and Figure (2.1-2) illustrates the corresponding idealized system used in this study. The values for the various lengths and masses of the idealized system are given in Table (4.1-1).

The numerical values for the elements of the M and K matrices of Eq. (2.6-5) were computed based on the data given above. The resulting values are presented in Table (4.1-2). The numerical values for the A and B matrices of Eq. (3.1-1) are given in Tables (4.1-3) and (4.1-4).

The eigenvalue problem for the balloon system was solved analytically. The solution for the eigenvalues $(\Omega^2)_j$ and corresponding eigenvectors are presented in Table (4.1-5). The values of Ω_j represent the natural frequencies of the system. The modal shape functions and periods corresponding to each natural frequency are shown in Table (4.1-6).

Results for the balloon observer system were obtained by employing two separate time intervals. The equations for predicting the body axis acceleration components from sensor outputs are presented in Appendix A. Plots of the body axis acceleration components over the two time intervals are given in Figures (4.1-1) through (4.1-6).

4.2 Results From Simulation Study

Eq. (3.1-1) was employed to simulate the balloon platform angular velocity and angular displacement. The inputs and outputs employed with the simulated system were of the same order of magnitude as predicted

TABLE 4.1-1

Idealized LACATE System Properties

r_1 (distance from point 0 to mass m_1) = 75 ft.

r_2 (distance from mass m_1 to m_2) = 15 ft.

m_1 (lumped mass) = 135 lb_m

m_2 (lumped mass) = 375 lb_m

TABLE 4.1-2

Coefficients of m and k Matrices

$$m_{11} = 89156 \text{ (lbf} \cdot \text{s}^2 \cdot \text{ft)}$$

$$m_{12} = 13111 \text{ (lbf} \cdot \text{s}^2 \cdot \text{ft)}$$

$$m_{21} = 13111 \text{ (lbf} \cdot \text{s}^2 \cdot \text{ft)}$$

$$m_{22} = 2622 \text{ (lbf} \cdot \text{s}^2 \cdot \text{ft)}$$

$$k_{11} = 38278 \text{ (lbf} \cdot \text{ft)}$$

$$k_{22} = 5629.4 \text{ (lbf} \cdot \text{ft)}$$

TABLE 4.1-3

Coefficients of A Matrix

$$a_{31} = -1.621 \text{ (s}^{-2}\text{)}$$

$$a_{32} = 1.1923 \text{ (s}^{-2}\text{)}$$

$$a_{41} = 8.107 \text{ (s}^{-2}\text{)}$$

$$a_{42} = 8.107 \text{ (s}^{-2}\text{)}$$

TABLE 4.1-4

Coefficients of B Matrix

$$b_3^{(1)} = -0.01334 \text{ (ft}^{-1}\text{)}$$

$$b_4^{(1)} = 0.0$$

$$b_3^{(2)} = 0.01334 \text{ (ft}^{-1}\text{)}$$

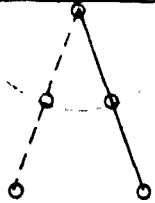

$$b_4^{(2)} = 0.0$$

TABLE 4.1-5Balloon Systems Eigenvalues Ω^2 ; and Corresponding Eigenvectors

j	Ω_j^2	X_j
1	.3711	1.000 1.048
2	9.3611	1.000 -6.488

TABLE 4.1-6

Balloon Systems Modal Shape Functions and Periods

j	Ω_j	Period (τ_j)	Modal Shape
1	.6092	10.314	
2	3.0596	2.053	

ORIGINAL PAGE IS
OF POOR QUALITY

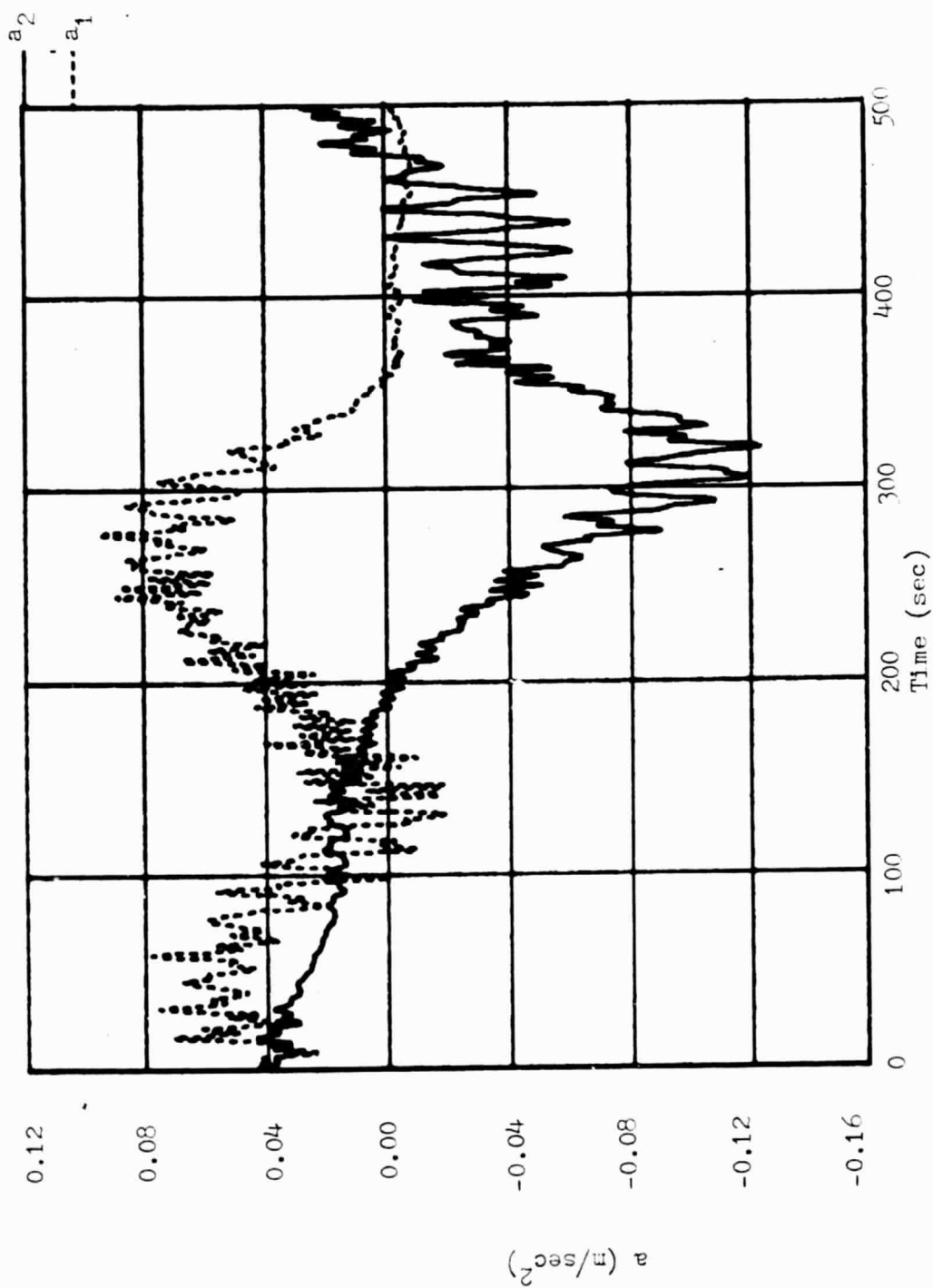


Fig. (4.1-1) Plot of Balloon's Translational Accelerations ($0 \leq t \leq 500$)

ORIGINAL PAGE IS
OF POOR QUALITY

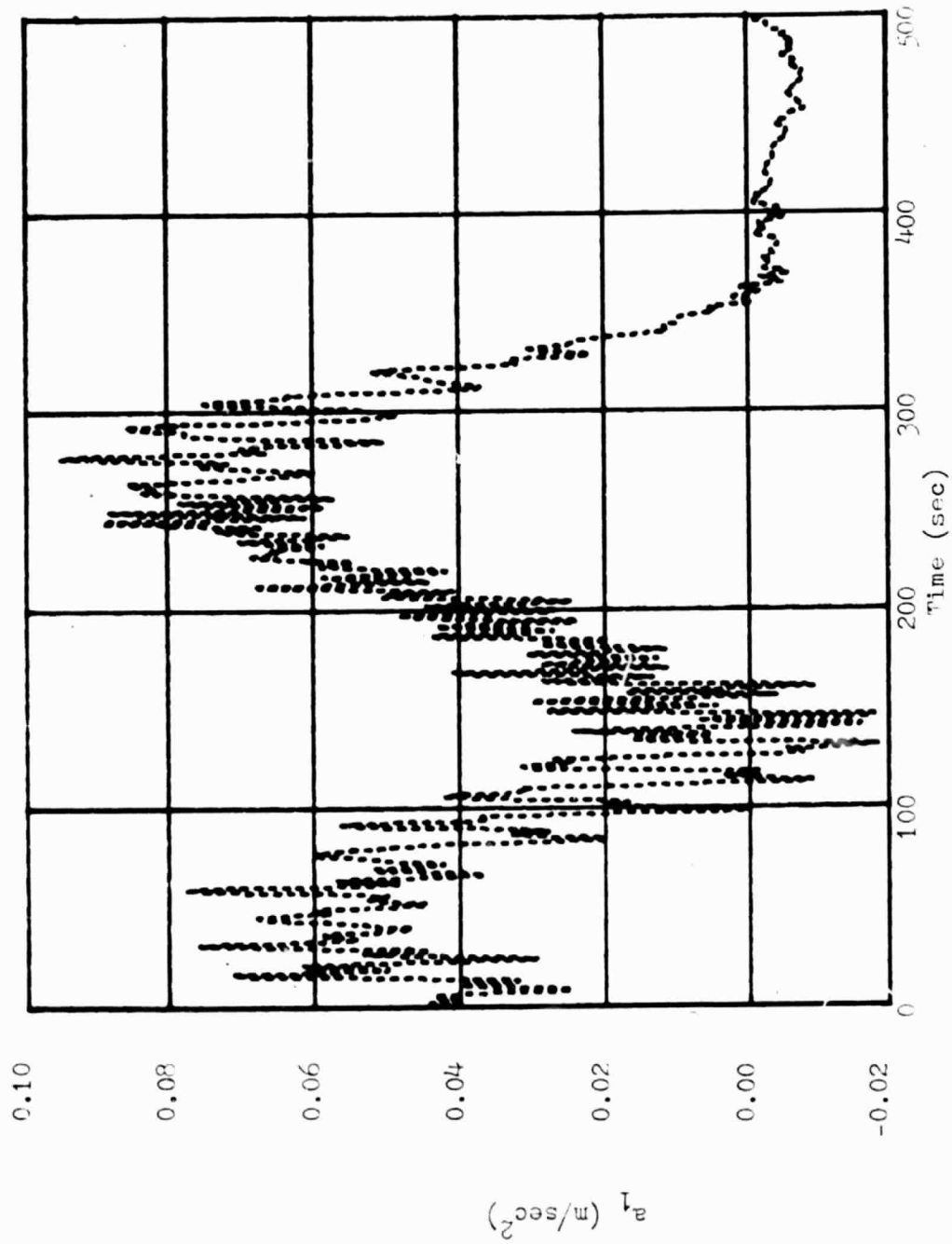


Fig. (4.1-2) Plot of Balloon's Translational Acceleration (a_1) ($0 \leq t \leq 500$)

ORIGINAL PAGE IS
OF POOR QUALITY

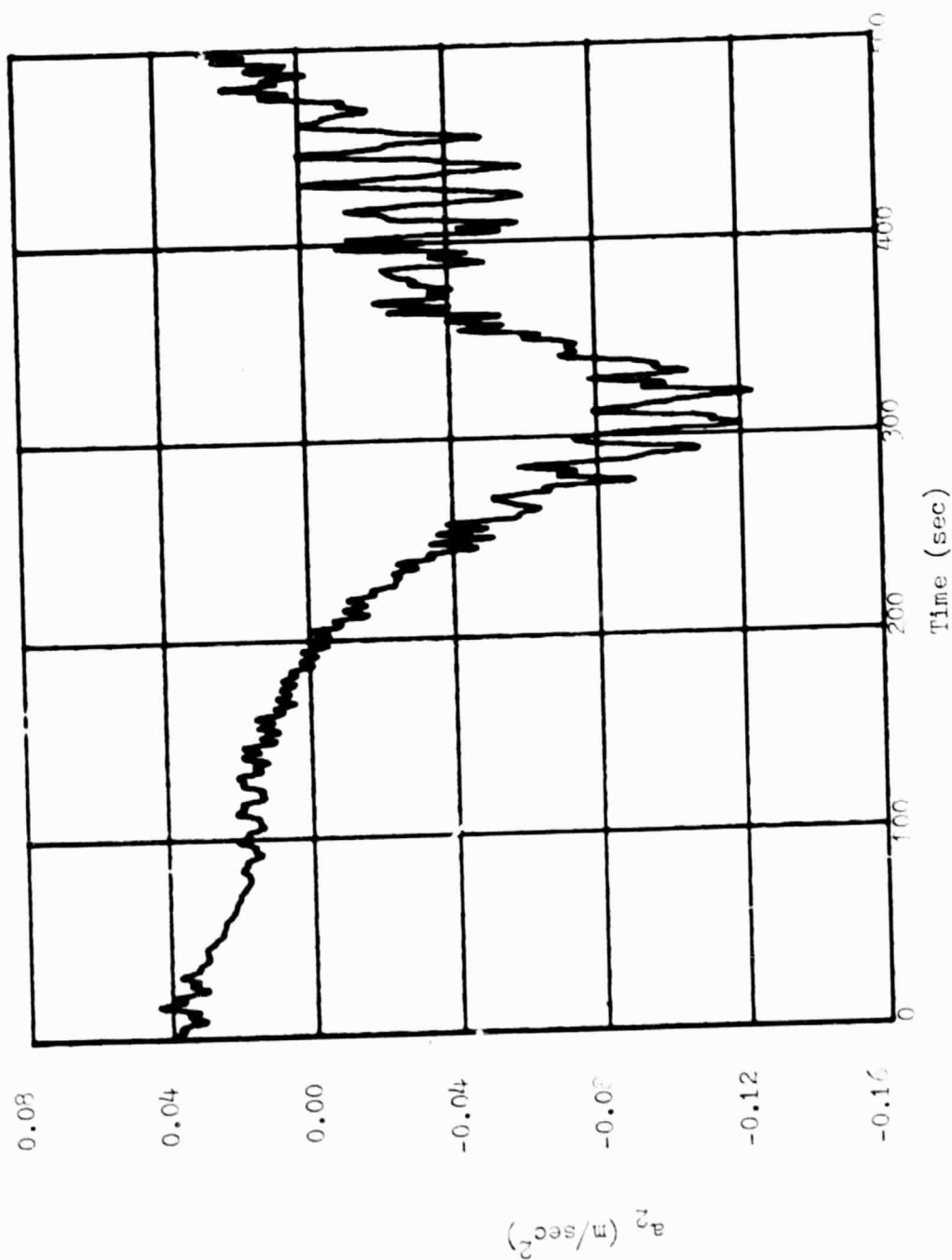


Fig. (4.1-3) Plot of Balloon's Translational Acceleration (a_2) ($0 \leq t \leq 500$)

ORIGINAL PAGE IS
OF POOR QUALITY

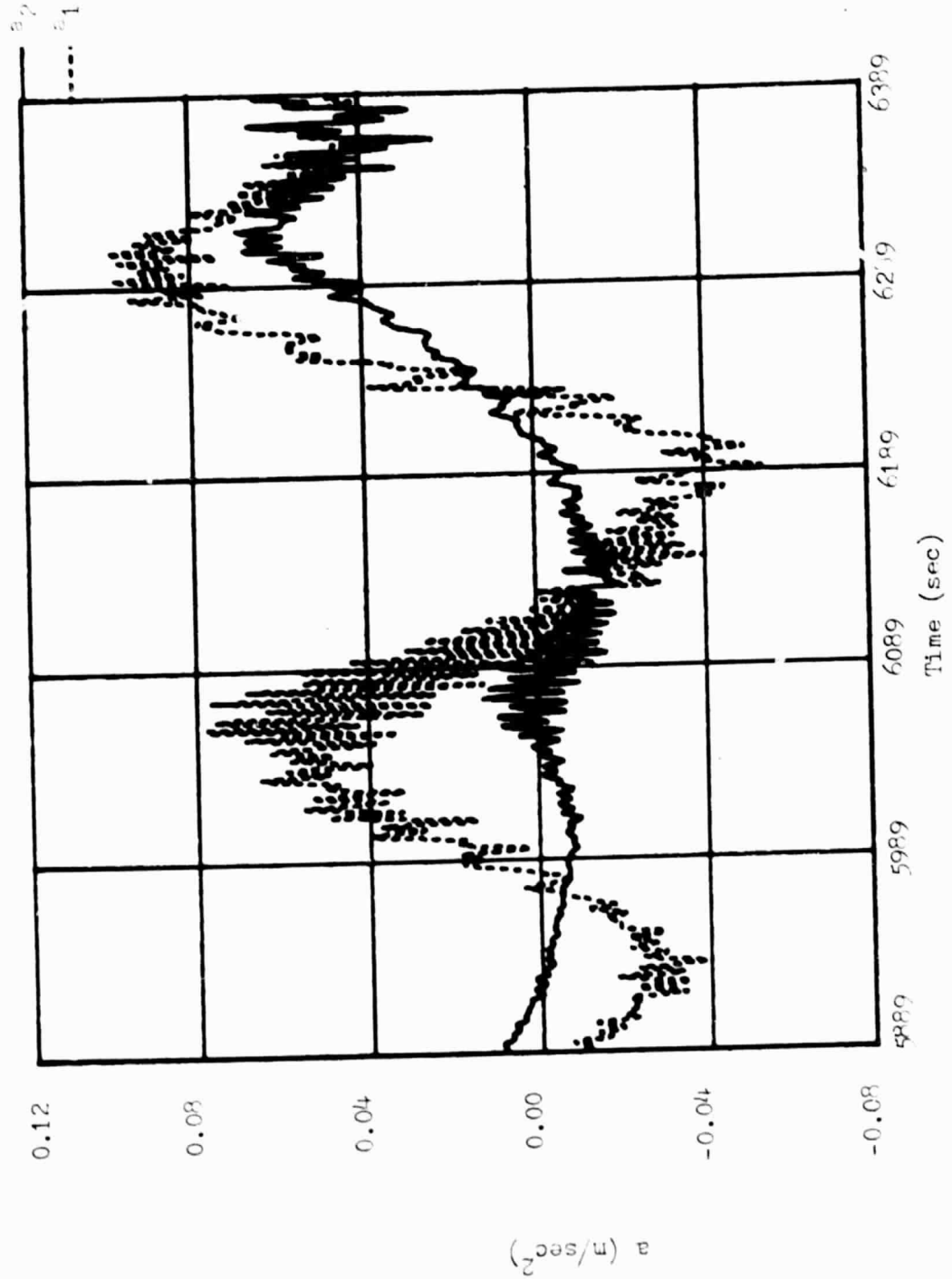


Fig. (4.1-4) Plot of Balloon's Translational Accelerations ($5889 \leq t \leq 6389$)

ORIGINAL PAGE IS
OF POOR QUALITY

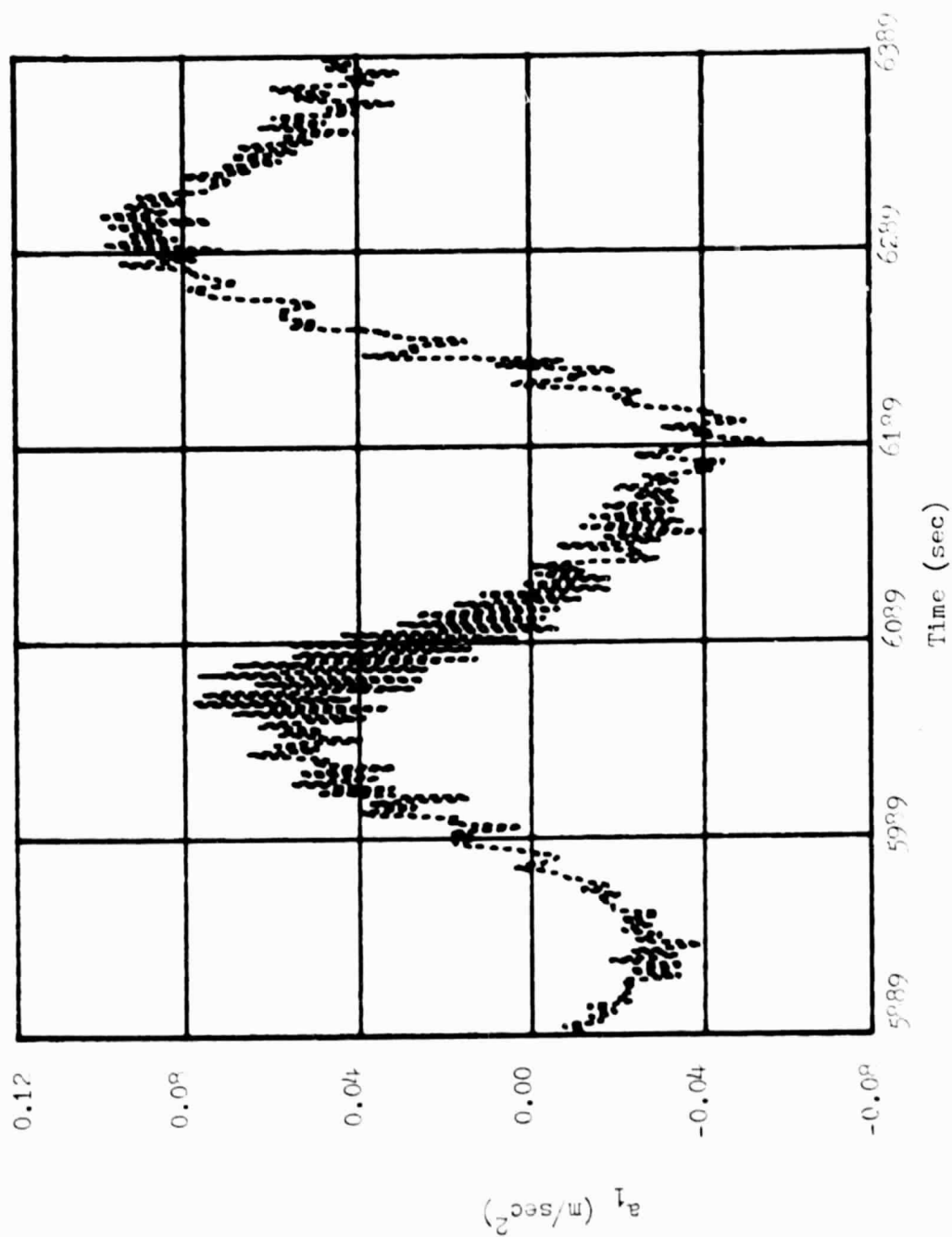


Fig. (4.1-5) Plot of Balloon's Translational Acceleration (a_1) (5989 ≤ t ≤ 6389)

ORIGINAL PAGE IS
OF POOR QUALITY

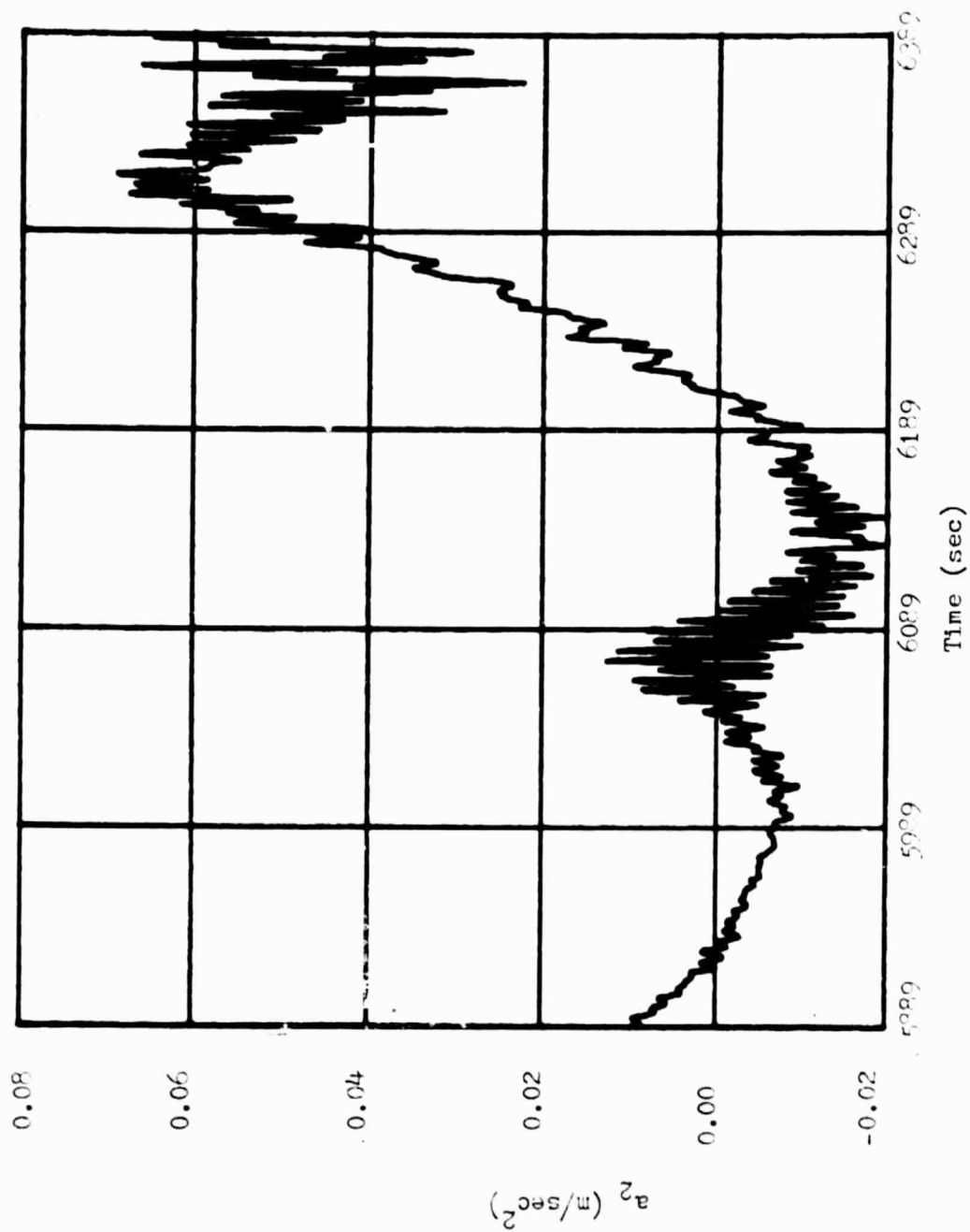


Fig. (4.1-6) Plot of Palloon's Translational Acceleration (a_2) (5989-6389)

by the actual LACATE flight data. For comparison purposes, all of the simulation runs employed identical initial conditions and eigenvalues; the magnitude of the latter was equal to -0.6 .

The angular velocity ($\dot{\theta}$) and angular displacement (θ) predicted by the fourth order observer system are shown in Figs. (4.2-1) - (4.2-4) for the case when bias is not present in the output. The free response case is illustrated in Figs. (4.2-1) and (4.2-2), while in Figures (4.2-3) and (4.2-4), results are given for the case when a ramp input was employed.

Figures (4.2-5) - (4.2-13) illustrate the free response of the fourth order observer system for the case when bias is present in the output. The plant output for the case shown in Figs. (4.2-5) and (4.2-6) contains a constant bias, while a linear bias was used to obtain the results shown in Figs. (4.2-7) and (4.2-8).

Figures (4.2-9) - (4.2-13) give the free response results for the fourth order observer system when a high frequency bias ($\beta = 0.005 \cos(13t)$) is present in the plant output. The results for the angular displacement from the fourth order observer system are presented in Figs. (4.2-9) and (4.2-10). Figs. (4.2-11) and (4.2-12) present the results for the angular velocity predicted by the fourth order observer model. Fig. (4.2-13) presents the results for the plant output (i.e., $y = q_4 + \beta$).

Figures (4.2-14) - (4.2-21) display the free response results from the fifth order observer system for the case when bias in the output is present. In the case of Figs. (4.2-14) and (4.2-15), the output contained a constant bias, while a linear bias was used to obtain the results shown in Figs. (4.2-16) and (4.2-17).

Figures (4.2-18) - (4.2-21) show the results from the fifth order observer system when the plant output contains a high frequency bias ($q_5 = 0.005 \cos(13t)$). Figs. (4.2-18) and (4.2-19) present results for the angular displacement predicted by the fifth order observer system. The angular velocity predicted by this system is shown in Figs. (4.2-20) and (4.2-21). The results for the plant output (i.e., $y = q_4 + q_5$) are presented in Fig. (4.2-13).

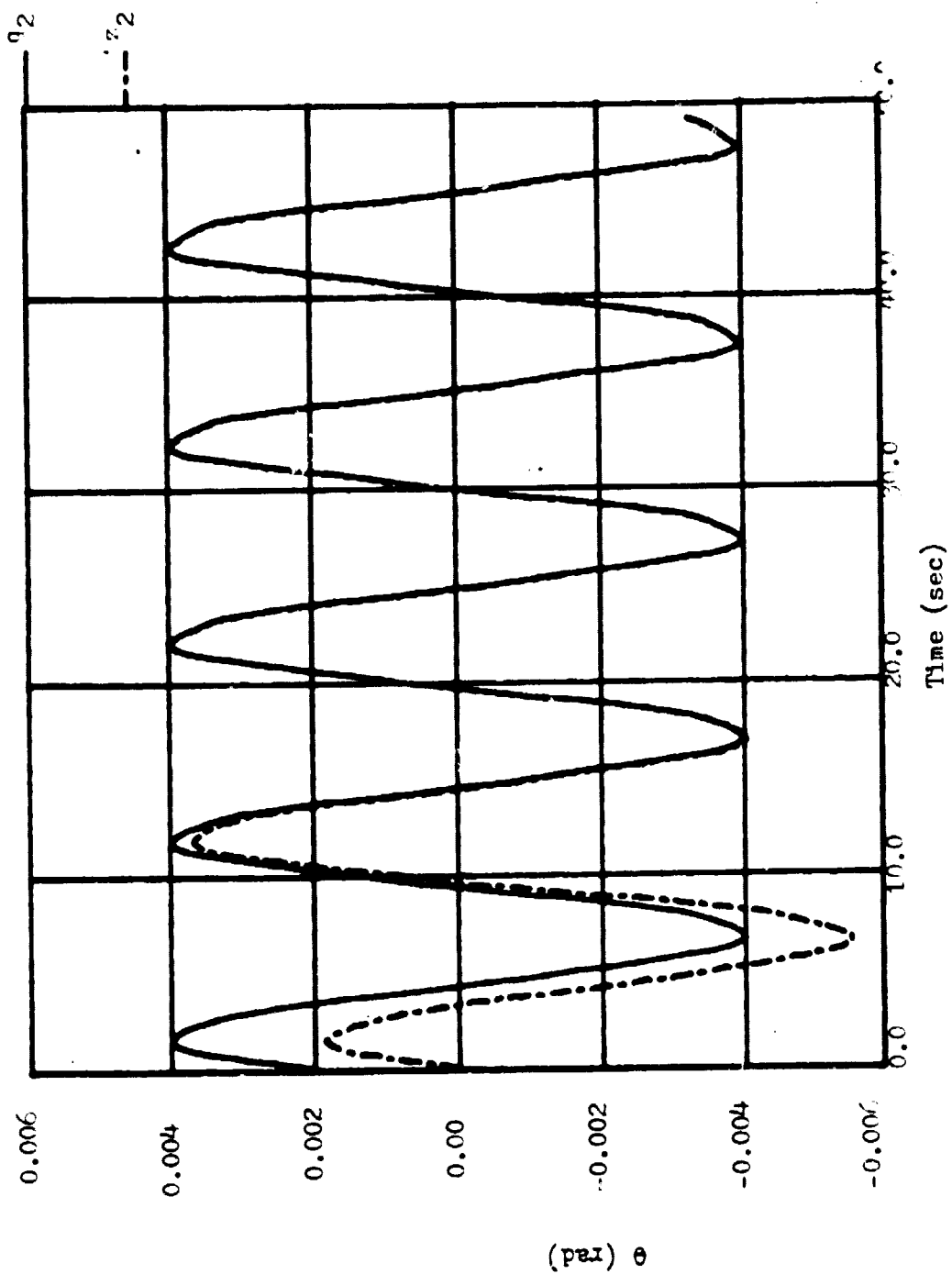


Fig.(4.2-1) Simulation Results For Angular Displacement
(4th Order Observer, $u=0$, $\lambda=-0.6$)

ORIGINAL PAGE IS
OF POOR QUALITY

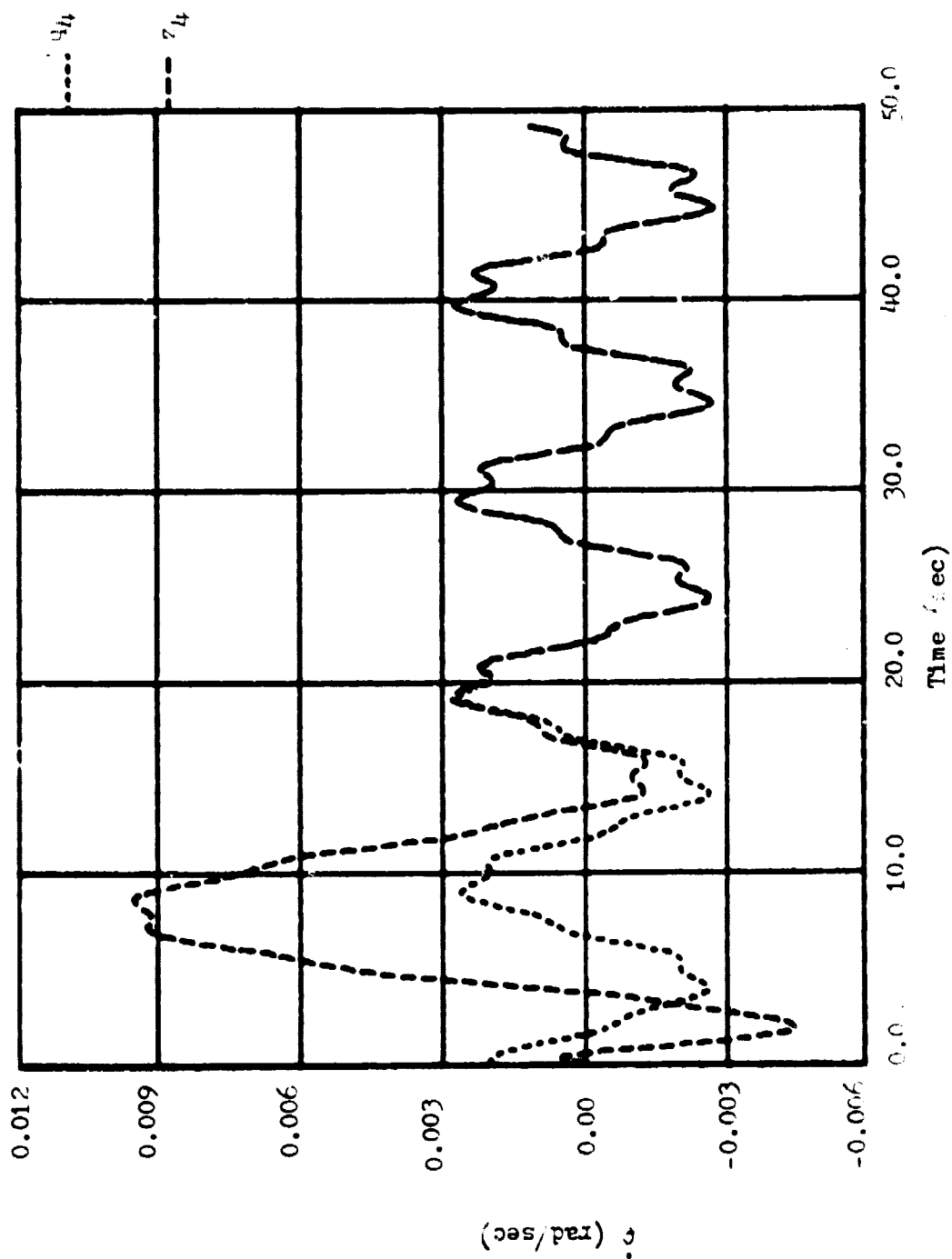


Fig.(4.2-2) Simulation Results For Angular Velocity
(4th Order Observer, $u=0.0$, $\lambda=-0.6$)

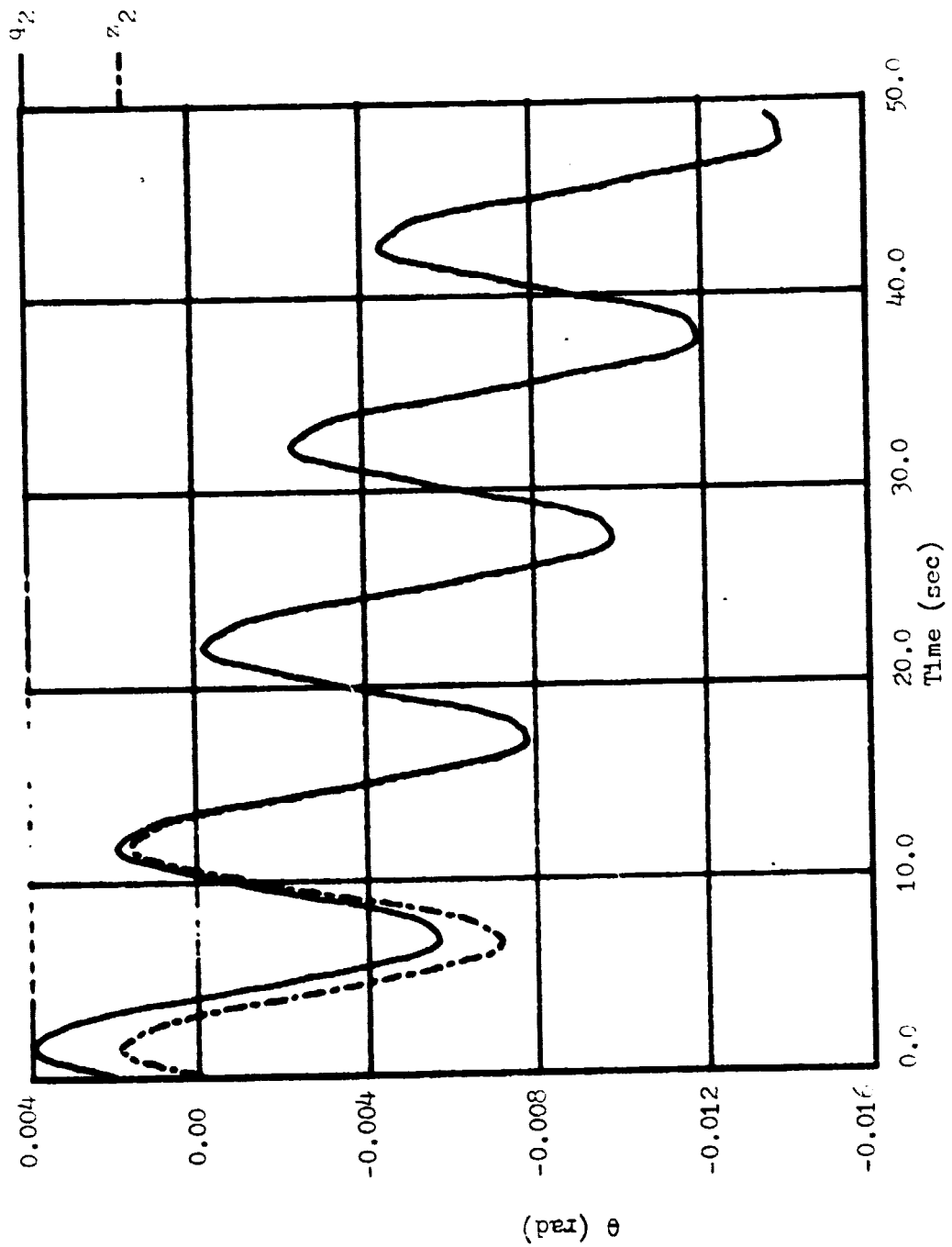


Fig.(4.2-3) Simulation Results For Angular Displacement
(4th Order Observer, $u=0.002t$, $\lambda=-0.6$)

ORIGINAL PAGE IS
OF POOR QUALITY

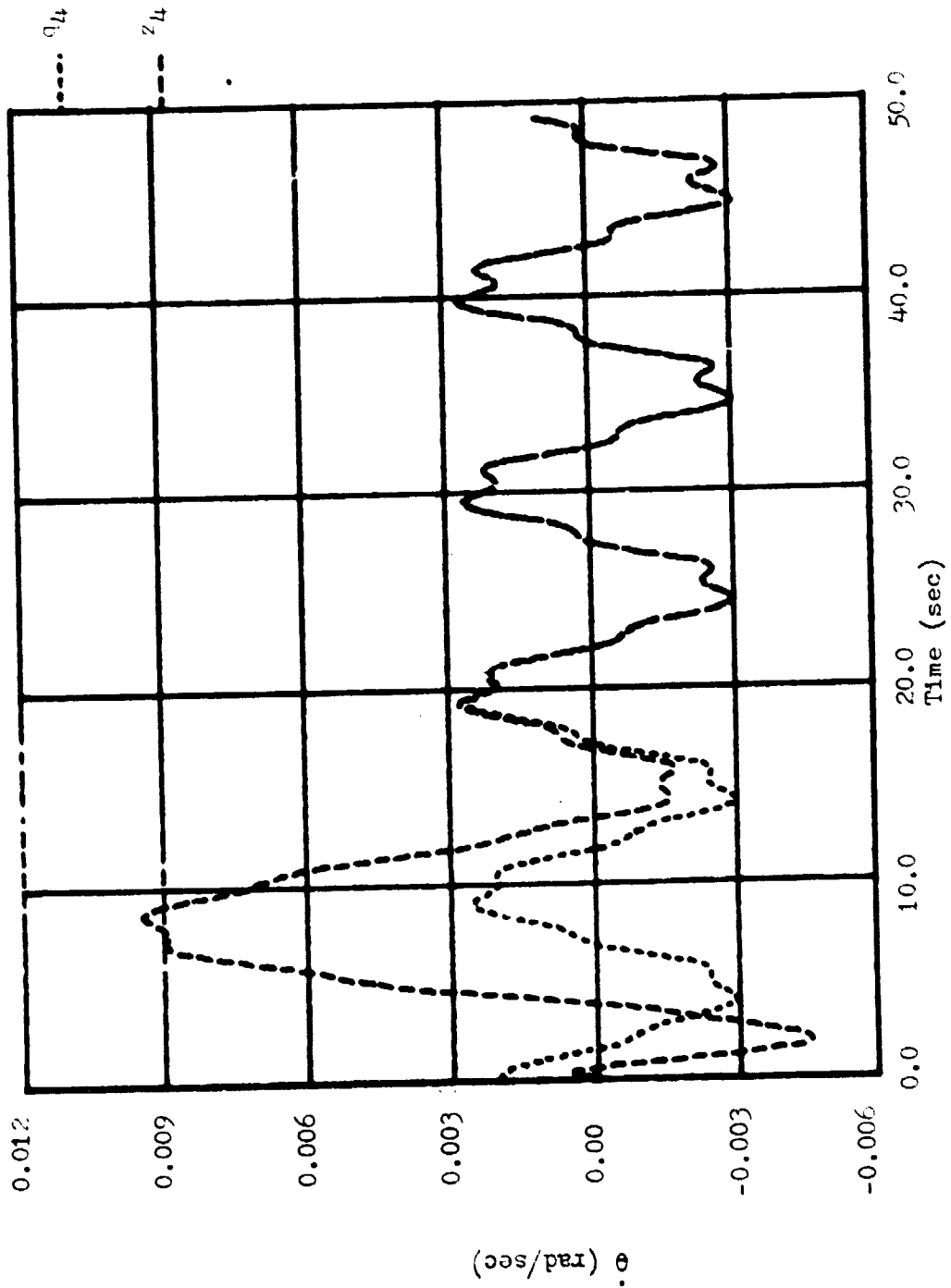


Fig.(4.2-4) Simulation Results For Angular Velocity
(4th Order Observer, $u=0.002t$, $\lambda=-0.6$)

ORIGINAL PAGE IS
OF POOR QUALITY

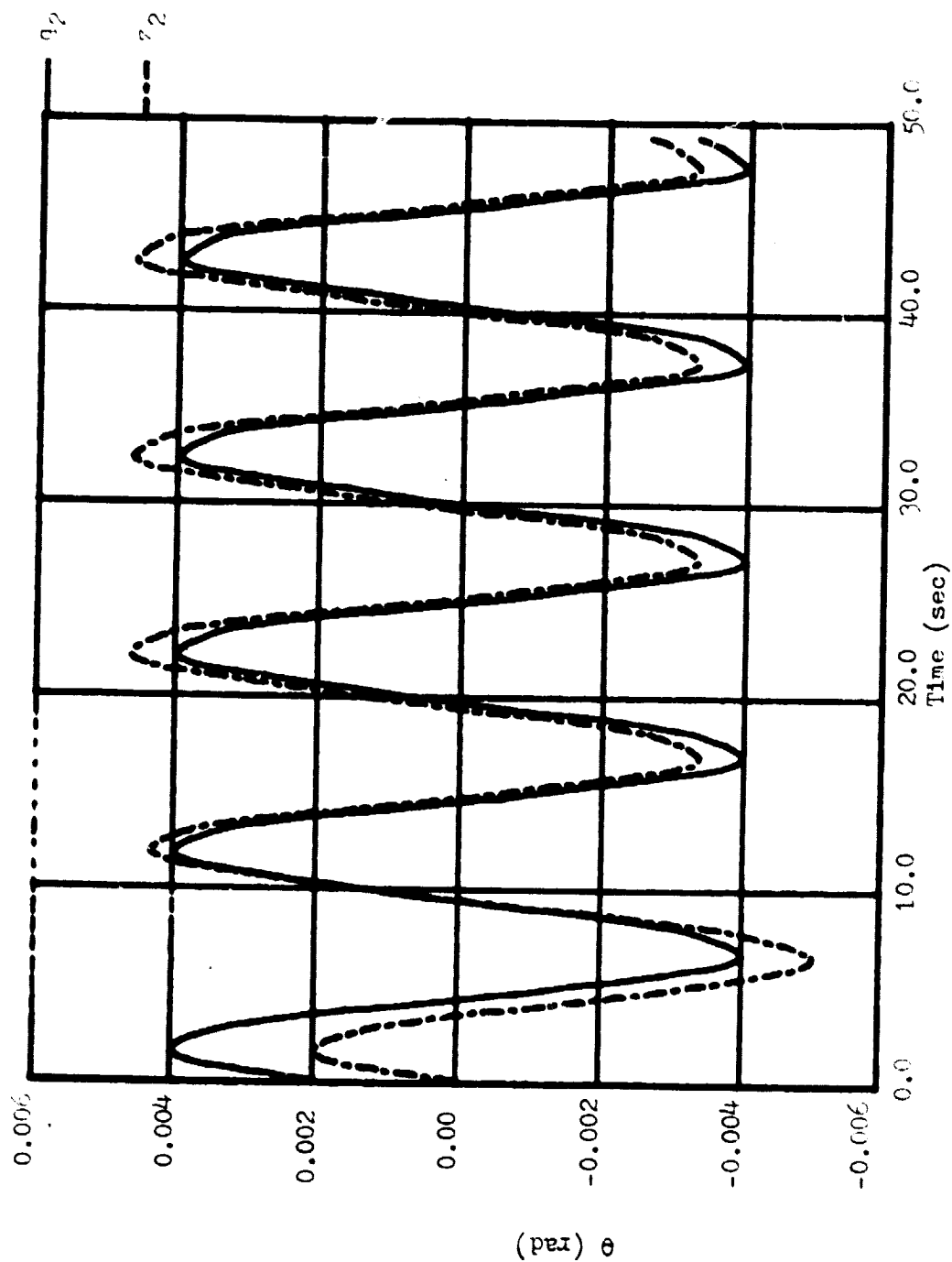


Fig.(4.2-5) Simulation Results For Angular Displacement
(4th Order Observer, $u=0$, $\lambda=-0.6$, $\text{bias}=1.0 \times 10^{-4}$)

ORIGINAL PAGE IS
OF POOR QUALITY

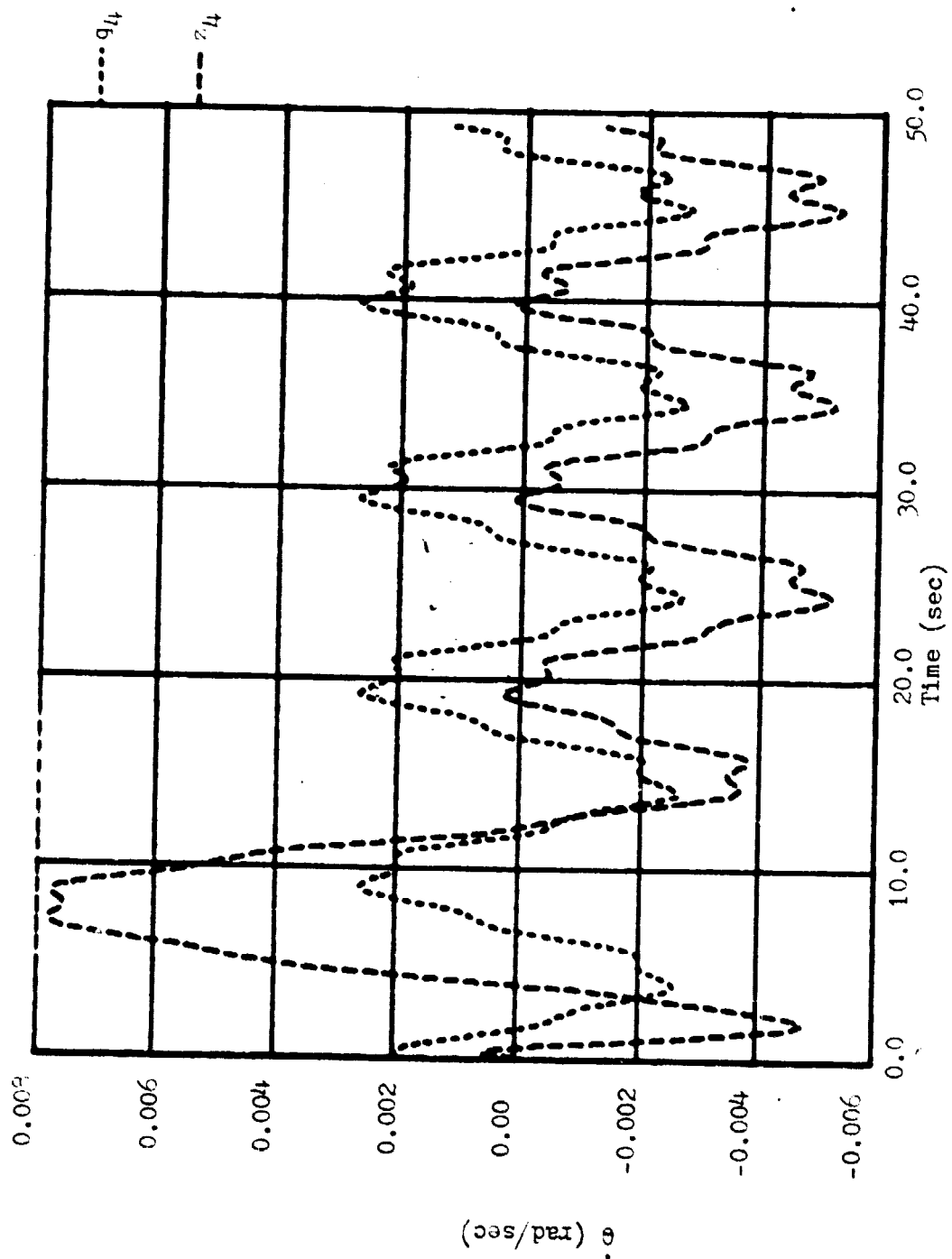


Fig.(4.2-6) Simulation Results For Angular Velocity
(4th Order Observer, $u=0$, $\lambda=-0.6$, Bias= 1.0×10^{-4})

ORIGINAL PAGE IS
OF POOR QUALITY

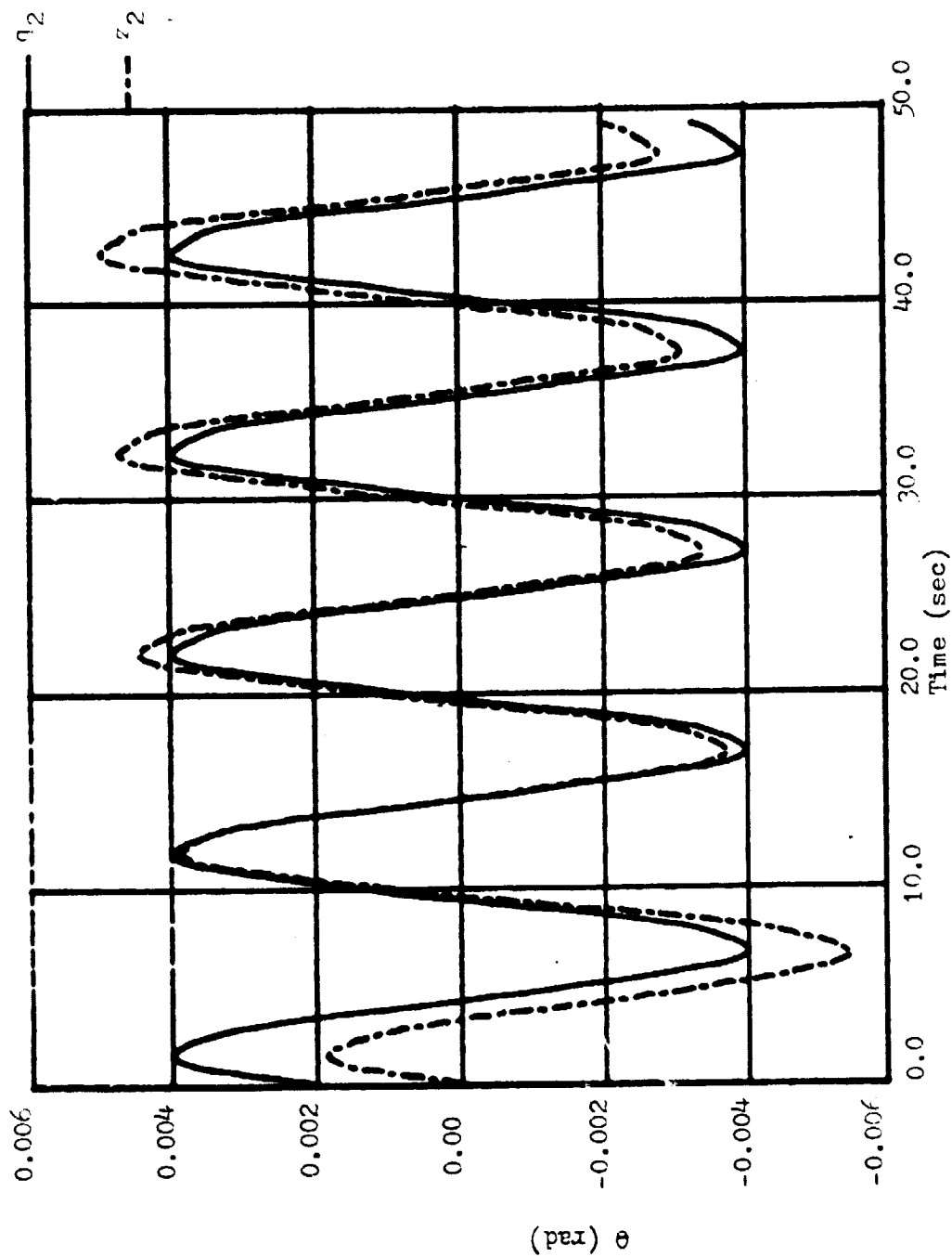


Fig.(4.2-7) Simulation Results For Angular Displacement
(4th Order Observer, $u=0$, $\lambda=-0.6$, $Bias=4.0 \times 10^{-6}$)

ORIGINAL PAGE IS
OF POOR QUALITY

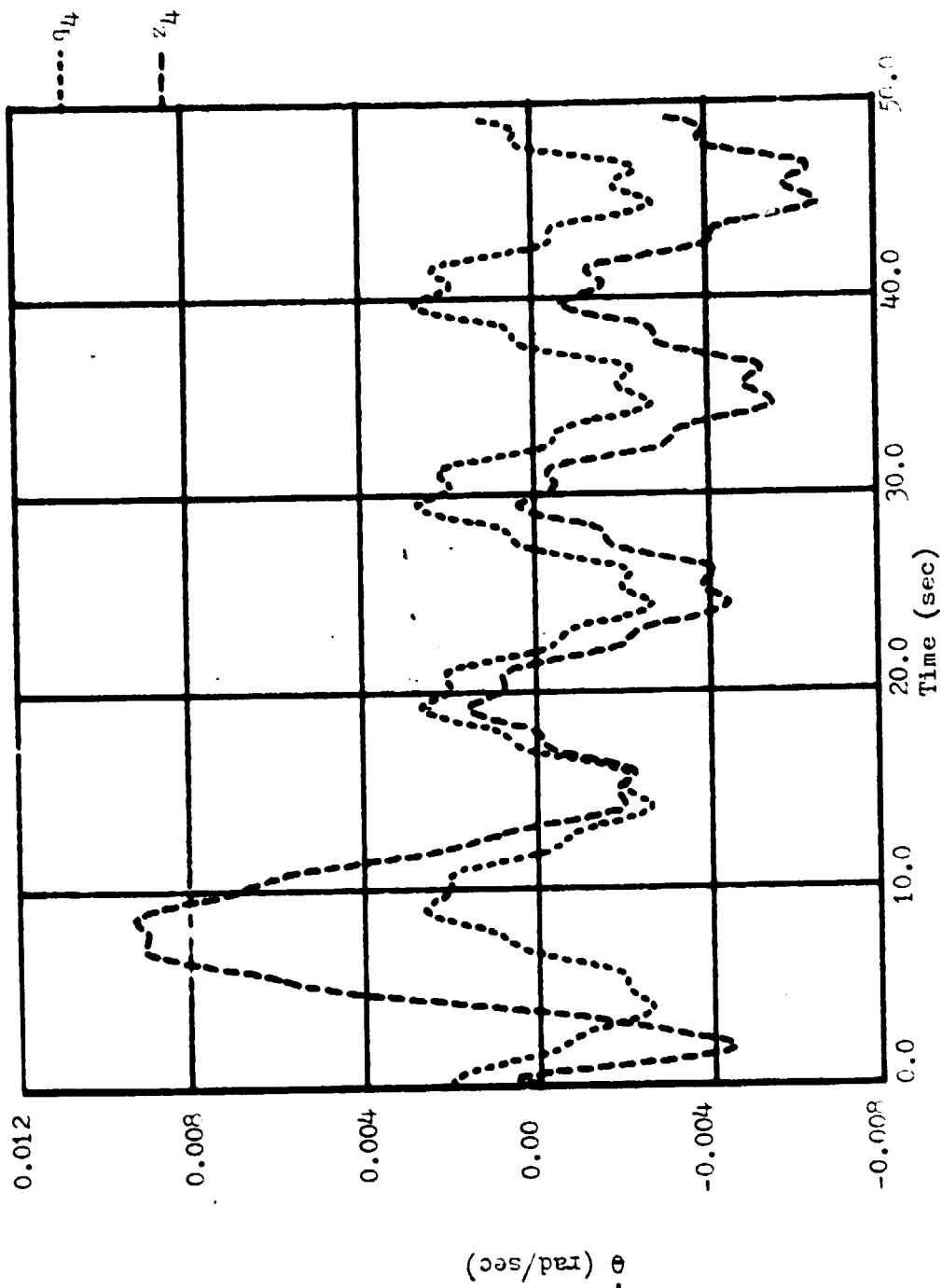


Fig. (4.2-8) Simulation Results For Angular Velocity
(4th Order Observer, $u=0$, $\lambda=-0.6$, Bias= $4.0 \times 10^{-6}t$)

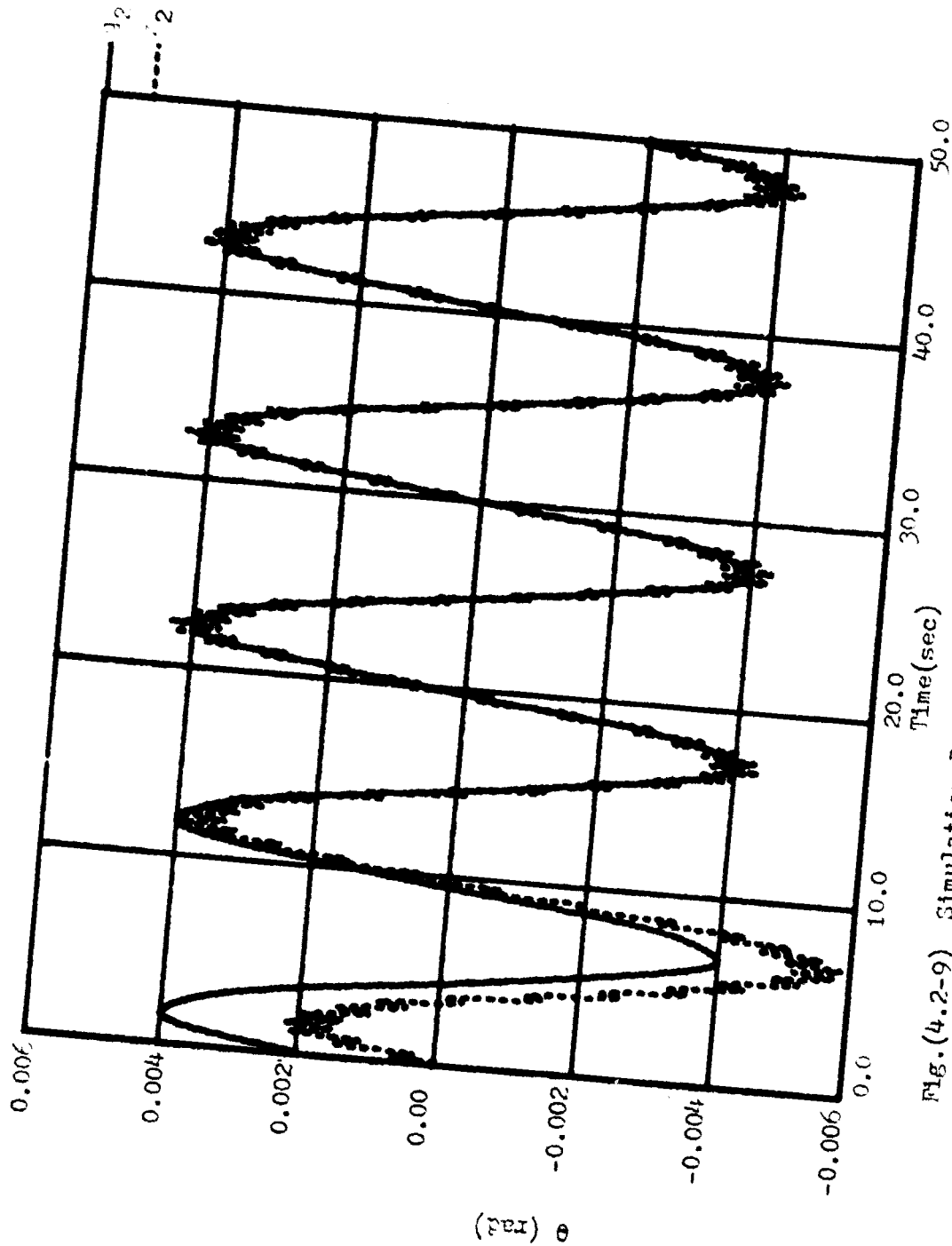


Fig.(4.2-9) Simulation Results For Angular Displacement
(4th Order Observer, $u=0$, $\lambda=-0.6$, Bias=0.005cos(13t))

ORIGINAL PAGE IS
OF POOR QUALITY

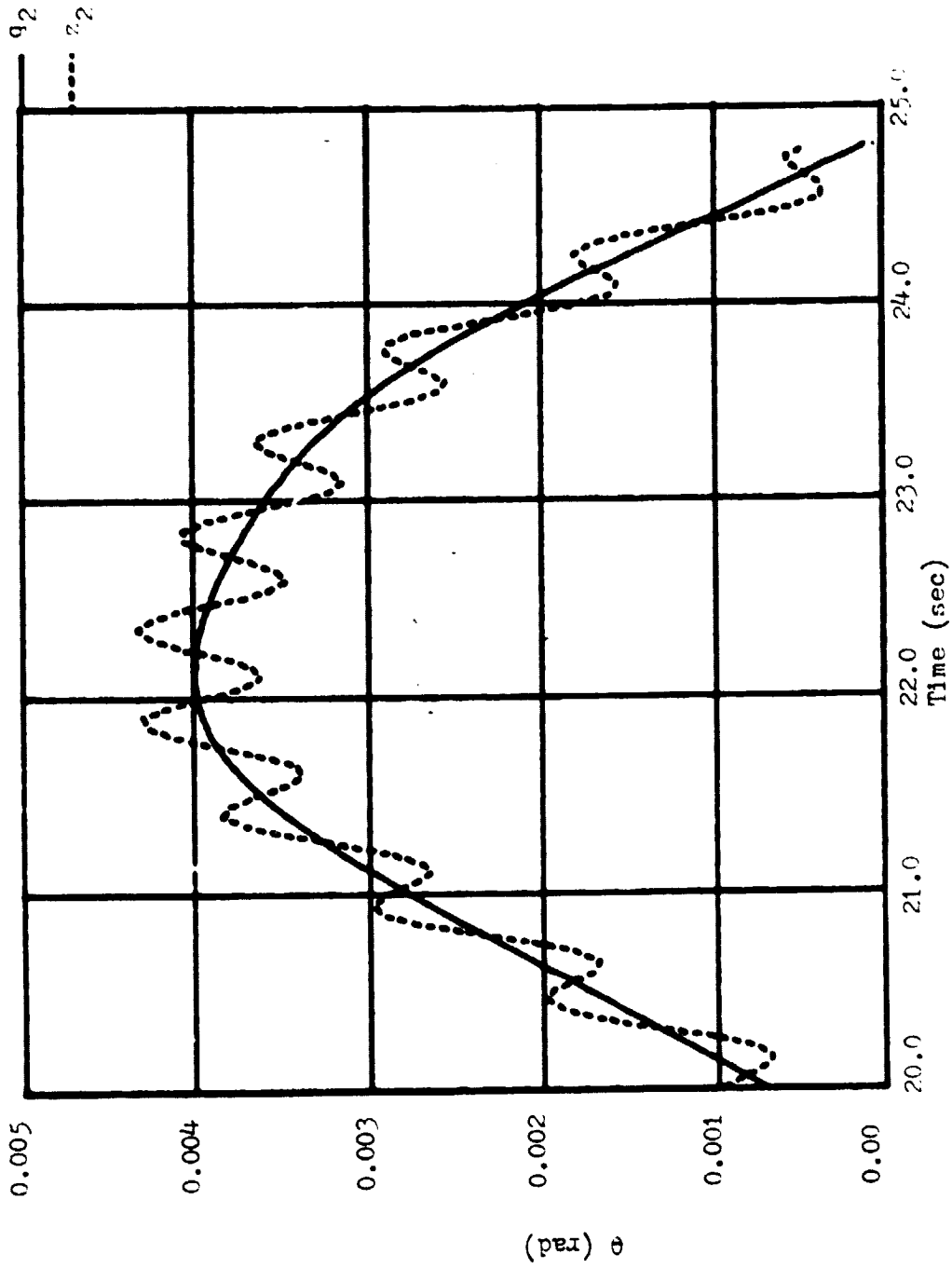


Fig. (4.2-10) Simulation Results For Angular Displacement
(4th Order Observer, $u=0$, $\lambda=-0.6$, $\text{Bias}=0.005\cos(13t)$)

ORIGINAL PAGE IS
OF POOR QUALITY

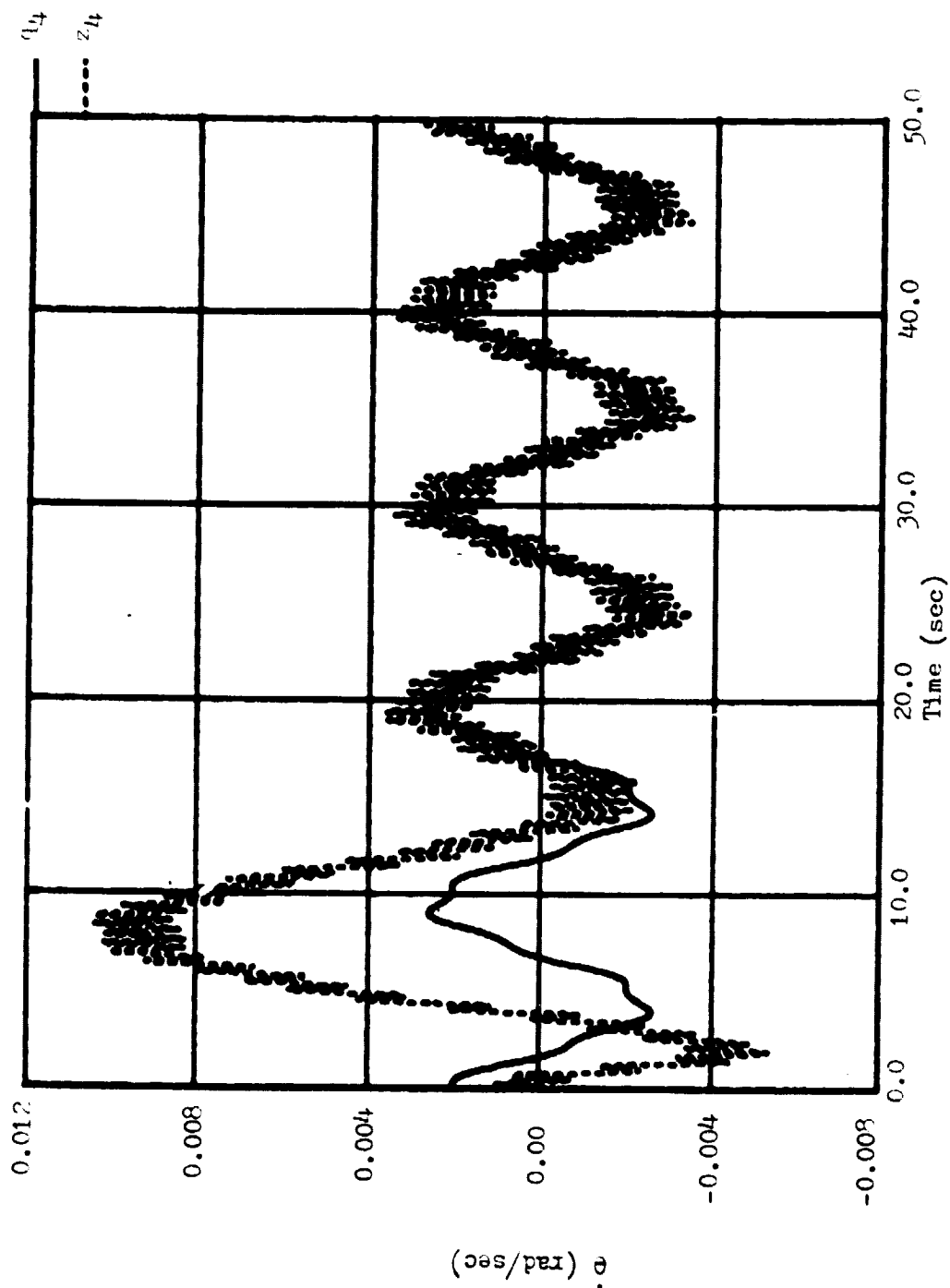


Fig.(4.2-11) Simulation Results For Angular Velocity

(4th Order Observer, $u=0$, $\lambda=-0.6$, $\text{Bias}=0.005\cos(13t)$)

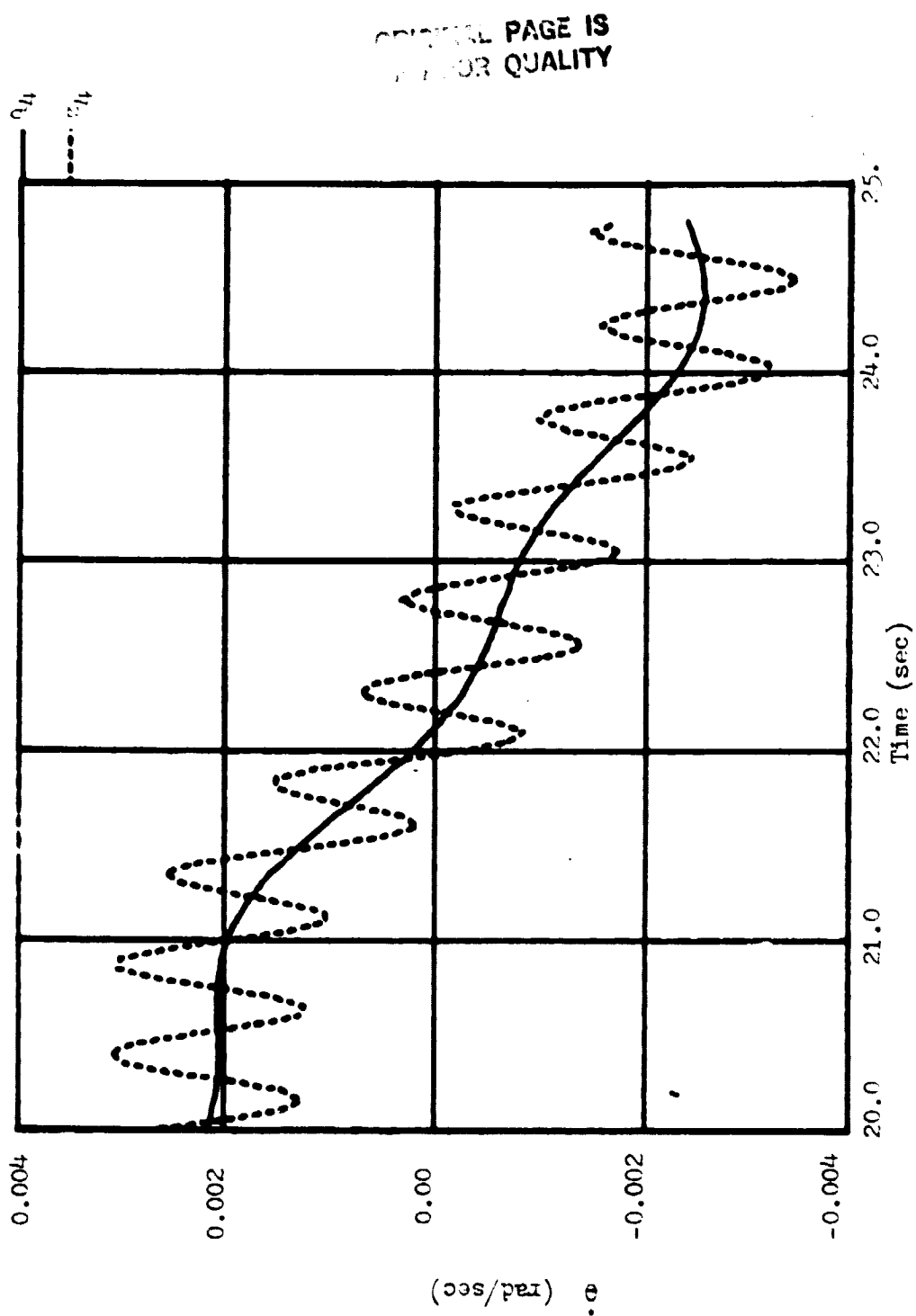


Fig. (4.2-12) Simulation Results For Angular Velocity

(4th Order Observer, $u=0$, $\lambda=-0.6$, Bias= $0.005\cos(13t)$)

ORIGINAL PAGE IS
OF POOR QUALITY

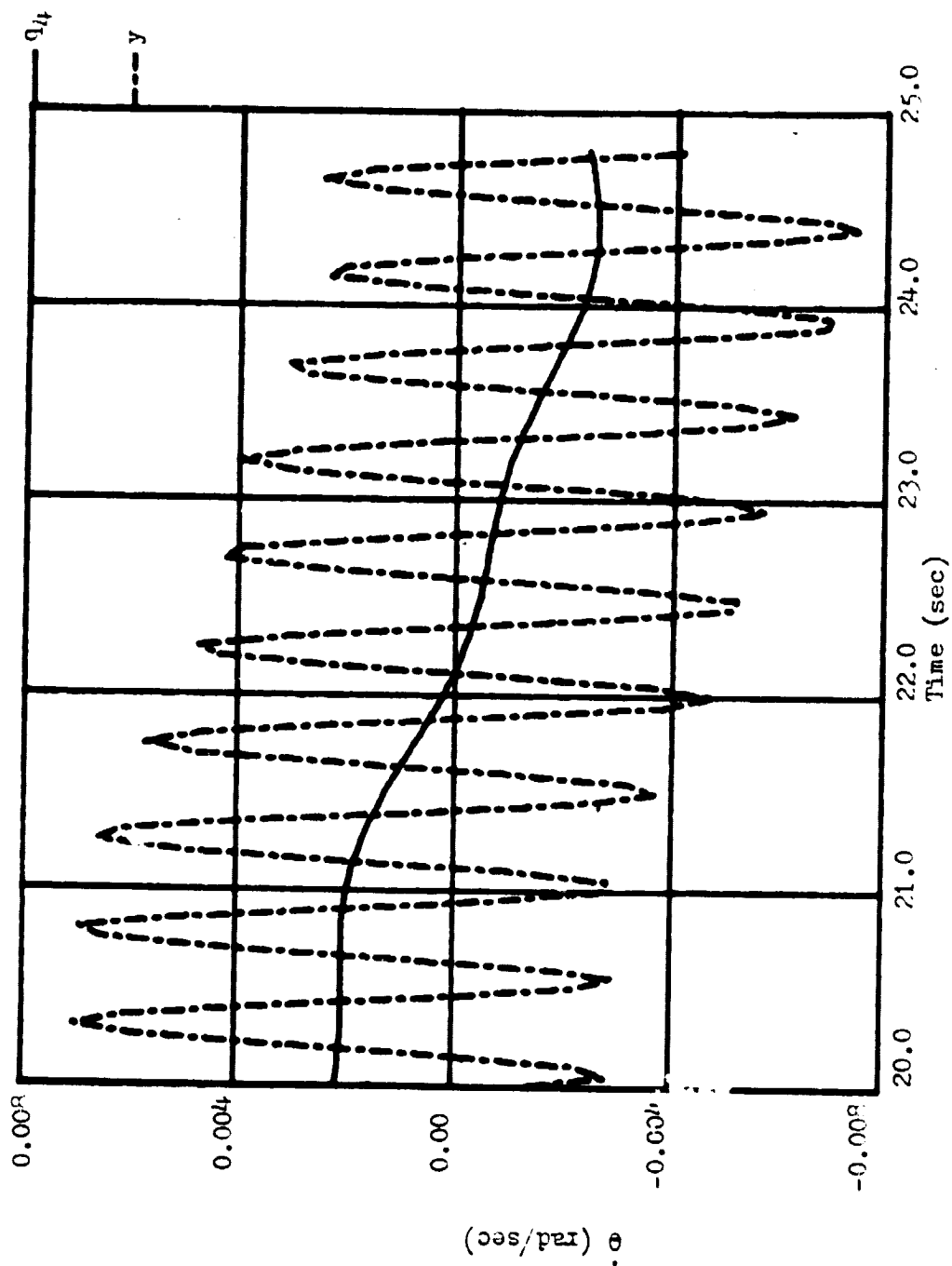


Fig.(4.2-13) Simulation Results For Output (Bias=0.005cos(13t))

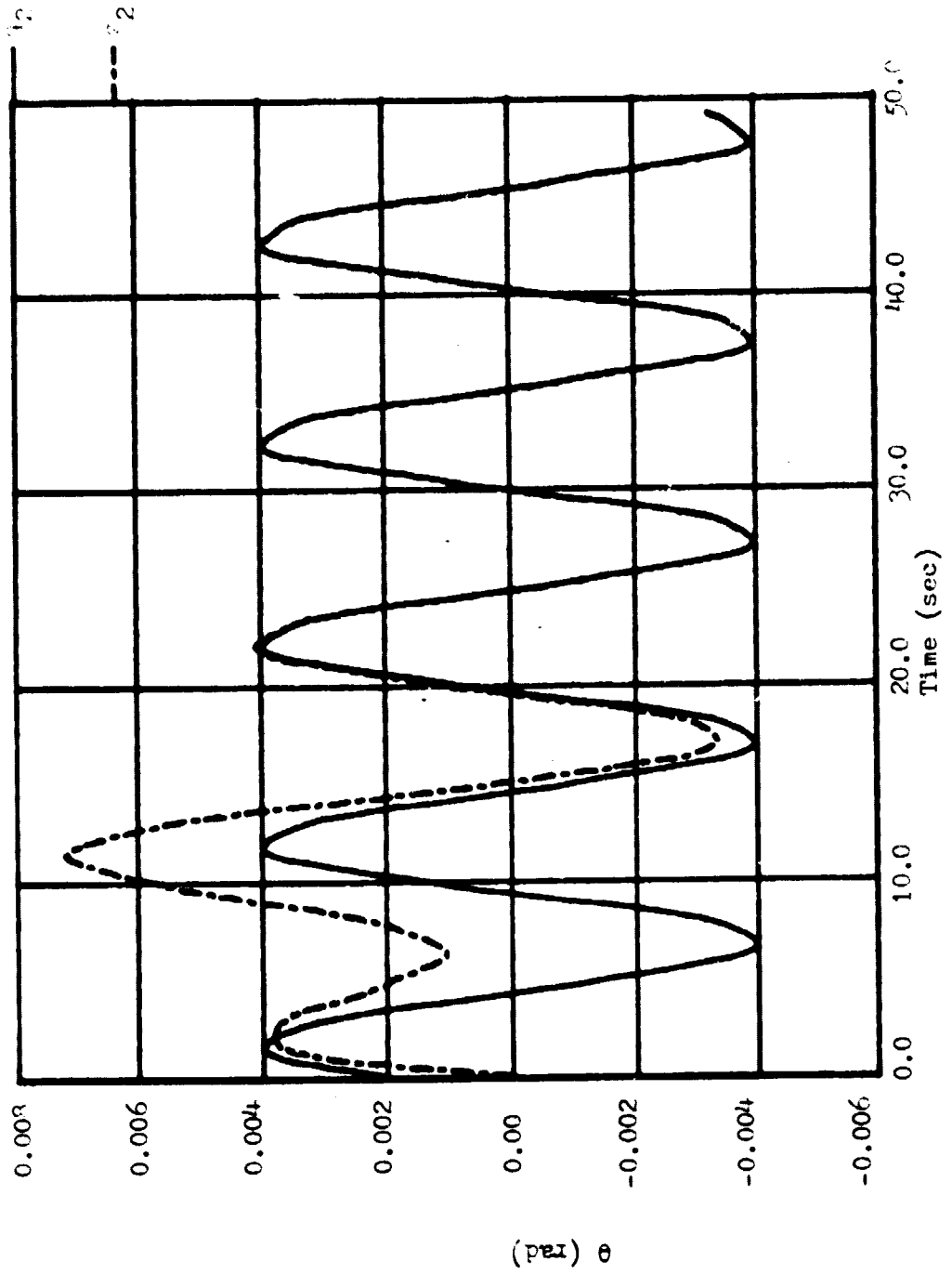


Fig. (4.2-14) Simulation Results For Angular Displacement
(5th Order Observer, $u=0$, $\lambda=-0.6$, Bias=0.002)

ORIGINAL PAGE IS
OF POOR QUALITY

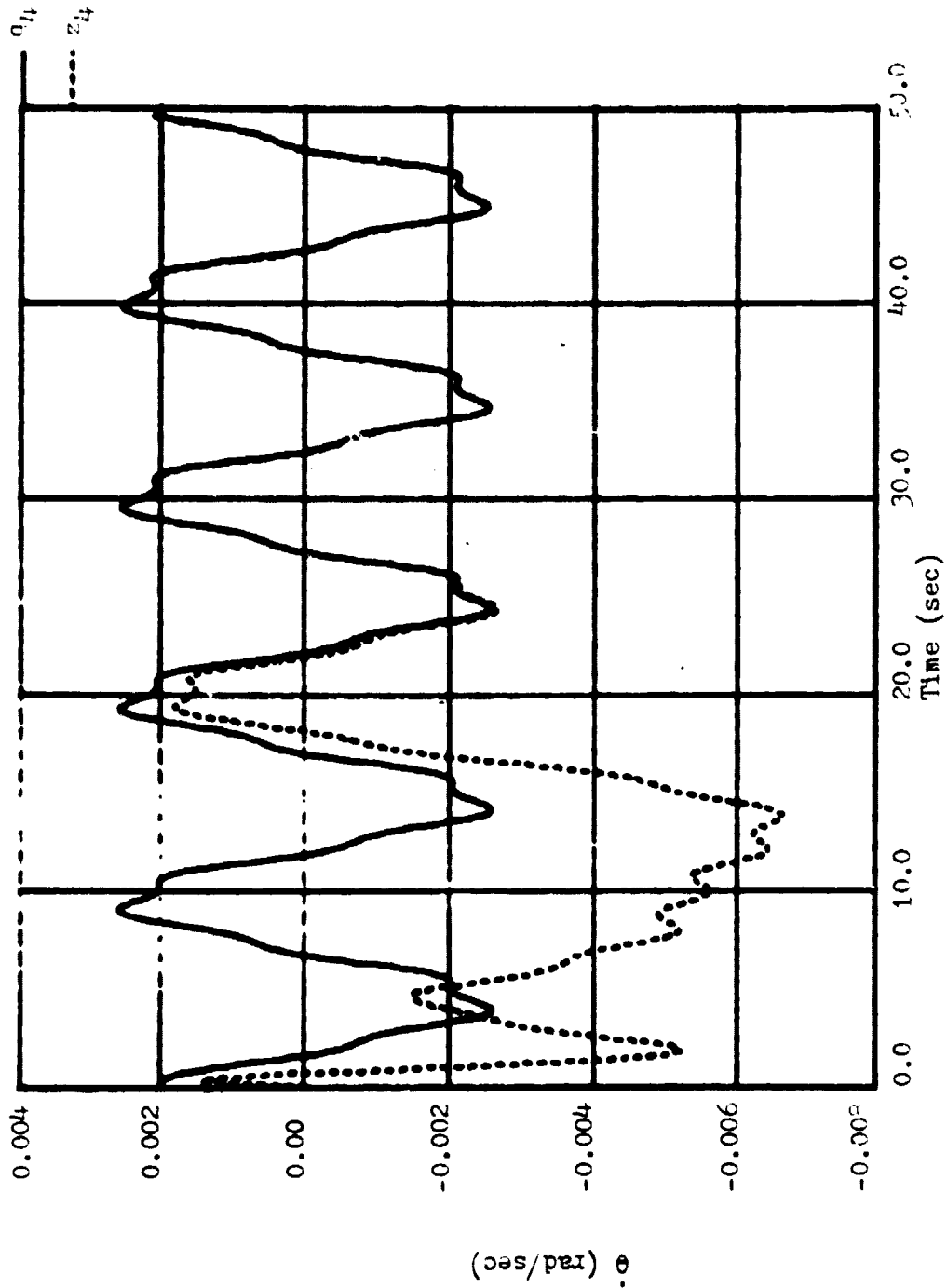


Fig. (4.2-15) Simulation Results For Angular Velocity

(5th Order Observer, $u=0$, $\lambda=-0.6$, Bias=0.002)

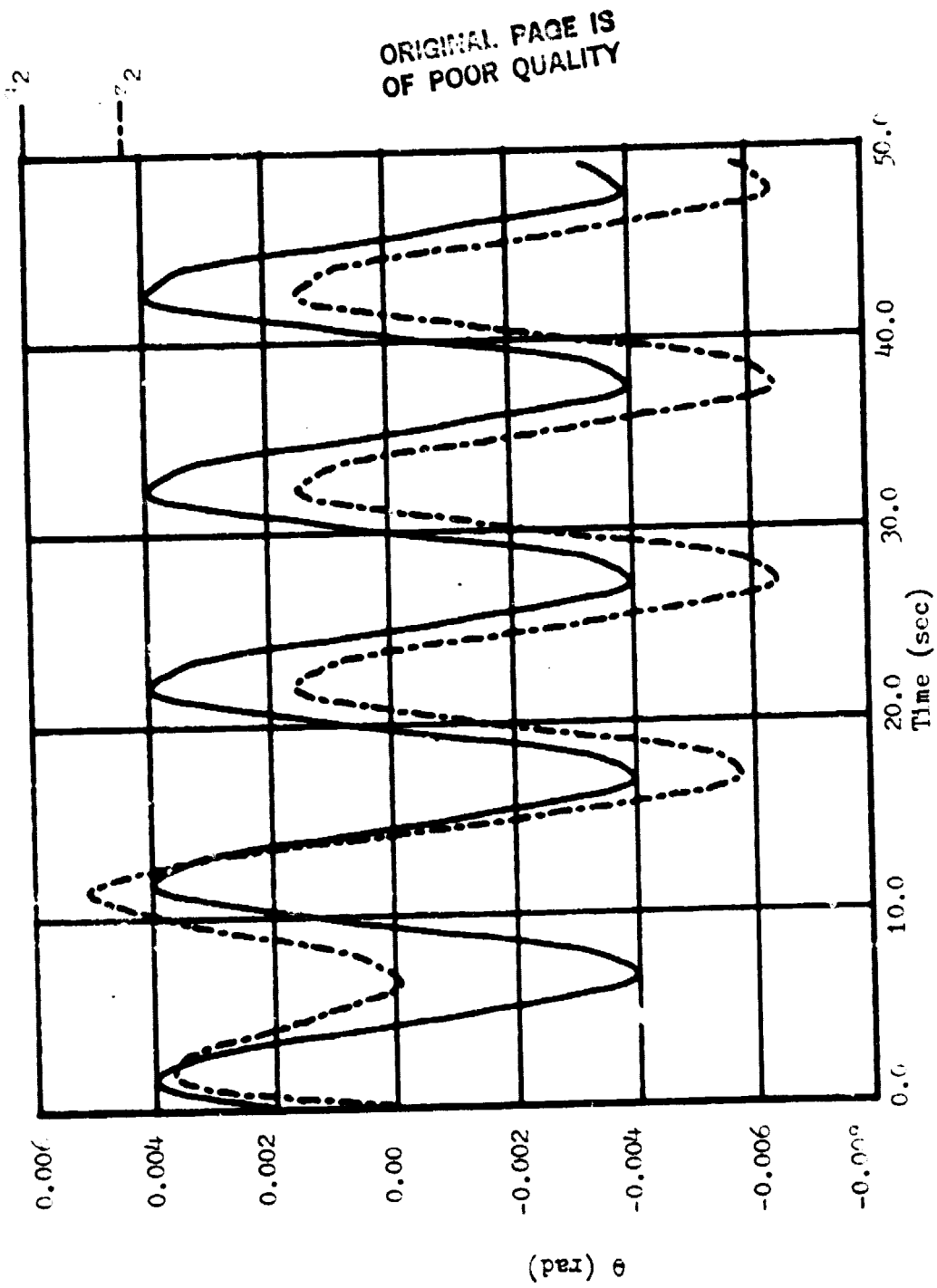


Fig. (4.2-16) Simulation Results For Angular Displacement
(5th Order Observer, $u=0$, $\lambda=-0.6$, Bias= $-1.0 \times 10^{-4}t + 0.002$)

ORIGINAL PAGE IS
OF POOR QUALITY

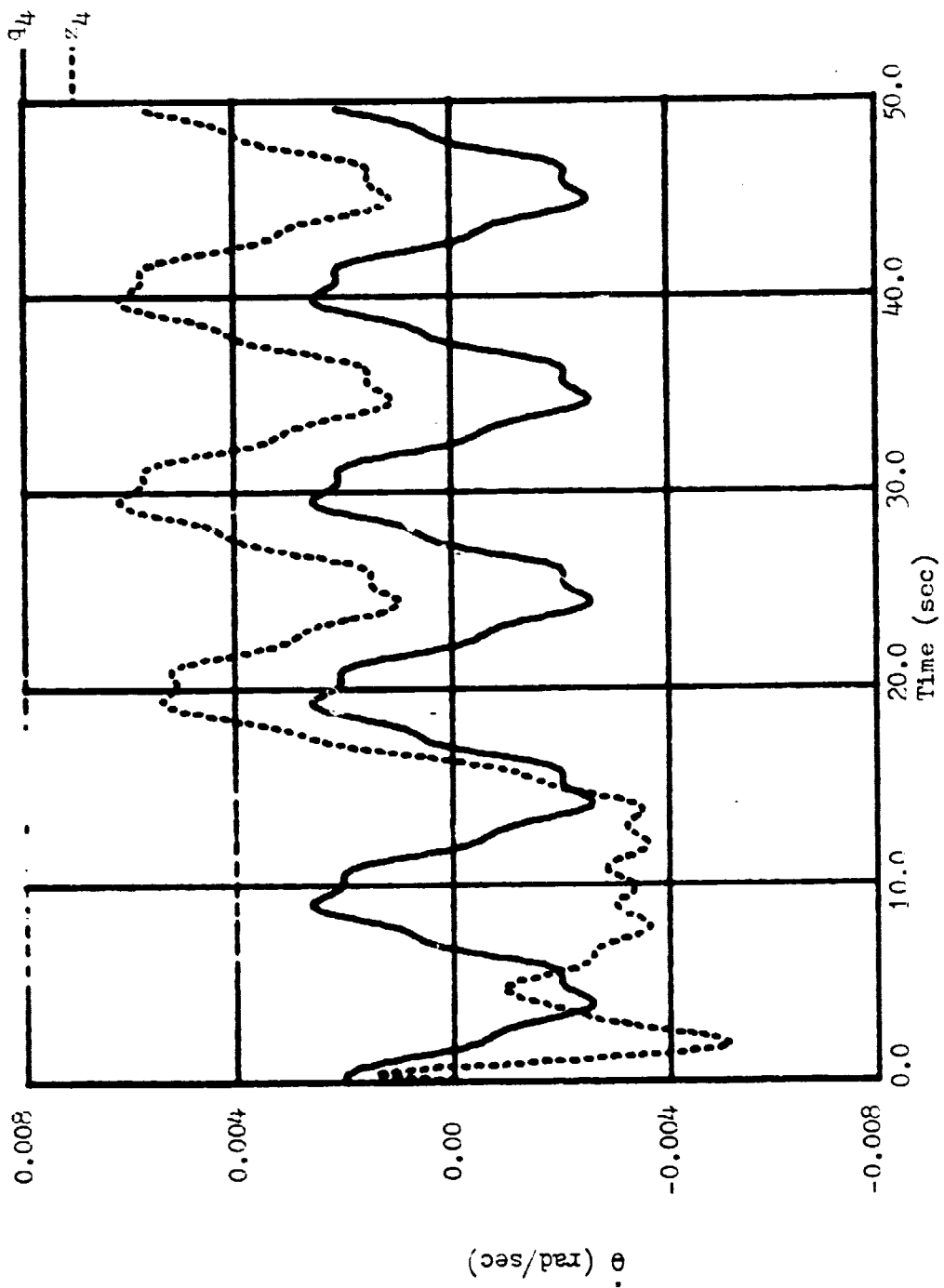


Fig. (4.2-17) Simulation Results For Angular Velocity
(5th Order Observer, $u=0$, $\lambda=-0.6$, Bias= $-1.0 \times 10^{-4}t + 0.002$)

ORIGINAL PAGE IS
OF POOR QUALITY

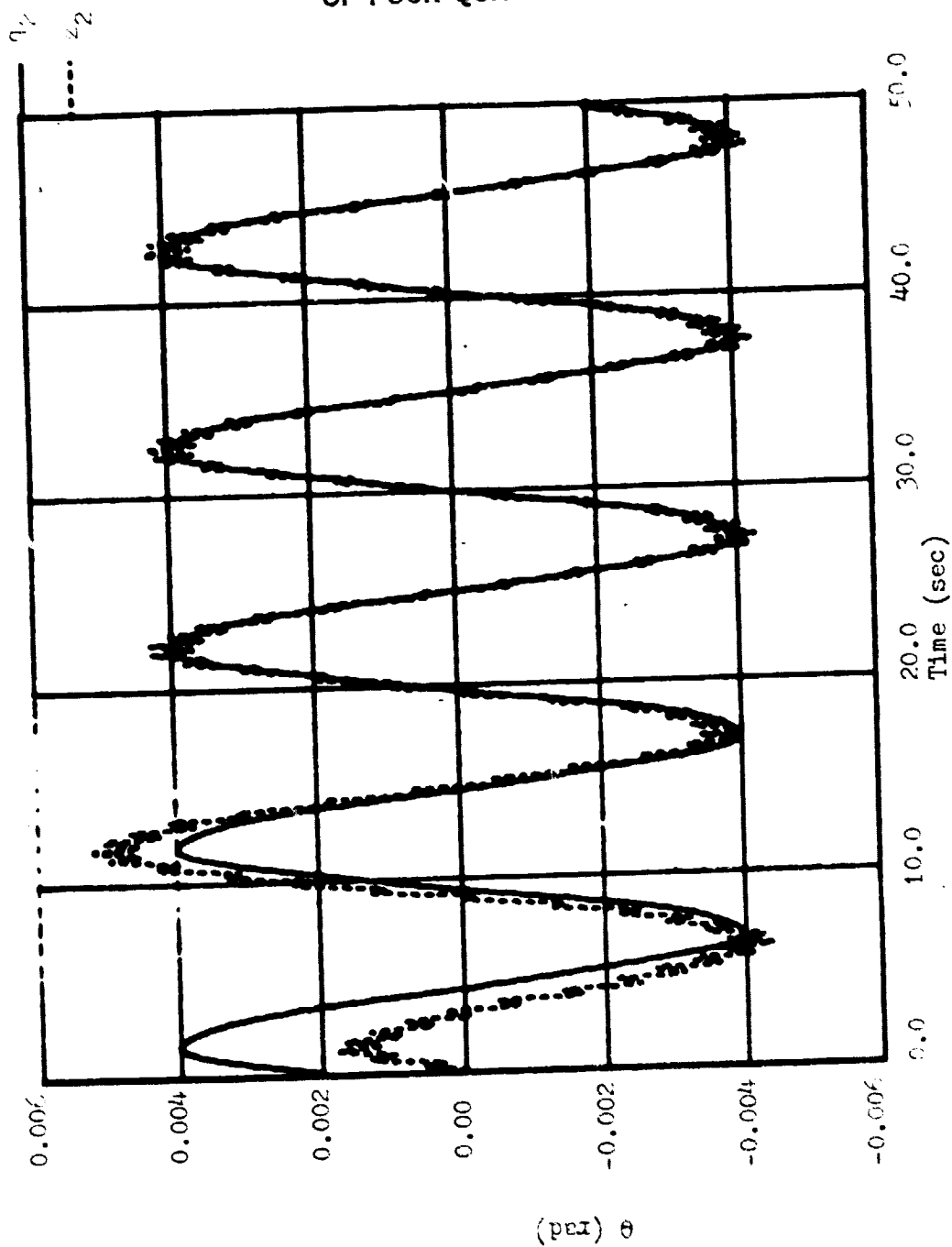


Fig. (4.2-18) Simulation Results For Angular Displacement
(5th Order Observer, $u=0$, $\lambda=-0.6$, Bias=0.005cos(13t))

ORIGINAL PAGE IS
OF POOR QUALITY

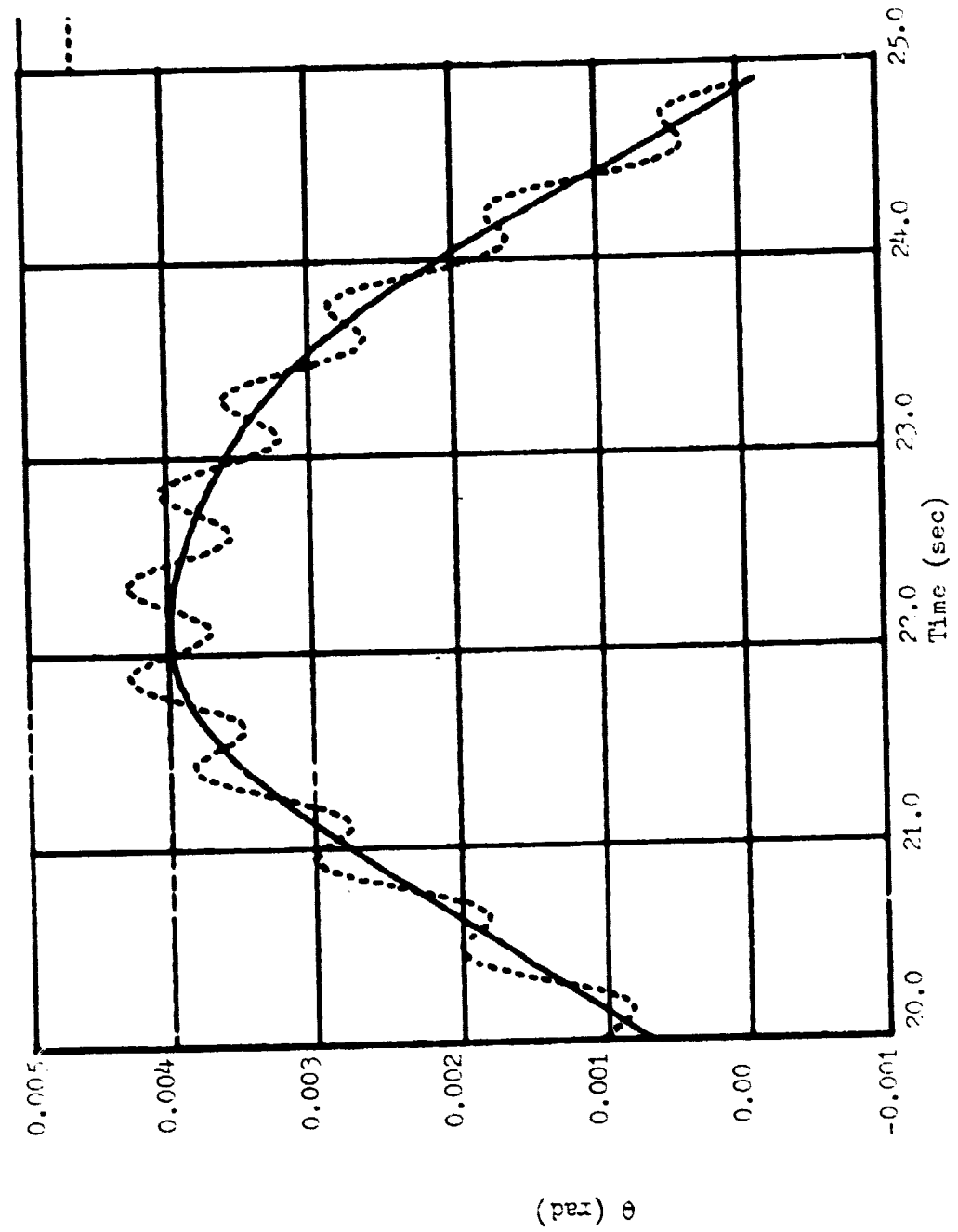


Fig. (4.2-19) Simulation Results For Angular Displacement
(5th Order Observer, $u=0$, $\lambda=-0.6$, Bias=0.005cos(13t))

ORIGINAL PAGE IS
OF POOR QUALITY

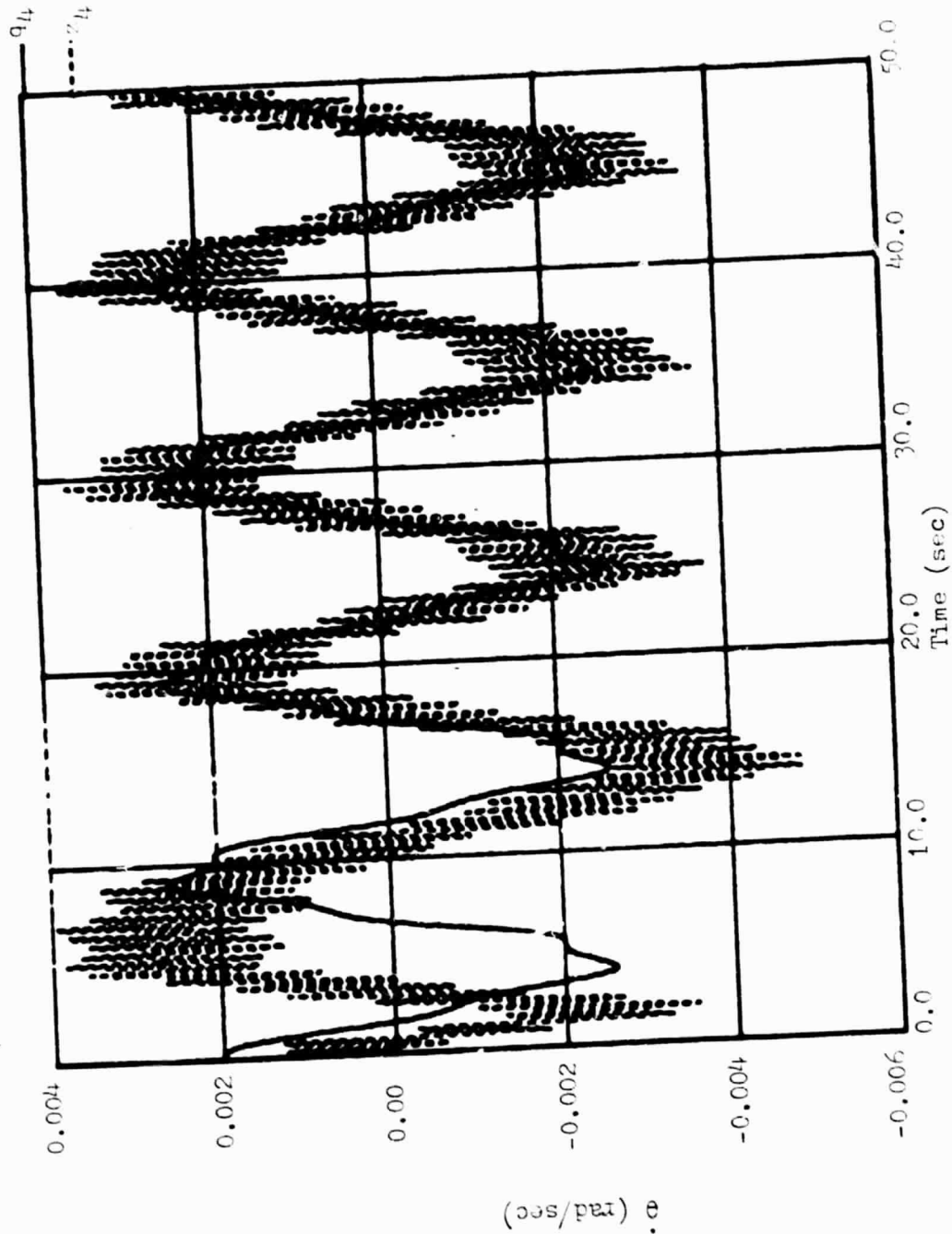


Fig. (4.2-20) Simulation Results For Angular Velocity
(5th Order Observer, $u=0$, $\lambda=-0.6$, Bias=0.005cos(13t))

ORIGINAL PAGE IS
OF POOR QUALITY

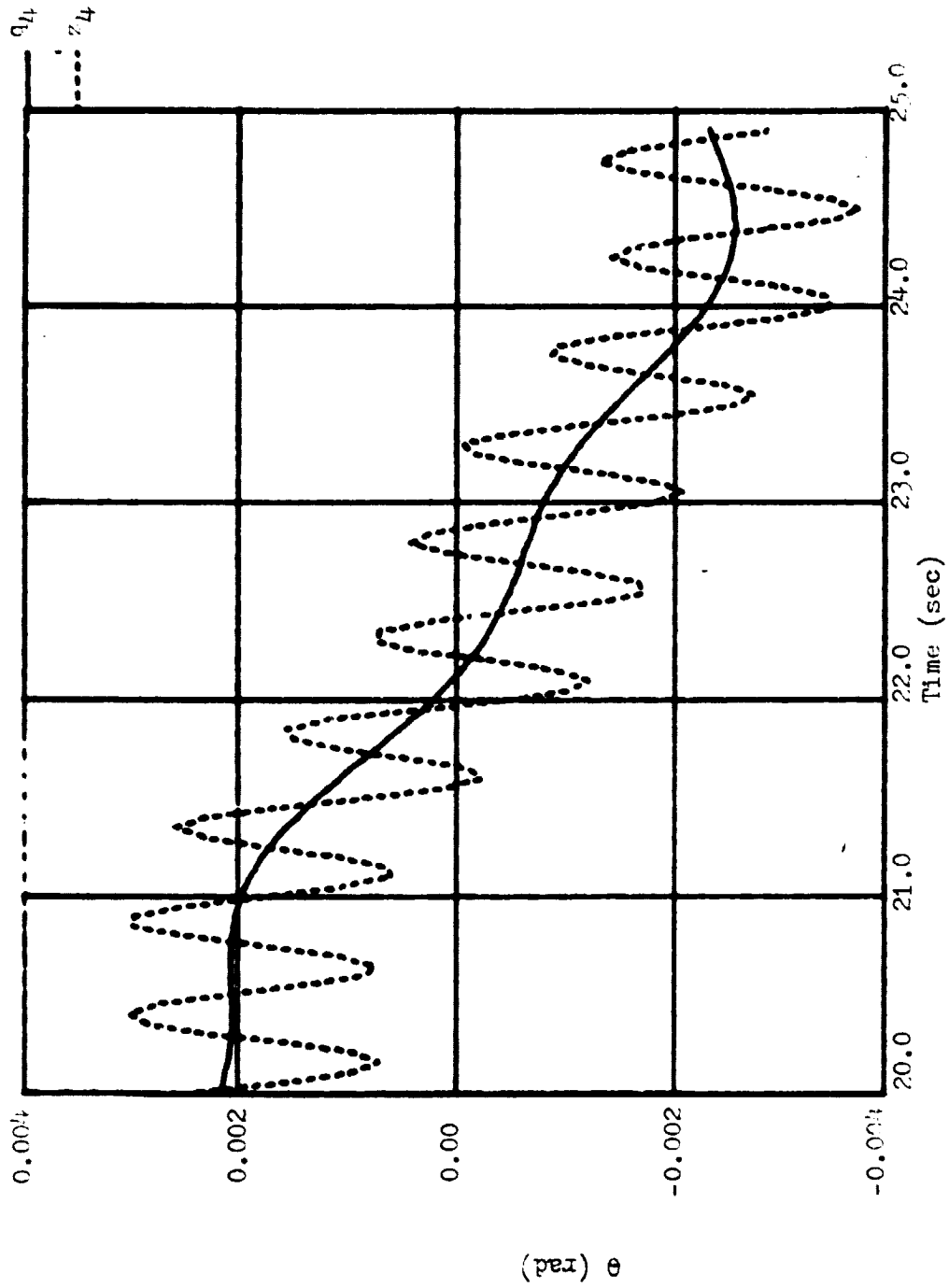


Fig.(4.2-21) Simulation Results For Angular Velocity
(5th Order Observer, $u=0$, $\lambda=-0.6$, Bias=0.005cos(13t))

4.3 Discussion of Simulation Study Results

The results in Figs. (4.2-1)-(4.2-4) verify that, after a finite time interval, the fourth order observer system will reconstruct the plant state exactly if all plant inputs and outputs are known. The use of repeated eigenvalues (i.e., $\lambda_1 = -0.6$) resulted in an error free response after a period of 20 seconds.

The fourth order observer results in Figs. (4.2-5)-(4.2-13) were obtained for the case when the plant output contained a bias ($\beta(t)$). From Figs. (4.2-5)-(4.2-13), it is seen that the reconstructed states contained an error resulting from the bias present in the plant output.

Two methods can be used to determine the steady state error in this reconstructed state due to output bias:

1. Revise Eq. (3.4-3) to include the error due to bias and then solve this equation.
2. Compare the results for the reconstructed state to the actual state directly by employing the curves in Figs. (4.2-5)-(4.2-13).

For purposes of this work the latter method will be employed.

For comparing the reconstructed state to the actual state, a relative error, $ER_i(t_j)$ will be used. This is defined as follows; i.e.,

$$ER_i(t_j) = \left| \frac{EA_i(t_j)}{q_i(t_j)} \right|, \quad (4.3-1)$$

where

$EA_i(t_j)$ = magnitude of the error in the state q_i at $t = t_j$, and
 $q_i(t_j)$ = maximum value of the actual state variable at $t = t_j$.

The curves in Figs. (4.2-5) and (4.2-6) indicate that the error in the reconstructed state is a constant when the plant output contains a constant bias (i.e., $\beta = 0.001$). In particular, for this case, a 5%

relative error (ER_y) in the output resulted in errors (ER_2 and ER_4) of 17% and 100% in θ_2 and $\dot{\theta}_2$ respectively.

When a linear bias (i.e., $\beta = 4.0 \times 10^{-6}t$) is present in the plant output, a linear error resulted in the reconstructed state (see Figs. (4.2-7) and (4.2-8)). At $t = 43s$, $ER_y = 6\%$, $ER_2 = 23\%$ and $ER_4 = 133\%$.

The results shown in Figs. (4.2-9)-(4.2-13) indicate that when the plant output contained a high frequency bias (i.e., $\beta = 0.005 \cos(13t)$), the angular displacement (θ) and the angular velocity ($\dot{\theta}$) predicted by the fourth order observer contained a sinusoidal error. The error in the reconstructed state at peak amplitudes are $ER_y = 167\%$, $ER_2 = 9\%$ and $ER_4 = 33\%$.

The results obtained from the fifth order observer are shown in Figs. (4.2-14)-(4.4-21). Figs. (4.2-14)-(4.2-16) indicate that, for the case when the plant output contains a constant bias, the actual state will be reconstructed exactly after a finite interval of time.

Figs. (4.2-16) and (4.2-17) show that when the plant output contained a linear bias (i.e., $\beta = -1 \times 10^{-4}t$), a constant error resulted in the reconstructed state. At $t = 43s$, the resulting errors are given as follows; i.e., $ER_y = 153\%$, $ER_2 = 64\%$ and $ER_4 = 100\%$.

Figs. (4.2-18)-(4.2-21) show that when the plant output contains a high frequency bias (i.e., $\beta = 0.005 \cos(13t)$) the state predicted by the fifth order observer contains a sinusoidal error. The errors in the reconstructed state at peak amplitudes are $ER_y = 167\%$, $ER_2 = 6\%$ and $ER_4 = 35\%$.

In general, the results of the simulation study show that the form of the error in the reconstructed state will depend both on the order of the observer model and the type of bias (i.e., constant, linear, etc.)

present in the plant output. When an n th order bias is present in the plant output, the fifth order observer will yield a more accurate response than the fourth order observer. For this case, the error in the fifth order observer will be of order $n-1$, while the error in the fourth order observer will be of order n .

For a specific form of bias, the magnitude of the errors in the reconstructed state will depend on the elements of the F and G matrices. For the particular case when $\lambda_1 = -0.6$, the magnitude of error in the reconstructed state Z_2 was much smaller than that in Z_4 . Moreover, for the case when the bias was of a sinusoidal nature ($\beta = 0.005 \cos(13t)$), the error in the reconstructed state Z_2 was less for the fifth order observer model; however, a more accurate response was obtained in state Z_4 for the fourth order observer.

4.4 Observer Results for Determining Orientation of Balloon Platform

The fourth and fifth order observer system models were employed to determine the orientation (θ_2) of the balloon platform in the X_2X_3 plane for the time interval $t = 0s$ (initial LACATE data recording time) to $t = 500s$. The observer transient error was assumed to decay to zero after an elapsed time period of 250s. At this time the initial condition for integrating the gyroscope was set equal to the angular displacement (Z_2) predicted by the observer. Fig. (4.4-1) illustrates the output (y) obtained from the gyroscope with sensing axis along the e_1''' body axis.

Figs. (4.4-2)-(4.4-5) give the angular velocity (Z_4) and angular displacement (Z_2) predicted by the fourth order observer model for the case when $\lambda_1 = -0.5$. The free response case is illustrated in Figs. (4.4-2) and (4.4-3), while Figs. (4.4-4) and (4.4-5) give the response when the wind acceleration is included.

Figs. (4.4-6)-(4.4-13) illustrate the free response of the fifth order observer system with $\lambda_1 = -0.2$ and -0.5 respectively. Figs. (4.4-6) and (4.4-10) present the results for the angular velocity while Figs. (4.4-7), (4.4-8), (4.4-11), and (4.4-12) present the results for the angular displacement. Figs. (4.4-9) and (4.4-13) contain the results for predicted bias (Z_5).

Figs. (4.4-14)-(4.4-25) present the fifth order observers response with wind acceleration for the case when $\lambda_1 = -0.2, -0.5$, and -0.7 respectively. Figs. (4.4-14), (4.4-18), and (4.4-22) present the results for the angular velocity while Figs. (4.4-15), (4.4-16), (4.4-19), (4.4-20), (4.4-23) and (4.4-24) present the angular displacement. The bias predicted from the fifth order observer for the respective cases is presented in Figs. (4.4-17), (4.4-21), and (4.4-25).

ORIGINAL PAGE IS
OF POOR QUALITY

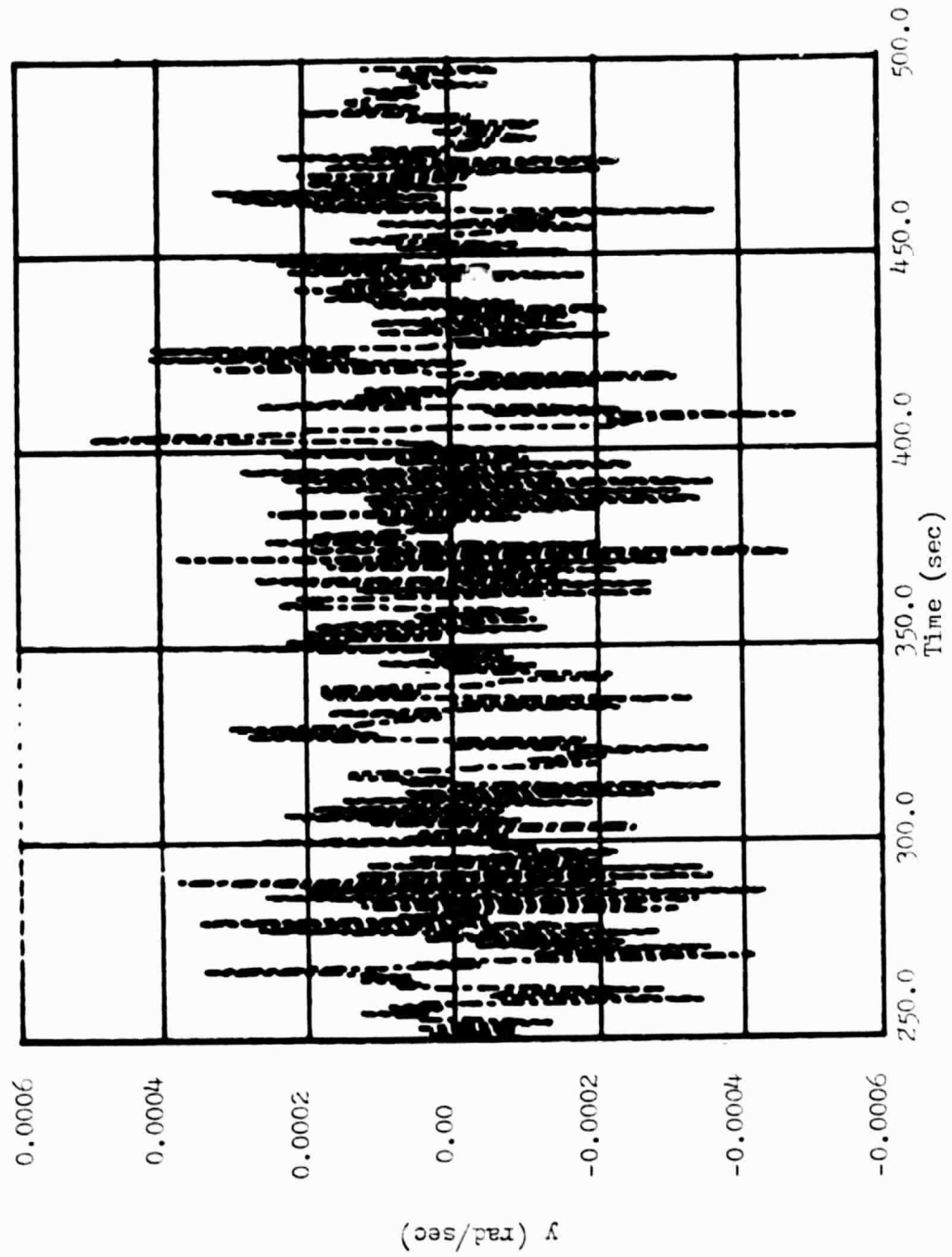


Fig.(4.4-1) Actual Output For Gyroscope Mounted Along X_1 Body Axis

ORIGINAL PAGE IS
OF POOR QUALITY

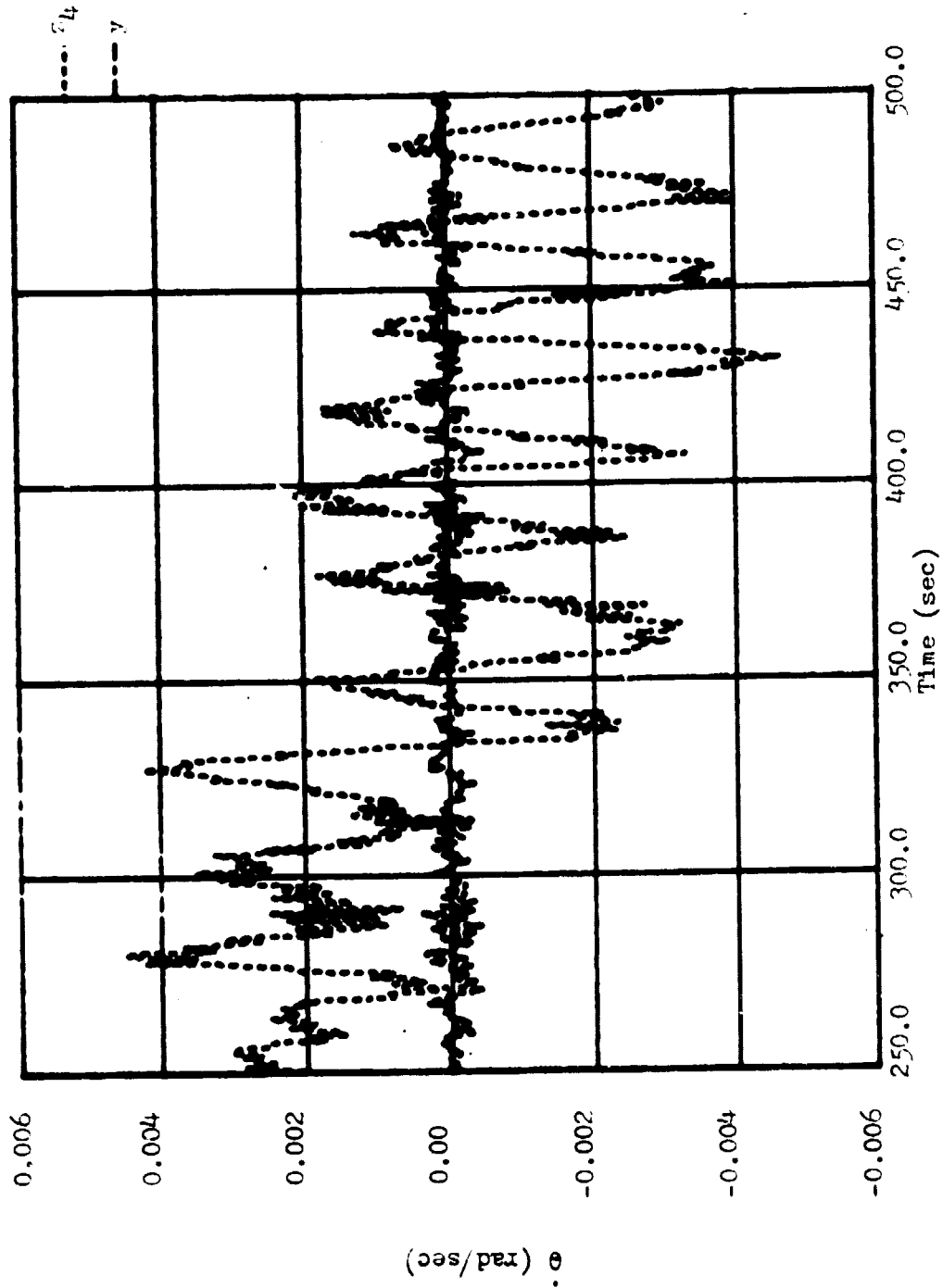


Fig. (4.4-2) Actual Results For Angular Velocity
(4th Order Observer, $u=0$, $\lambda=-0.5$)

ORIGINAL PAGE IS
OF POOR QUALITY

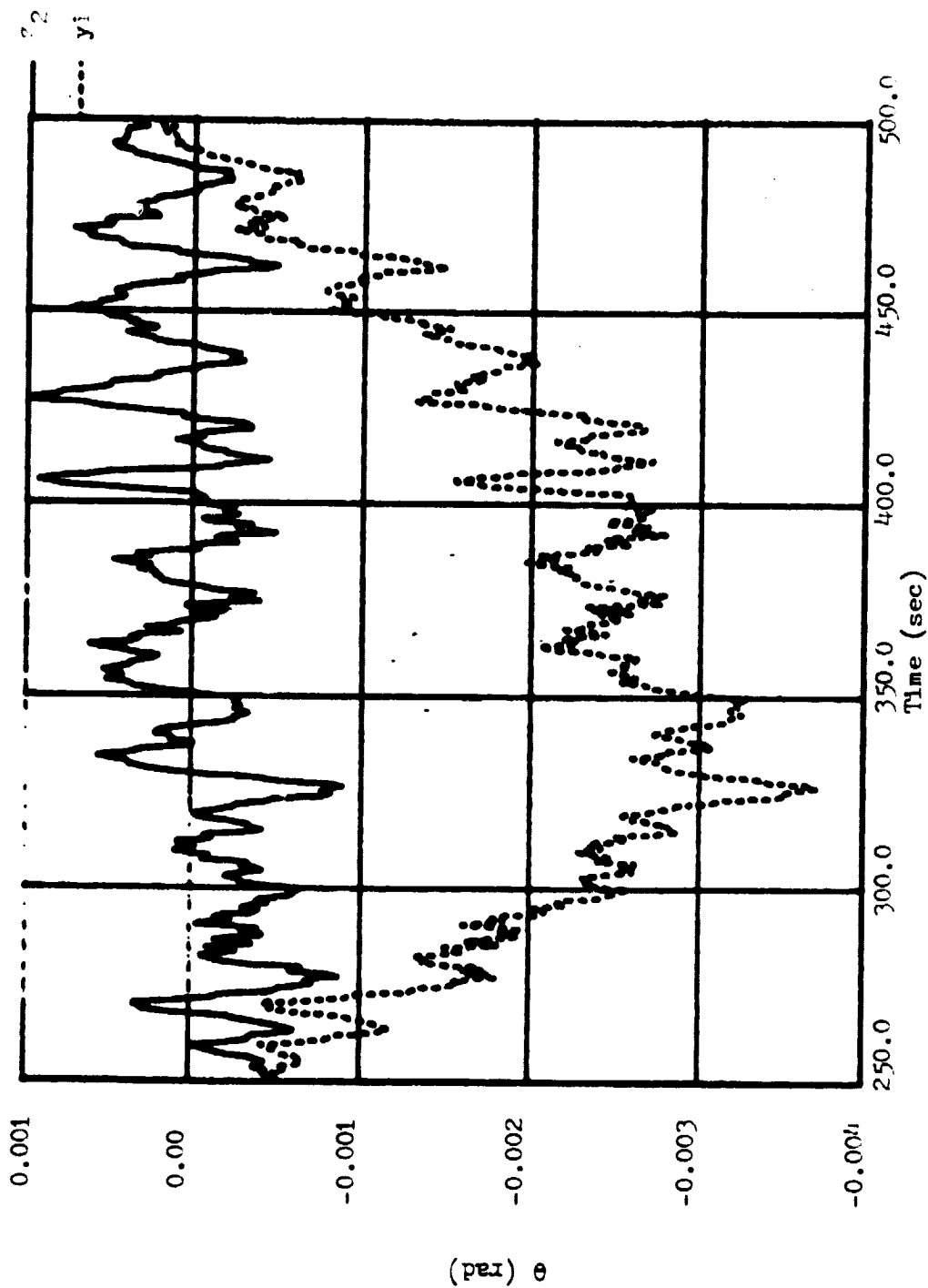


Fig.(4.4-3, Actual Results For Angular Displacement
(4th Order Observer, $u=0$, $\lambda=-0.5$)

ORIGINAL PAGE IS
OF POOR QUALITY

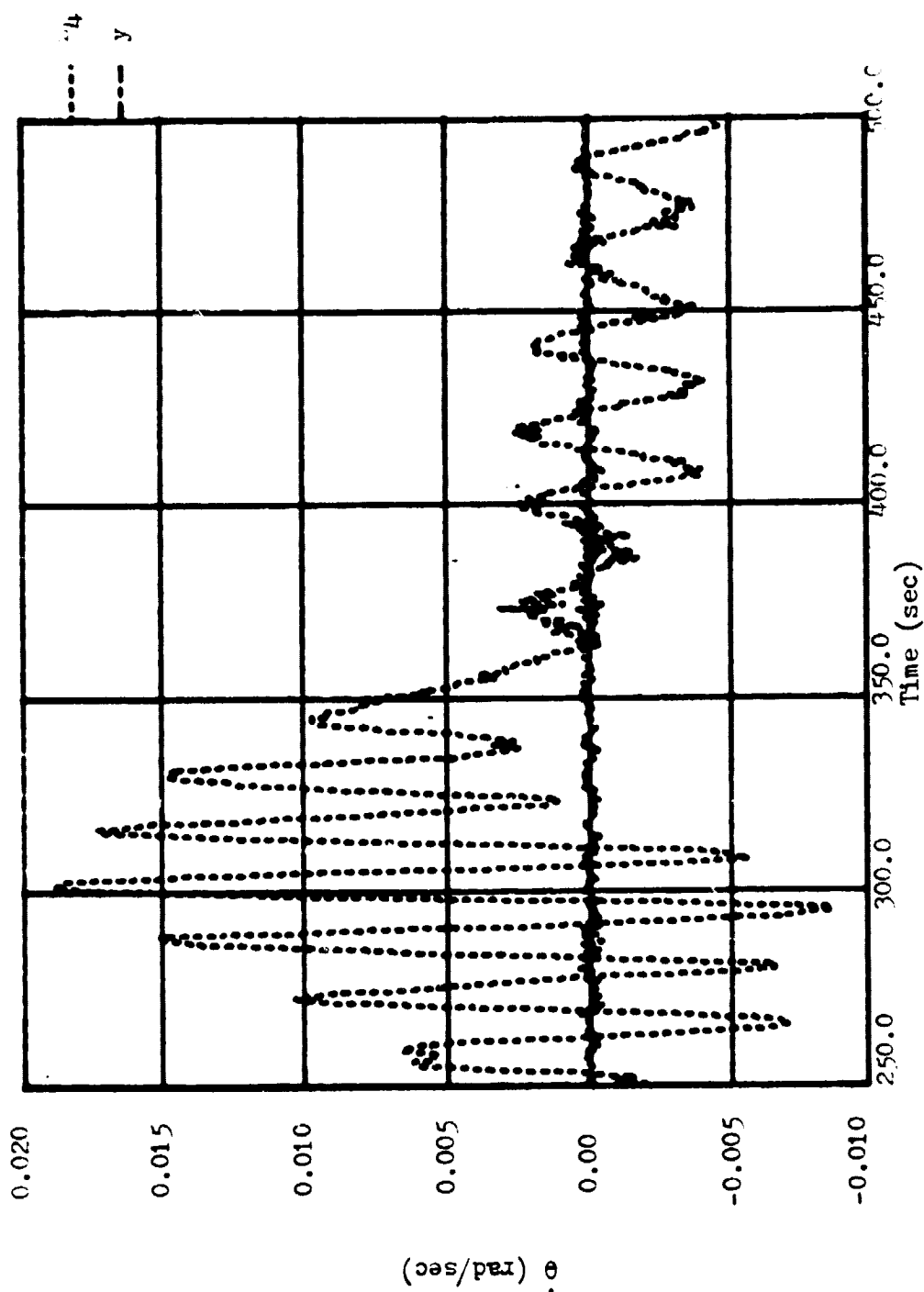


Fig.(4.4-4) Actual Results For Angular Velocity
(4 h Order Observer, $u=a_1, \lambda=-0.5$)

ORIGINAL PAGE IS
OF POOR QUALITY

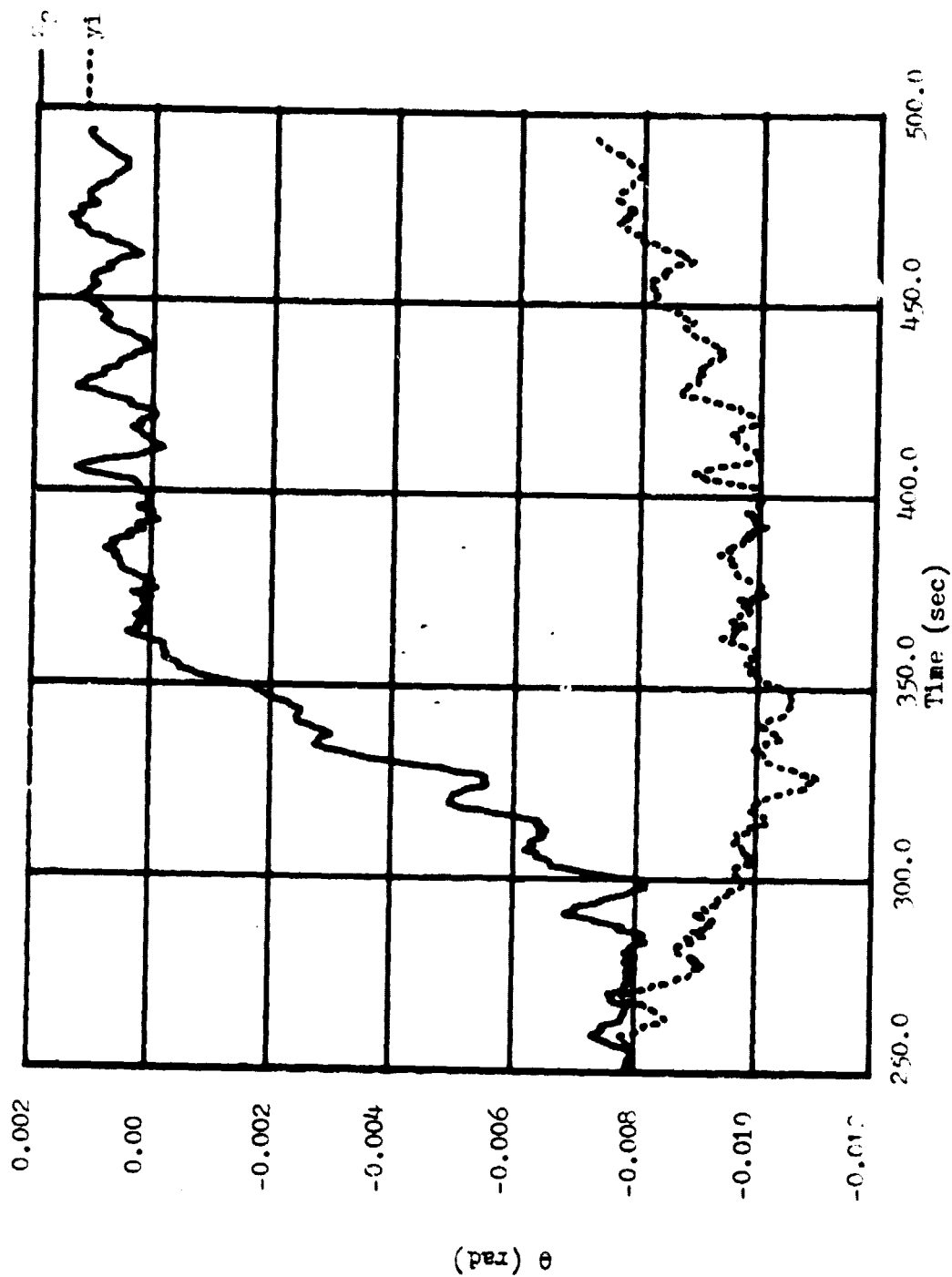


FIG. (4.4-5) Actual Results For Angular Displacement
(4th Order Observer, $u=a_1$, $\lambda=-0.5$)

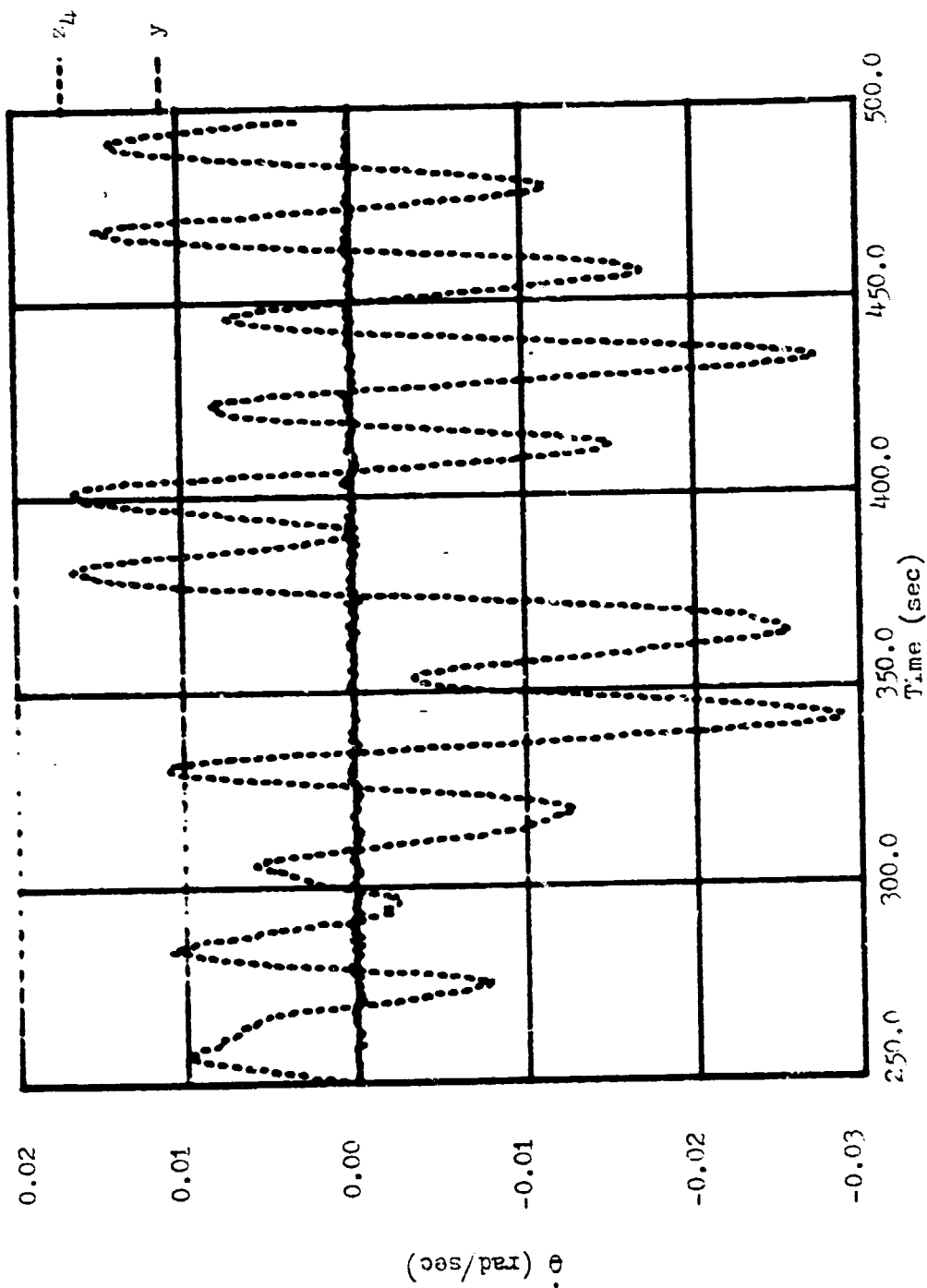


Fig.(4.4-6) Actual Results For Angular Velocity
(5th Order Observer, $u=0$, $\lambda=-0.2$)

ORIGINAL PAGE IS
OF POOR QUALITY

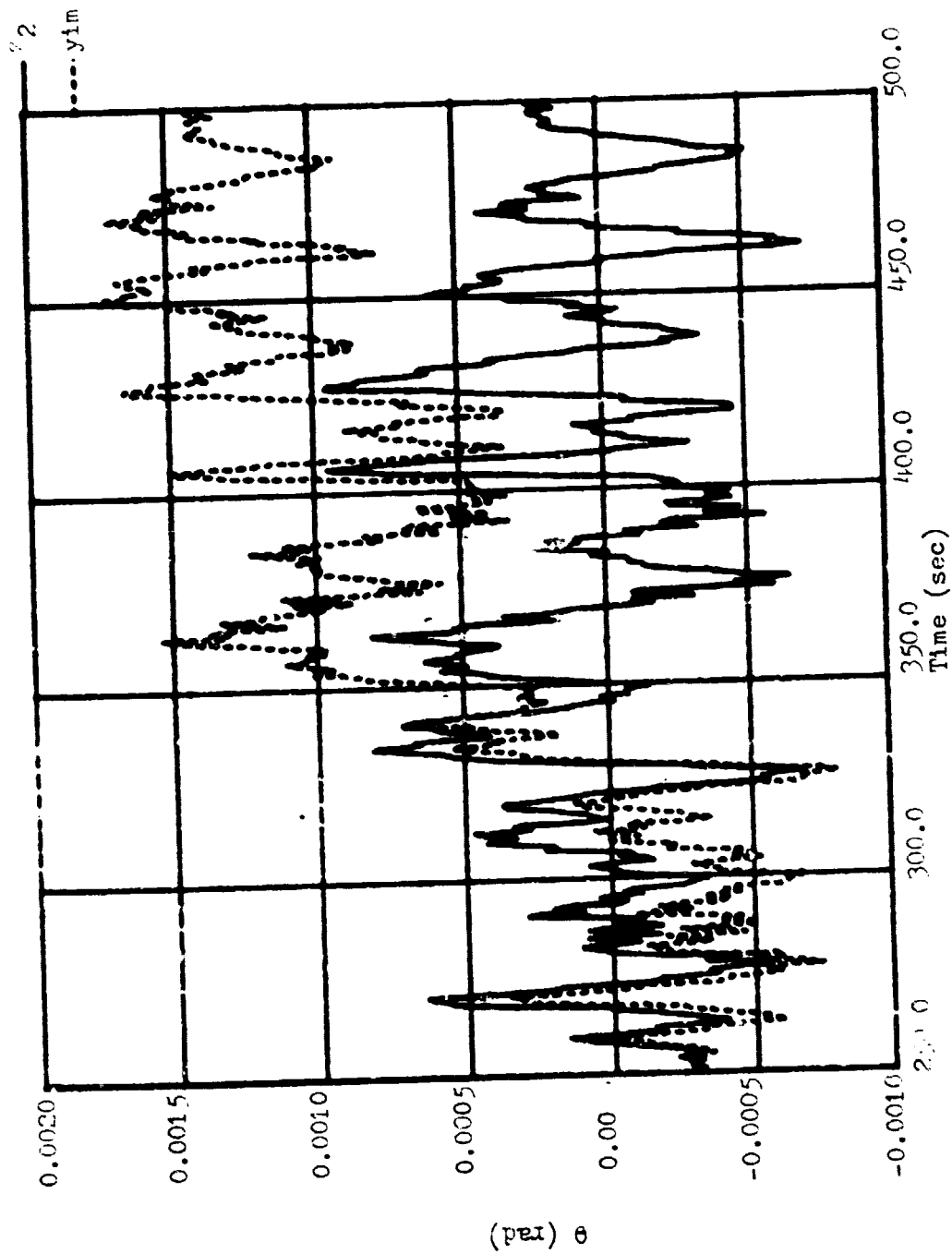


Fig. (4.4-7) Actual Results For Angular Displacement
(5th Order Observer, $u=0$, $\lambda=-0.2$)

ORIGINAL PAGE IS
OF POOR QUALITY

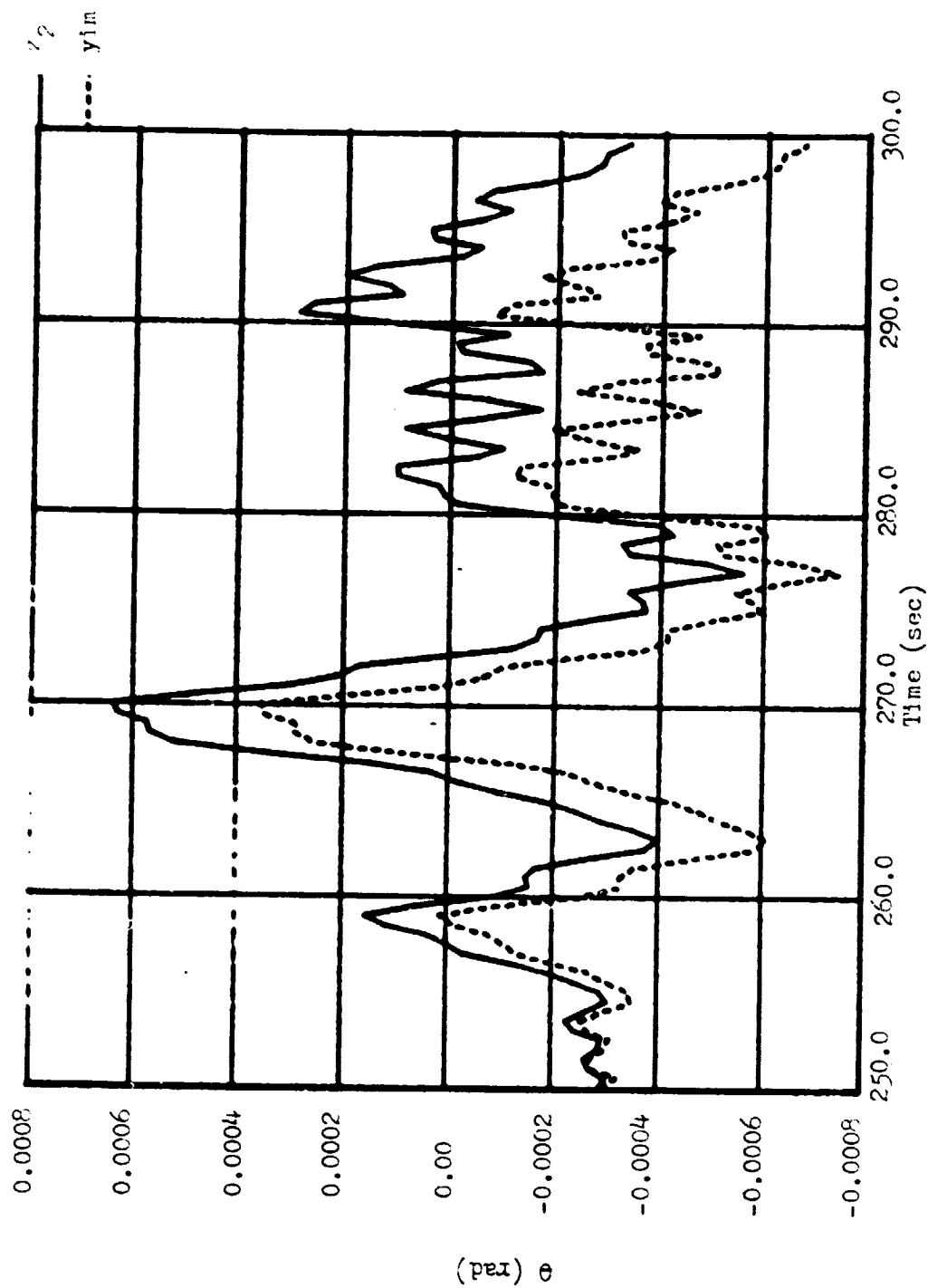


Fig. (4.4-8) Actual Results For Angular Displacement
(5th Order Observer, $u=0$, $\lambda=-0.2$)

ORIGINAL PAGE IS
OF POOR QUALITY

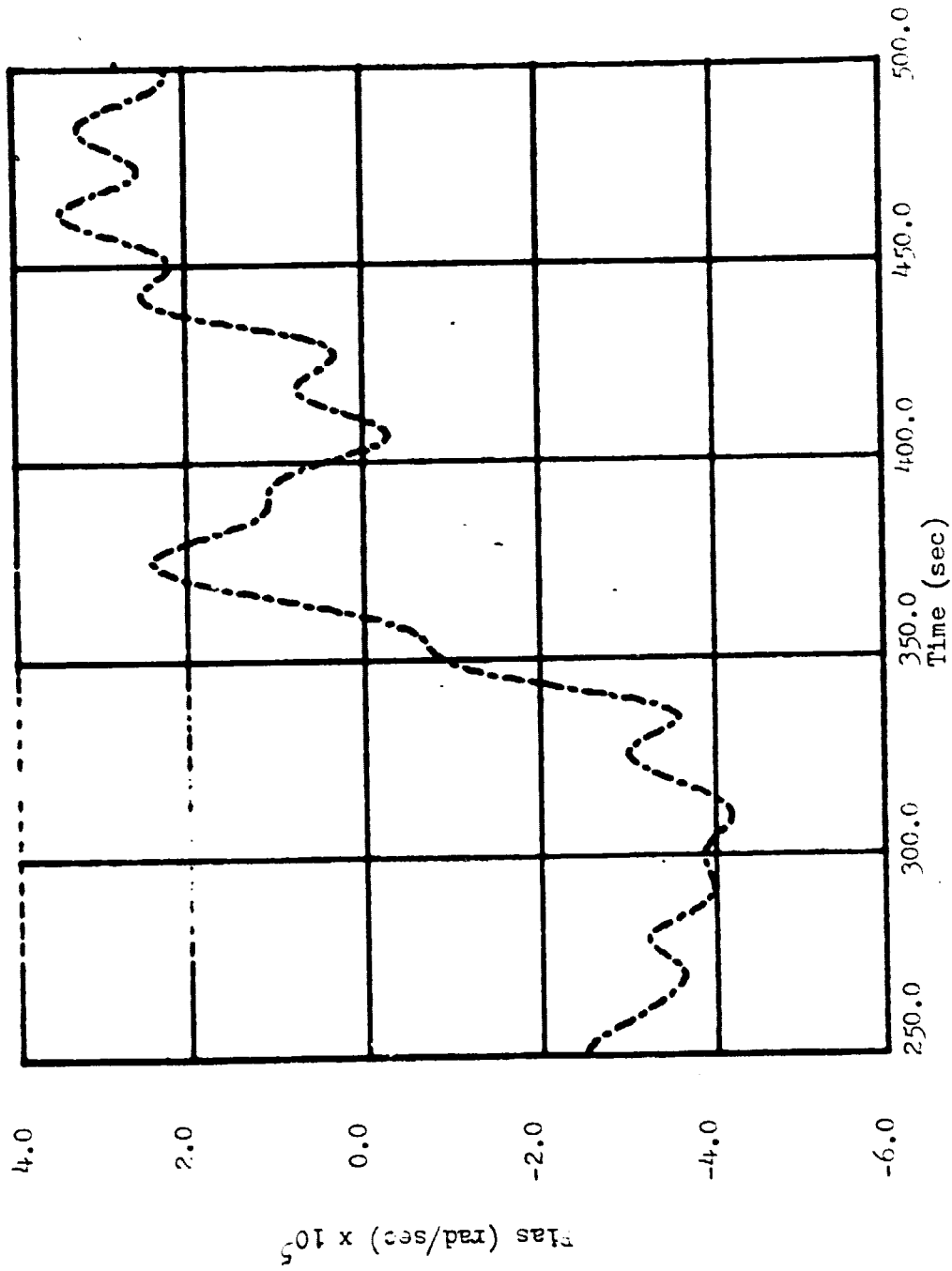


Fig. (4.4-9) Actual Results For Plas
(5th Order Observer, $u=0$, $\lambda=-0.2$)

ORIGINAL PAGE IS
OF POOR QUALITY.

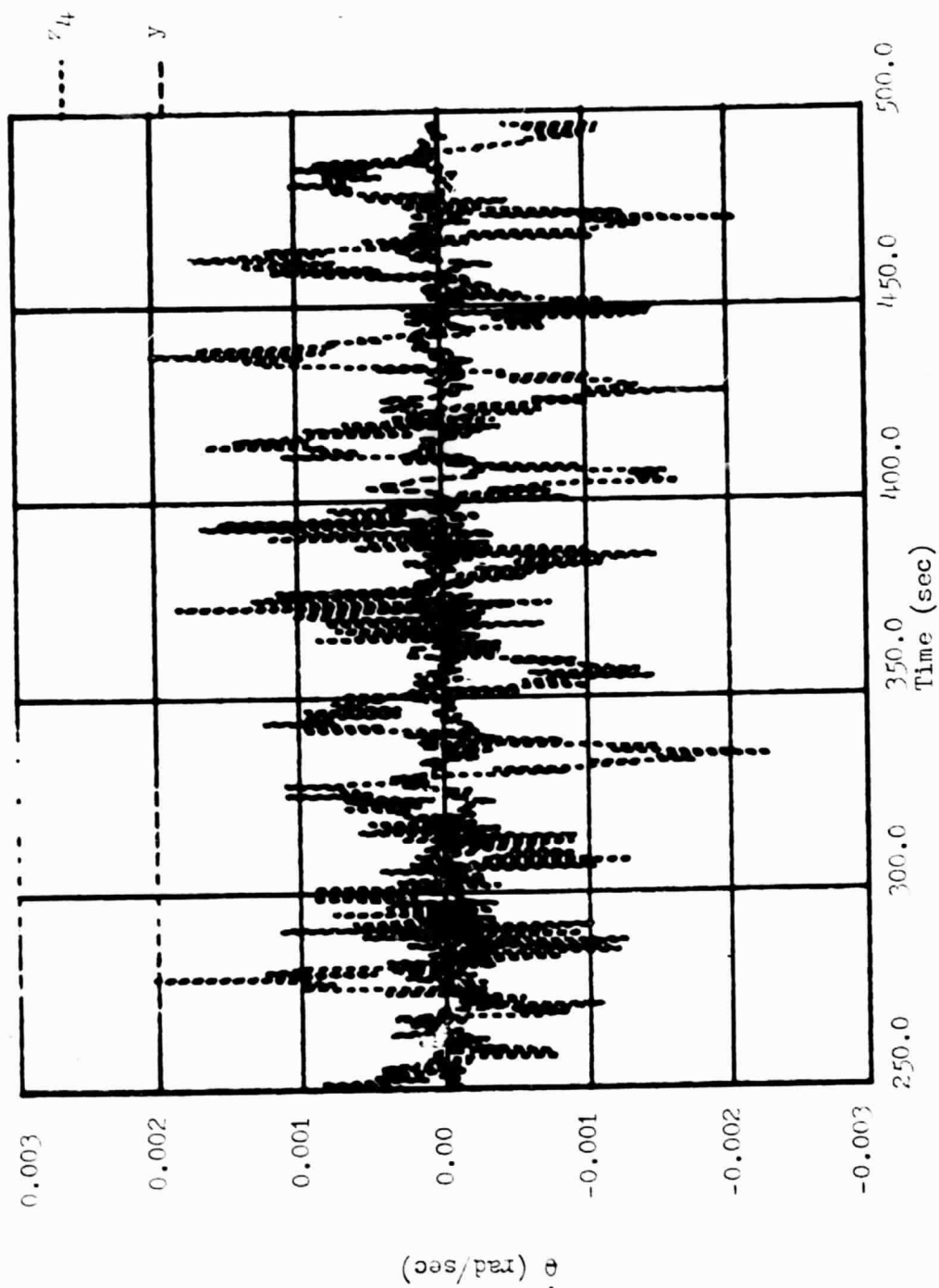


Fig. (4.4-10) Actual Results For Angular Velocity
(5th Order Observer, $u=0$, $\lambda=-0.5$)

ORIGINAL PAGE IS
OF POOR QUALITY

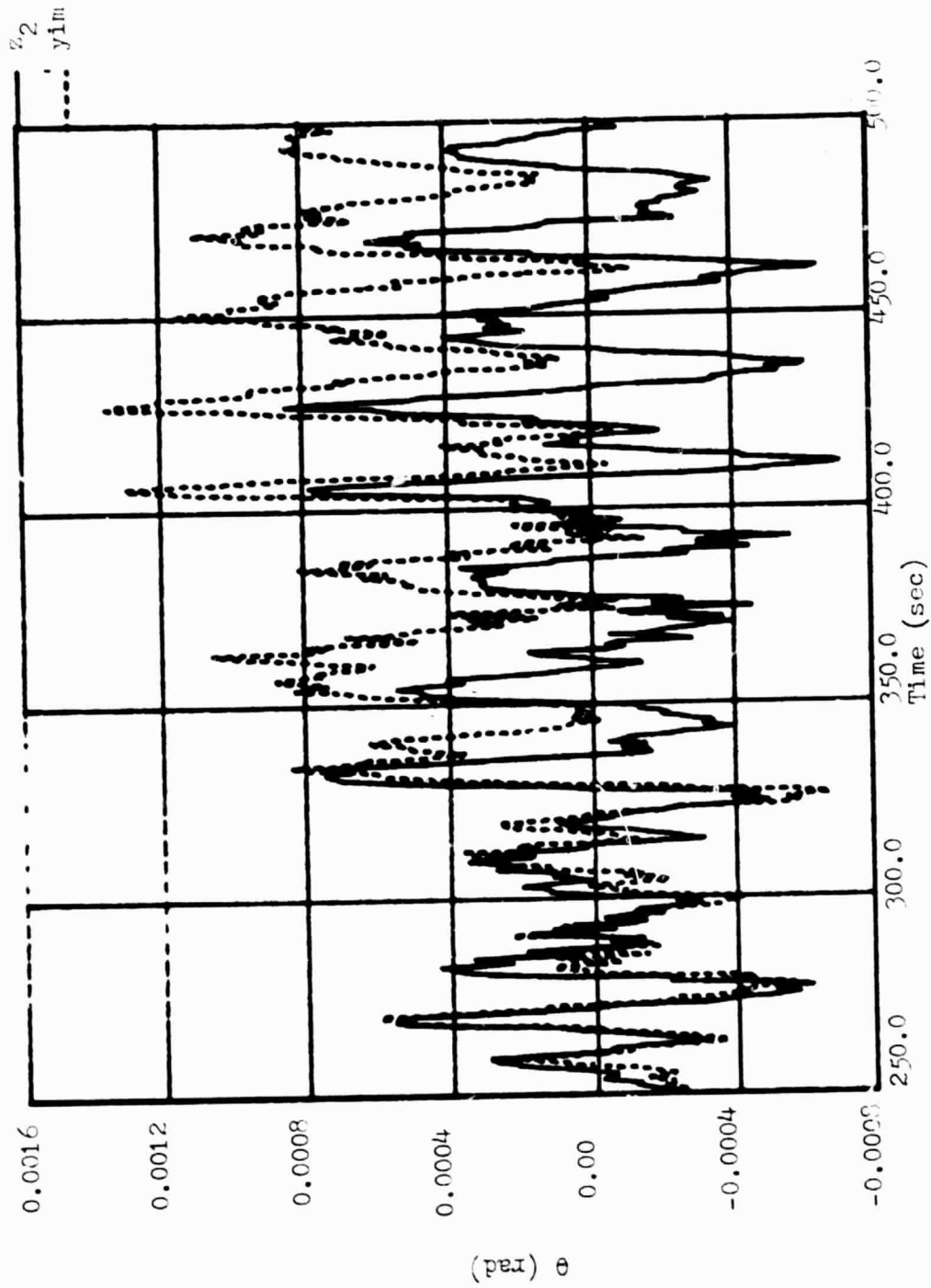


Fig. (4.4-11) Actual Results For Angular Displacement
(5th Order Observer, $u=0$, $\lambda=-0.5$)

ORIGINAL PAGE IS
OF POOR QUALITY

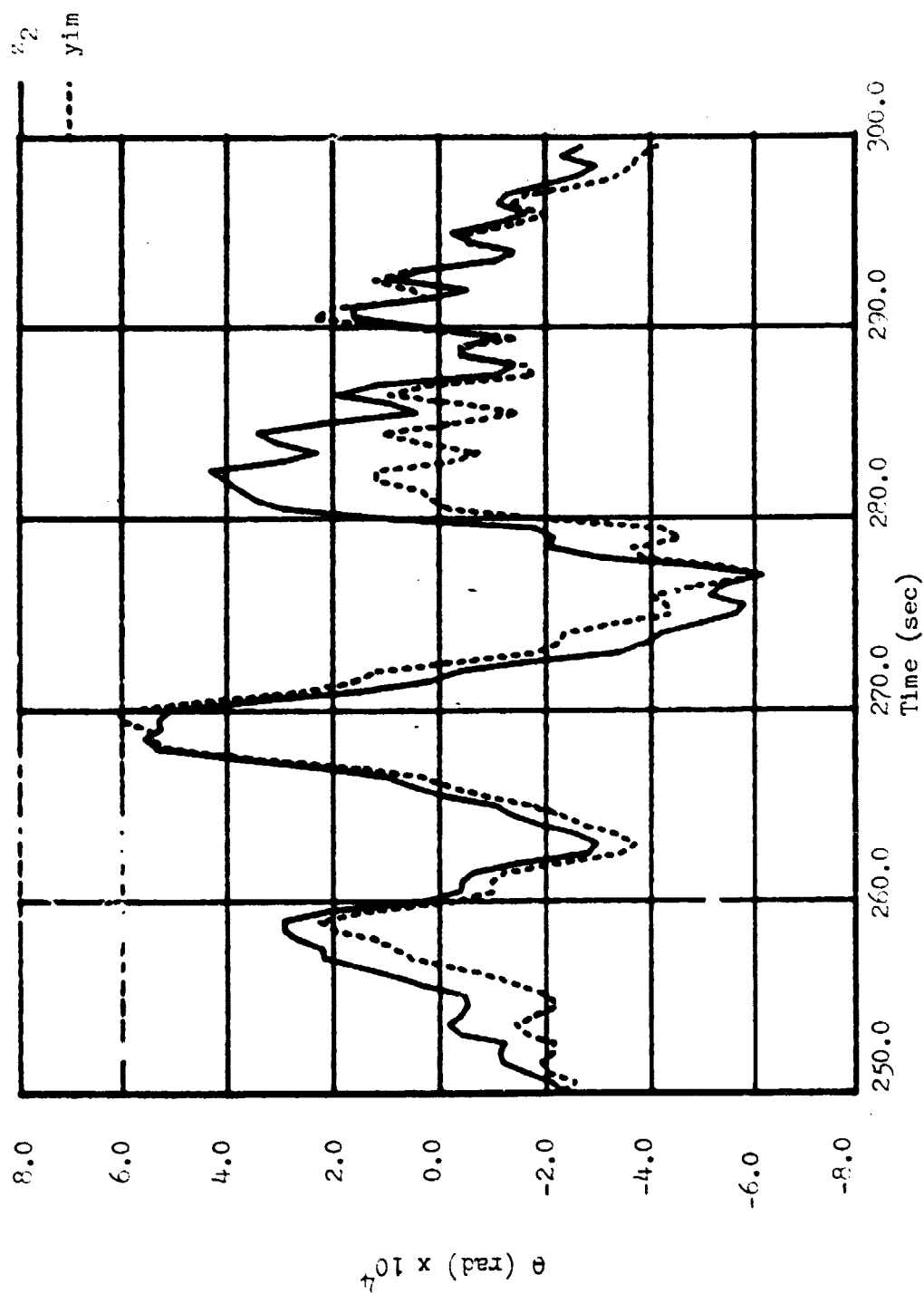


Fig. (4.4-12) Actual Results For Angular Displacement
(5th Order Observer, $u=0$, $\lambda=-0.5$)

CENTRAL PAGE IS
OF POOR QUALITY

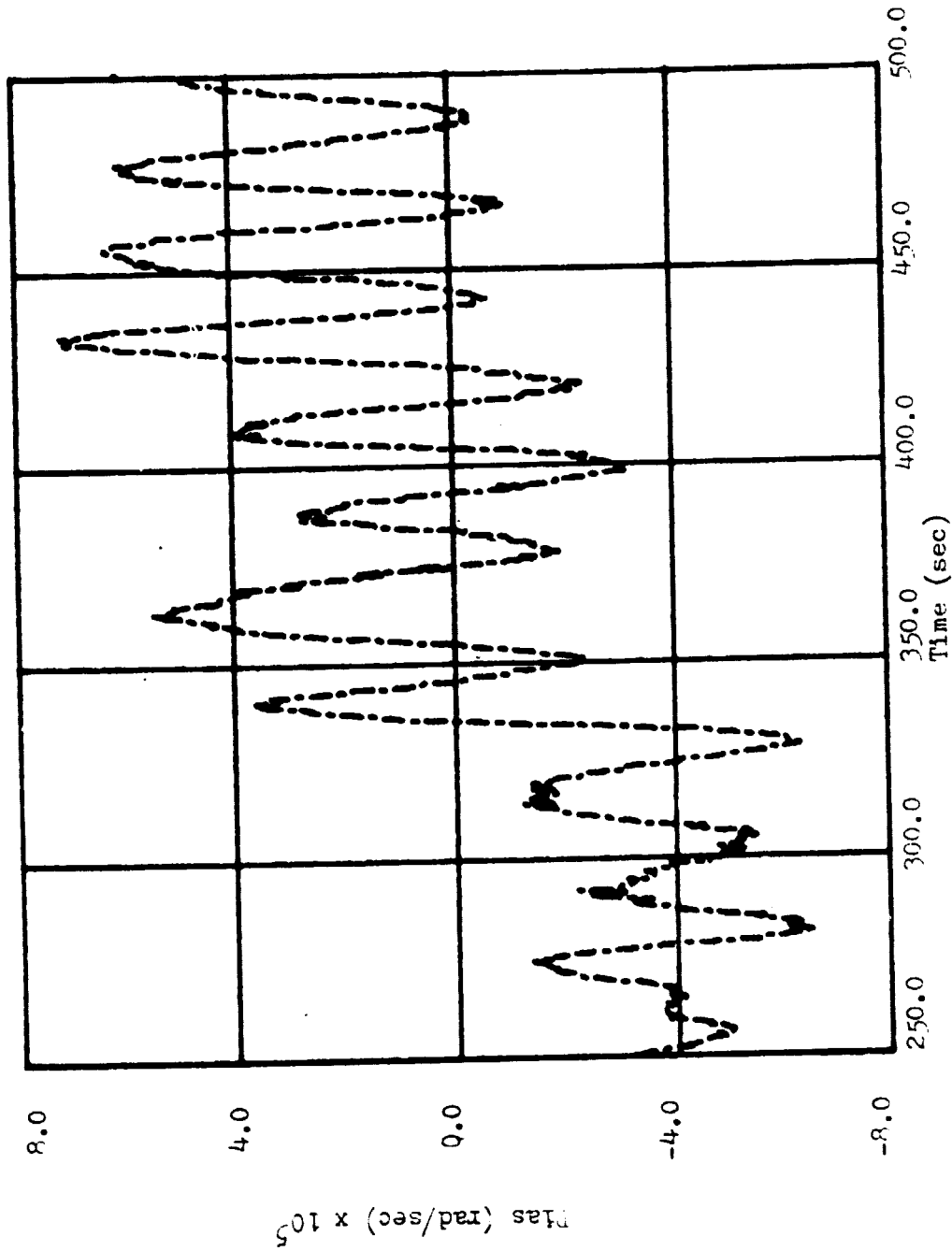


Fig.(4.4-13) Actual Results For Bias
(5th Order Observer, $u=0$, $\lambda=-0.5$)

ORIGINAL PAGE IS
OF POOR QUALITY

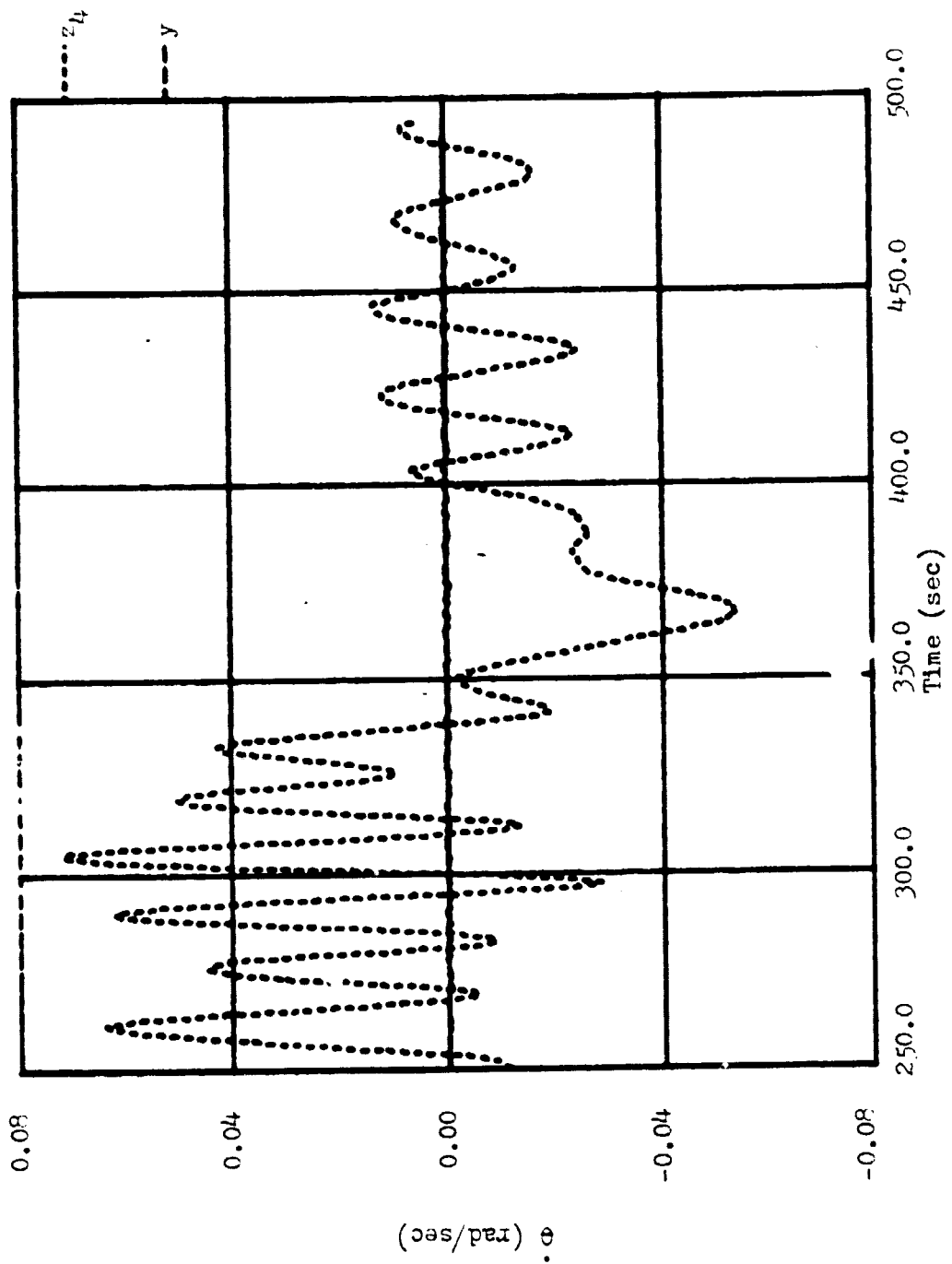


Fig.(4.4-14) Actual Results For Angular Velocity
(5th Order Observer, $u=a_1$, $\lambda=-0.2$)

ORIGINAL PAGE IS
OF POOR QUALITY

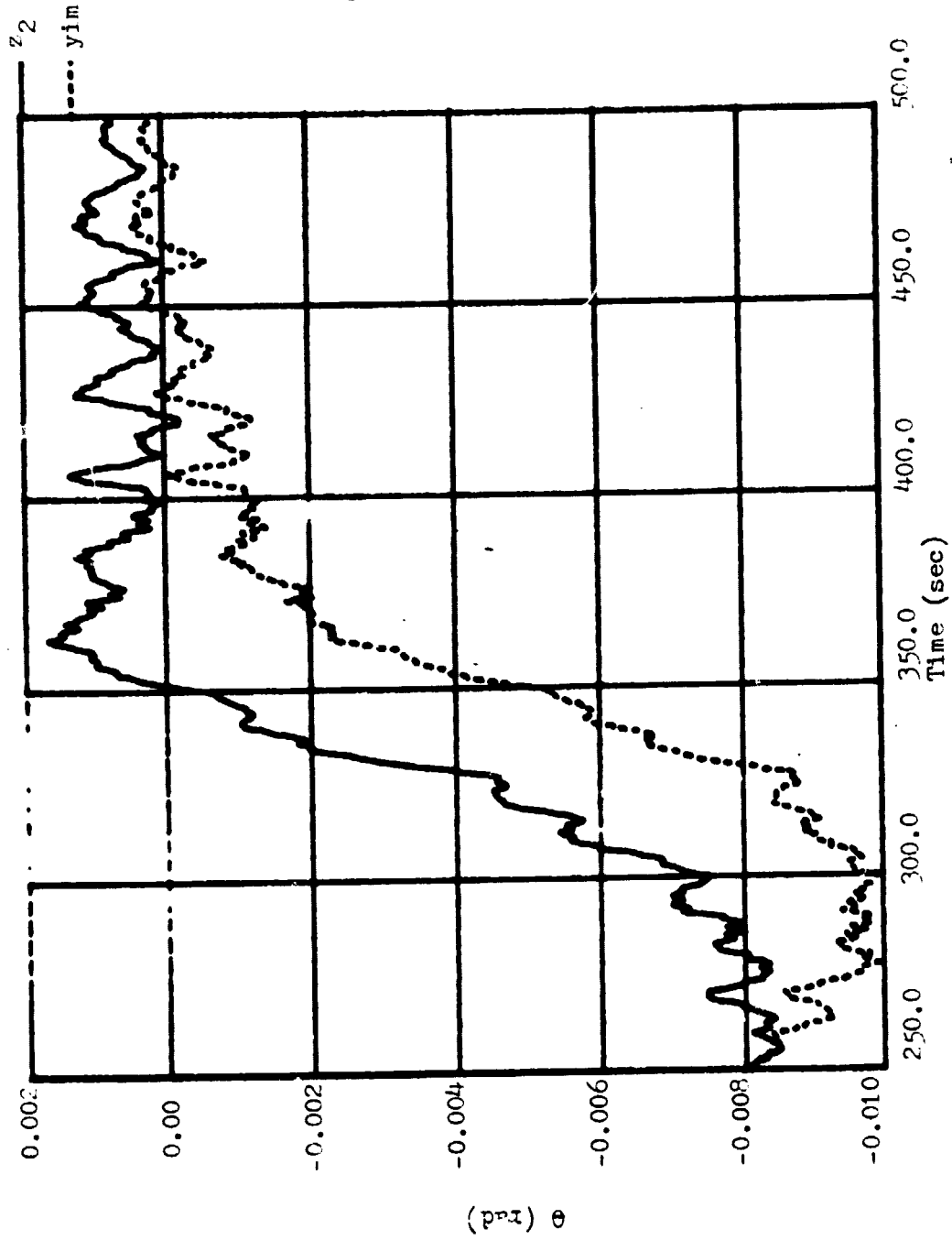


Fig. (4.4-15) Actual Results For Angular Velocity
(5th Order Observer, $u=a_1$, $\lambda=-0.2$)

ORIGINAL PAGE IS
OF POOR QUALITY

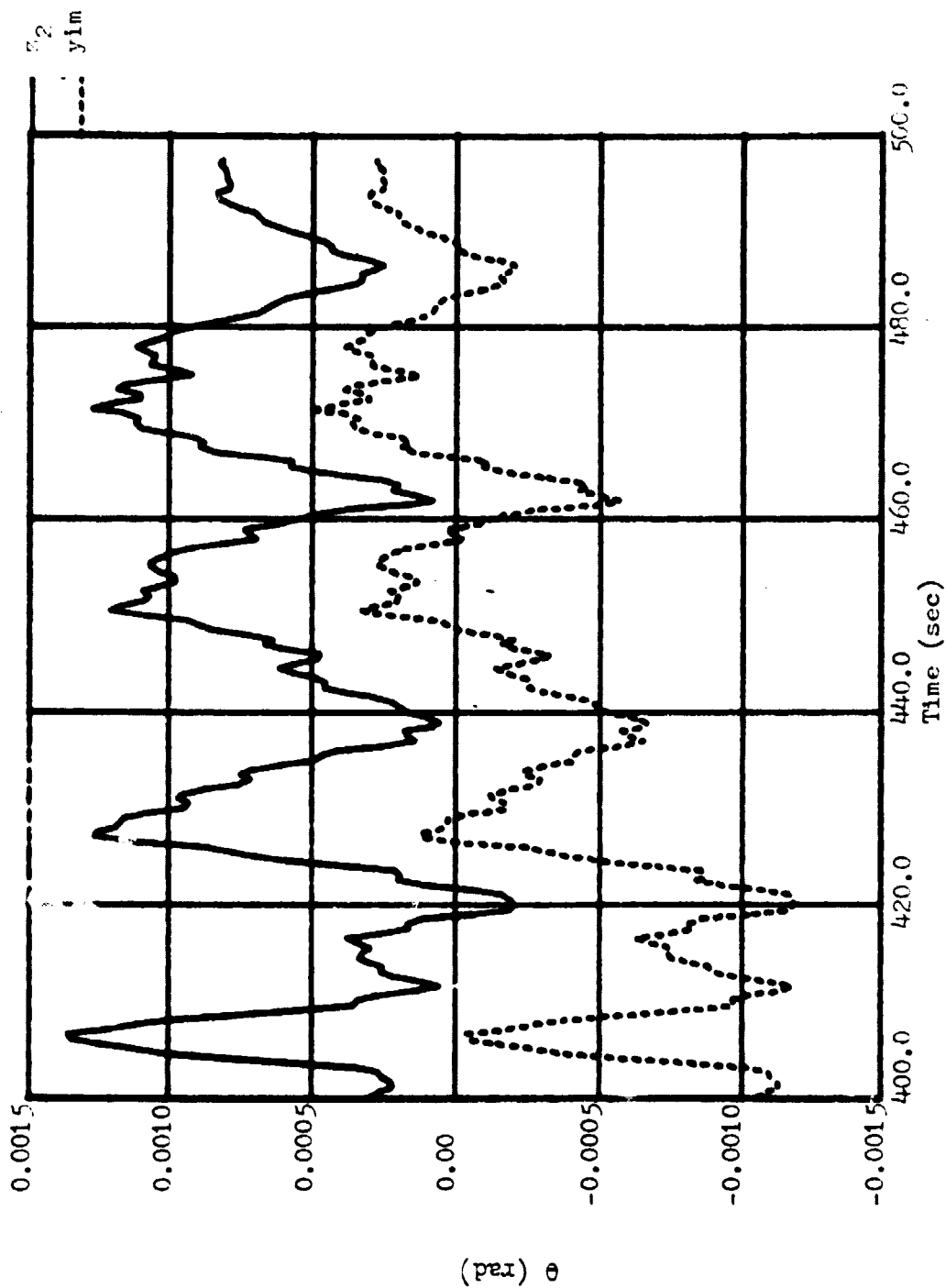


Fig. (4.4-16) Actual Results For Angular Displacement
(5th Order Observer, $u=a_1$, $\lambda=-0.2$)

ORIGINAL PAGE IS
OF POOR QUALITY

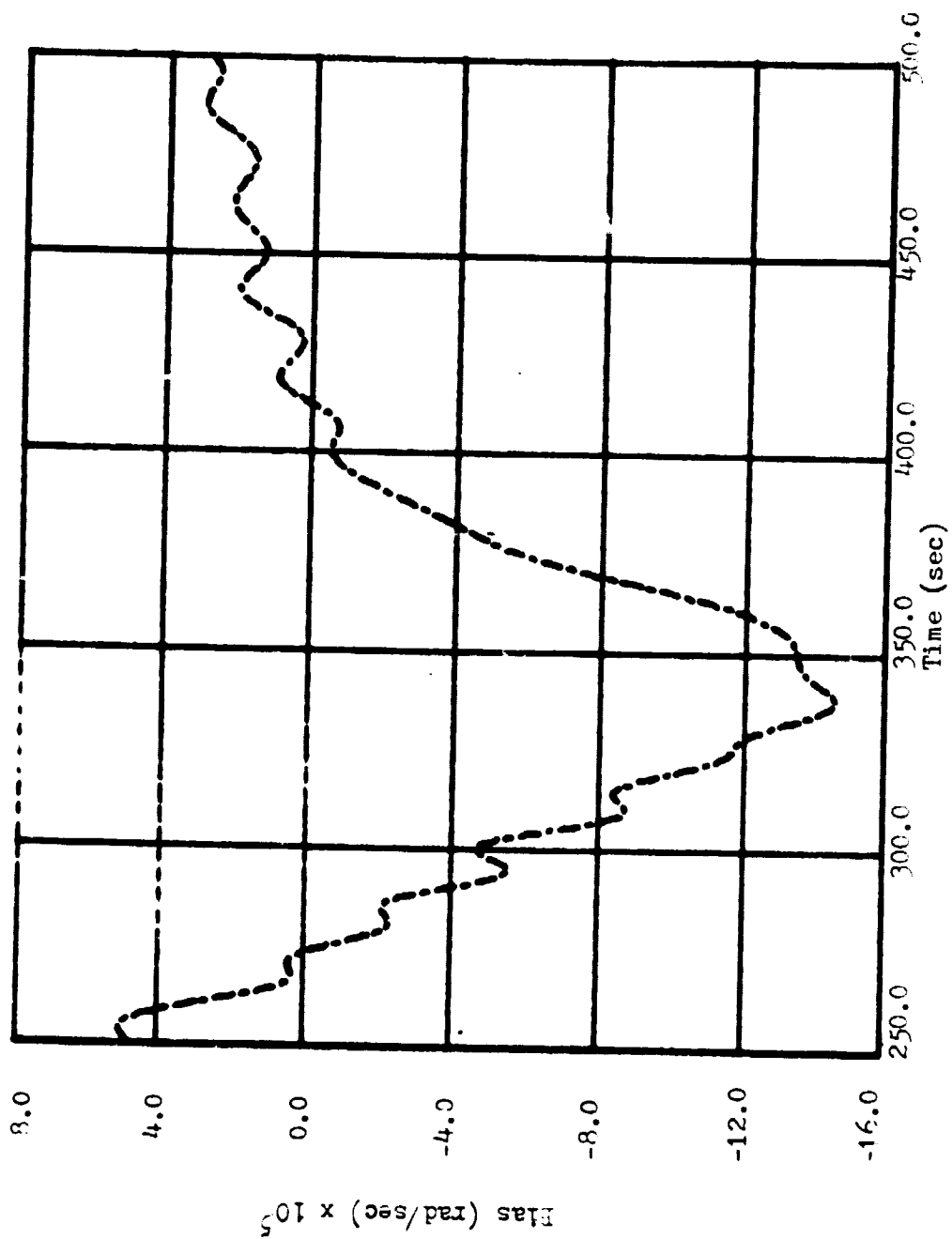


Fig.(4.4-17) Actual Results For Bias
(5th Order Observer, $u=a_1$, $\lambda=-0.2$)

ORIGINAL PAGE IS
OF POOR QUALITY

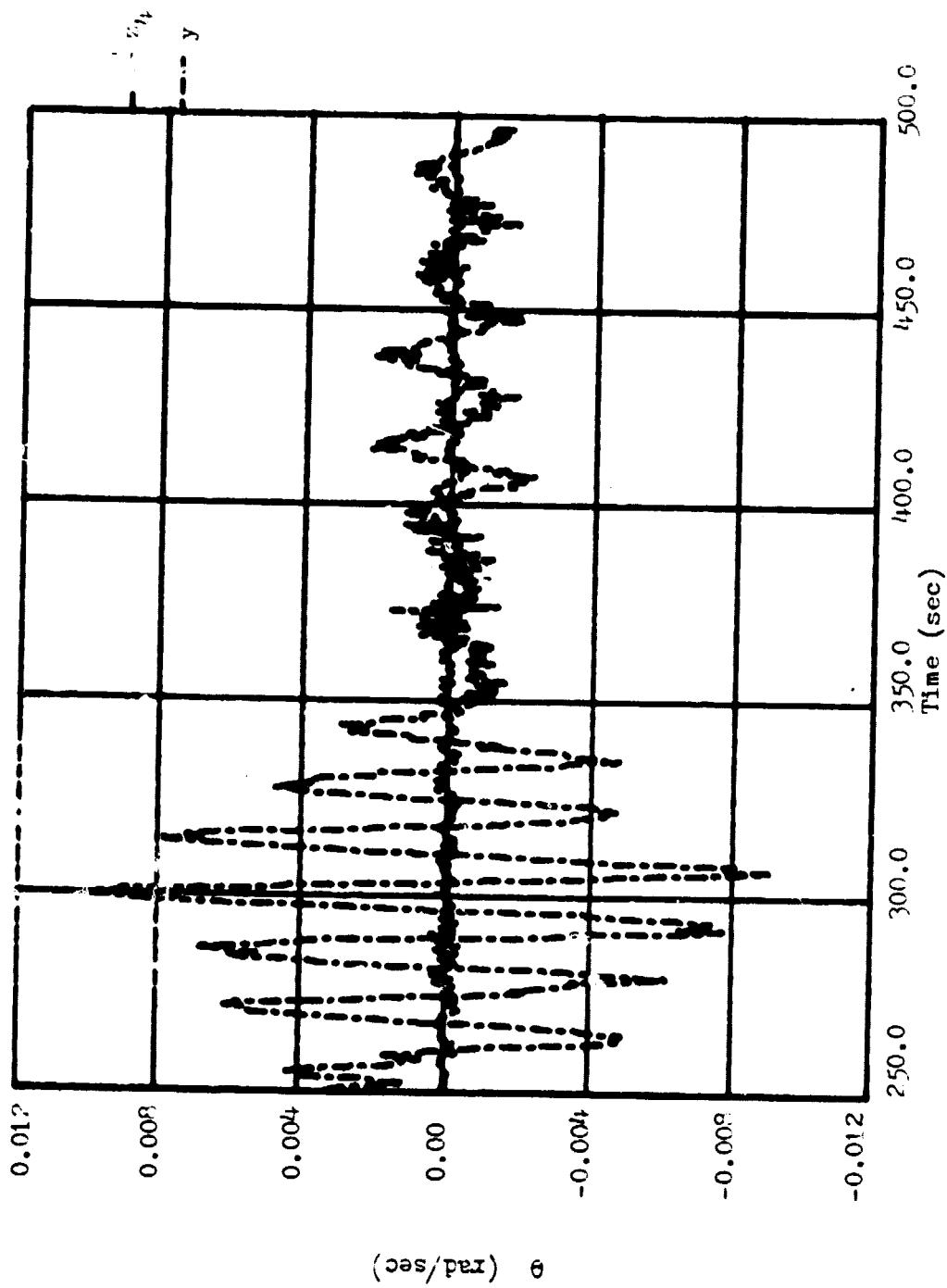


Fig. (4.4-12) Actual Results For Angular Velocity
(5th Order Observer, $u=a_1$, $\lambda=-0.5$)

ORIGINAL PAGE IS
OF POOR QUALITY

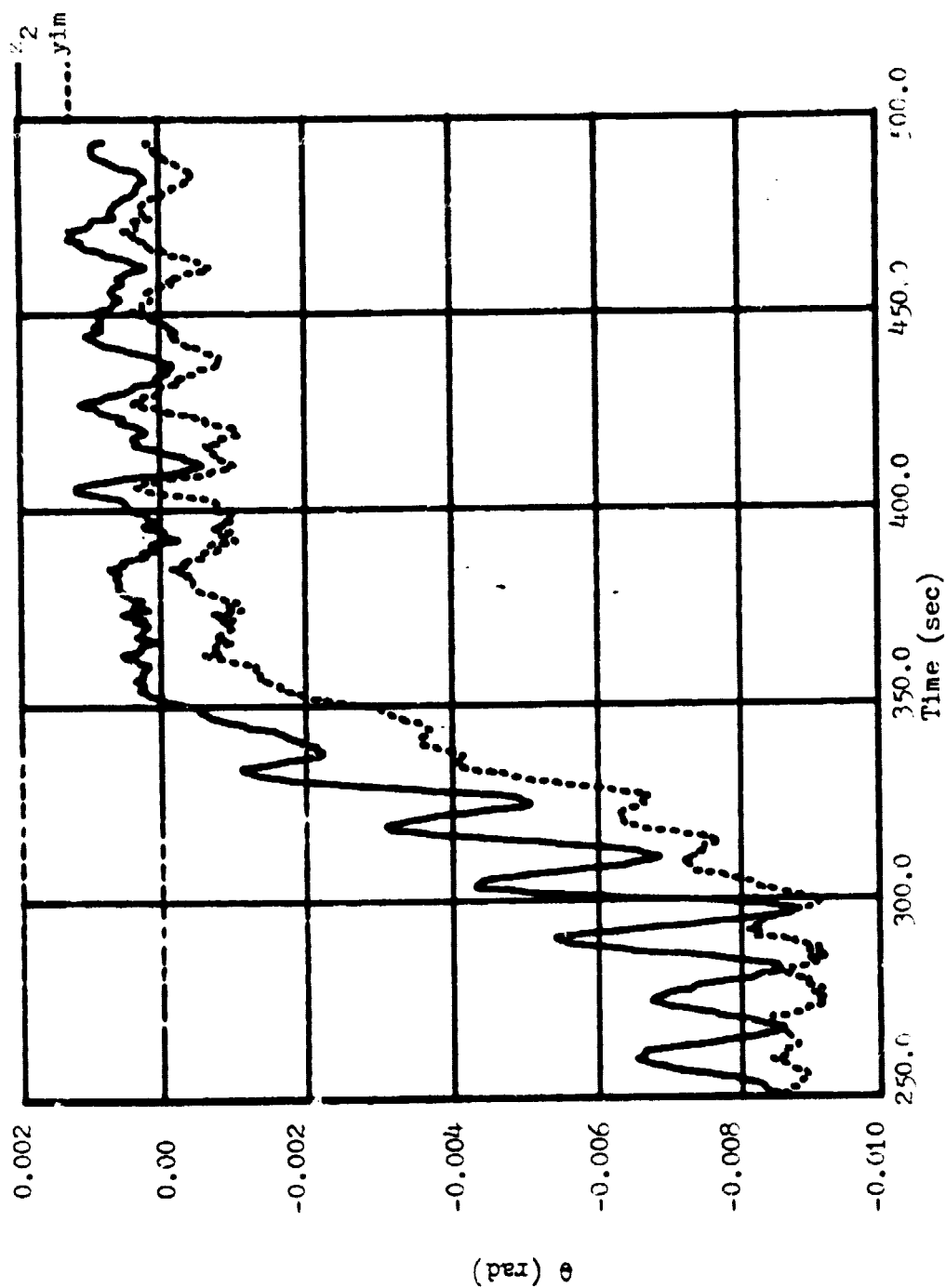


Fig.(4.4-19) Actual Results For Angular Displacement
(5th Order Observer, $u=a_1$, $\lambda=-0.5$)

ORIGINAL PAGE IS
OF POOR QUALITY

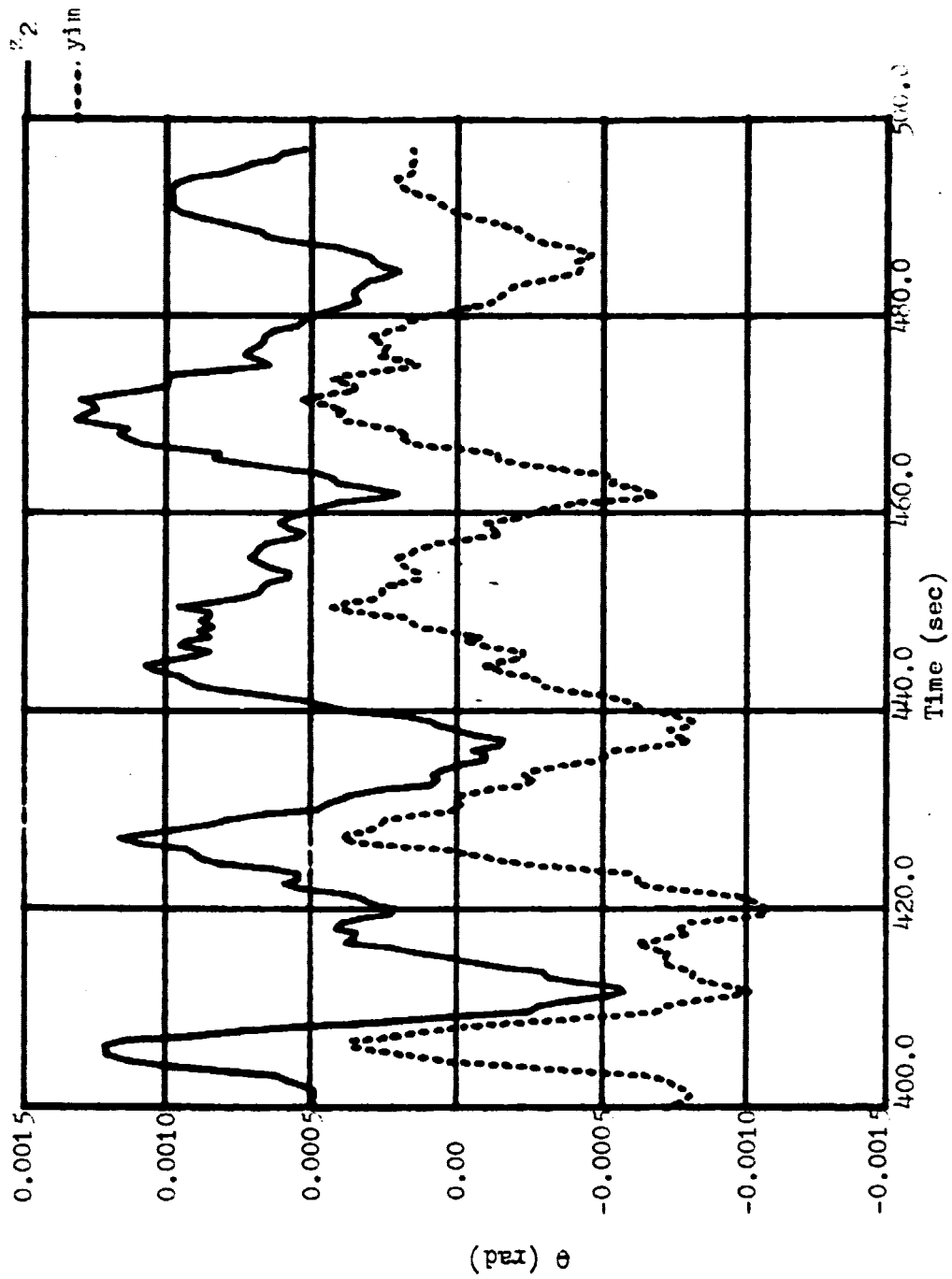


Fig.(4.4-20) Actual Results For Angular Displacement
(5th Order Observer, $u=a_1$, $\lambda=-0.5$)

7-2

ORIGINAL PAGE IS
OF POOR QUALITY

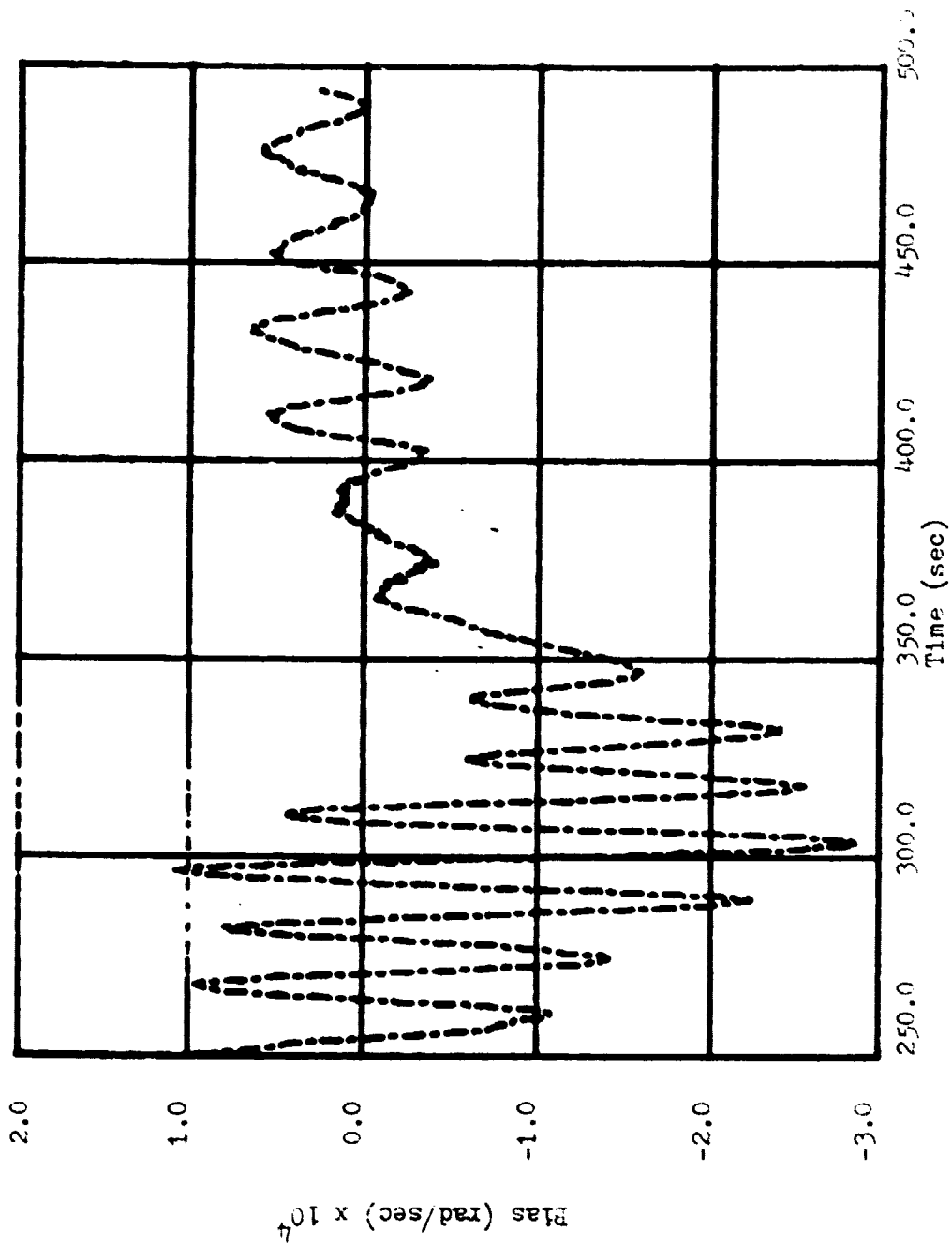


Fig.(4.4-21) Actual Results For Plas

(5th Order Observer, $u=a_1$, $\lambda=-0.5$)

ORIGINAL PAGE IS
OF POOR QUALITY.

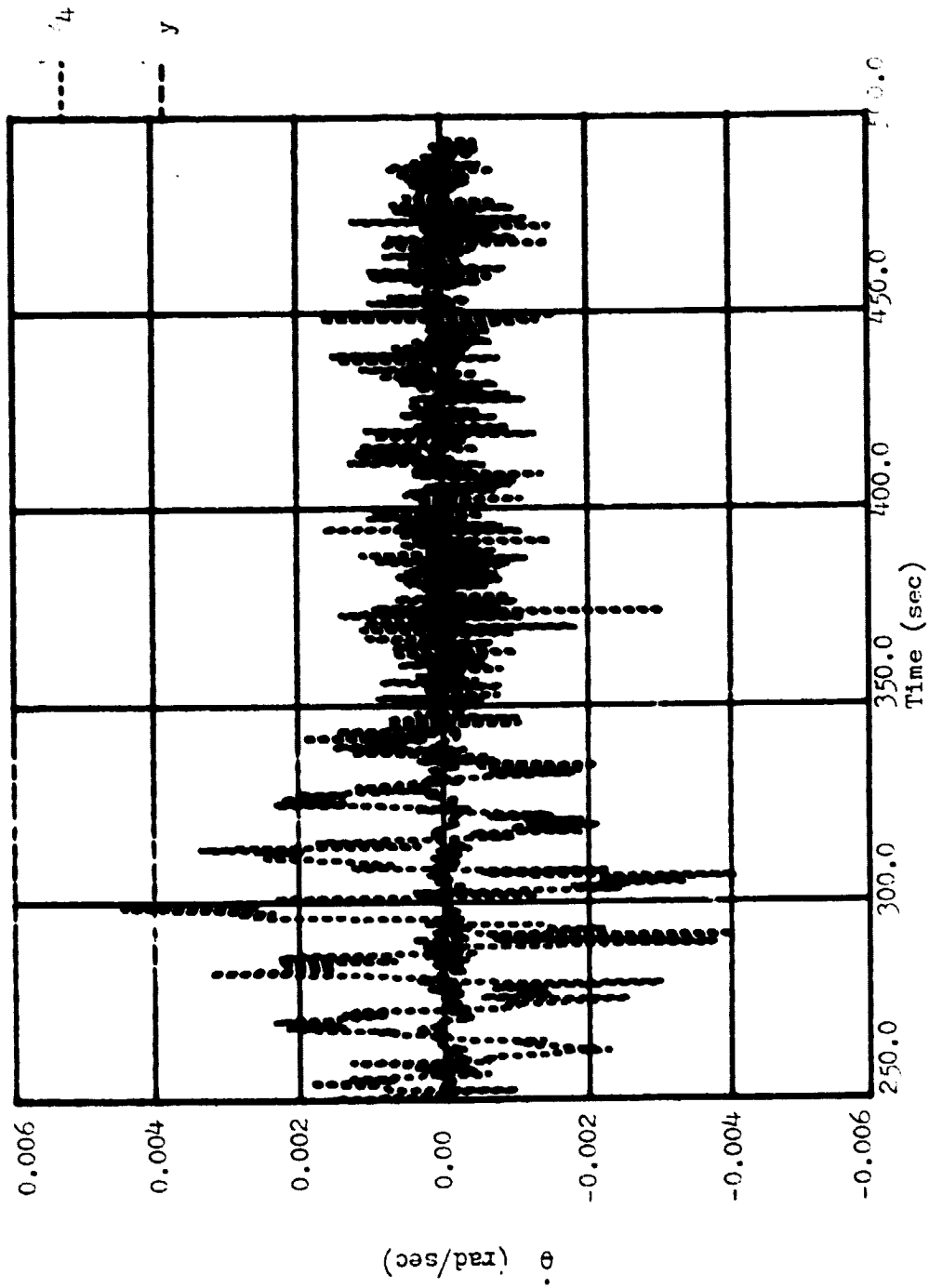


Fig.(4.4-22) Actual Results For Angular Velocity
(5th Order Observer, $u=a_1$, $\lambda=-0.7$)

ORIGINAL PAGE IS
OF POOR QUALITY

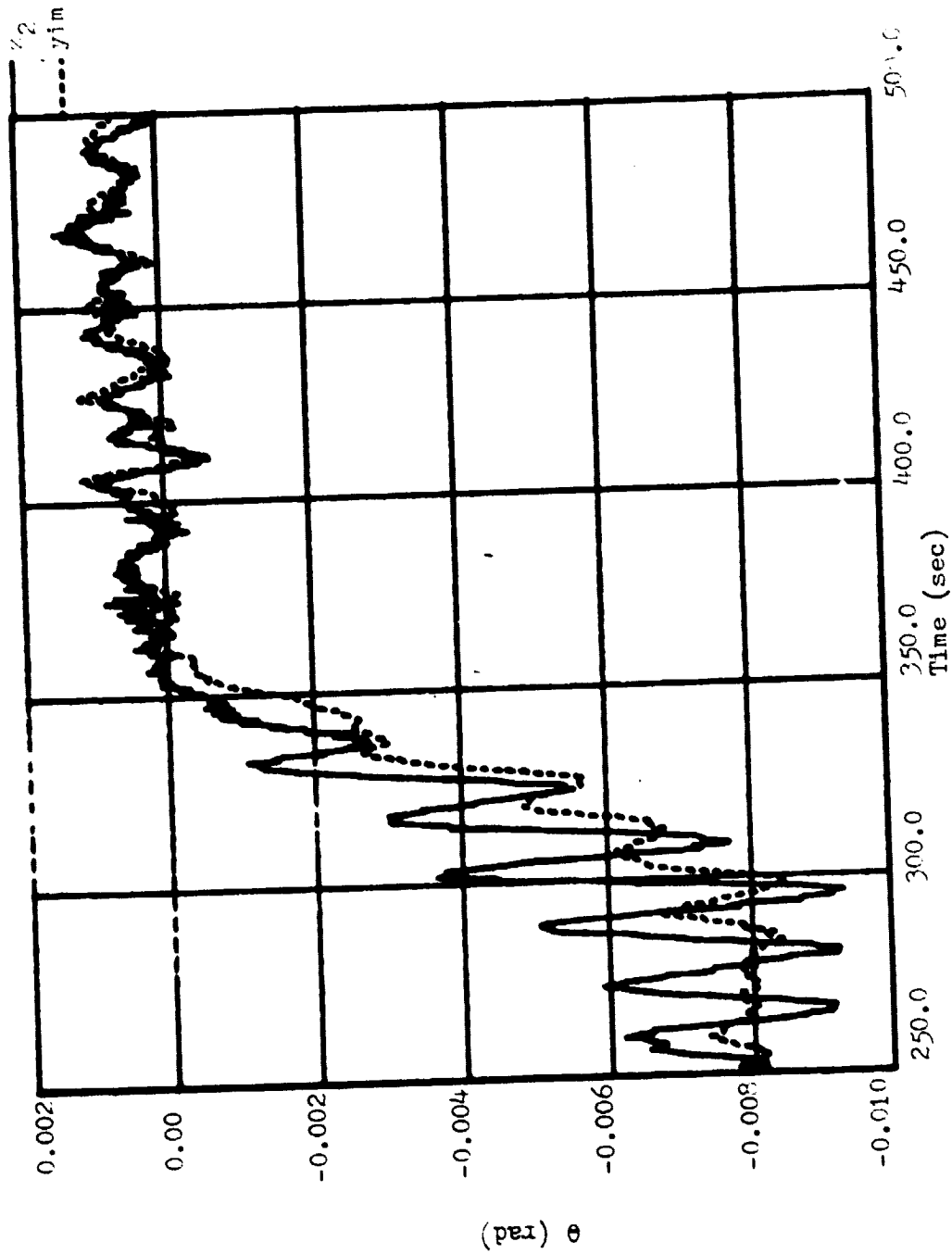


Fig. (4.4-23) Actual Results For Angular Displacement
(5th Order Observer, $u=a_1$, $\lambda=-0.7$)

ORIGINAL PAGE IS
OF POOR QUALITY

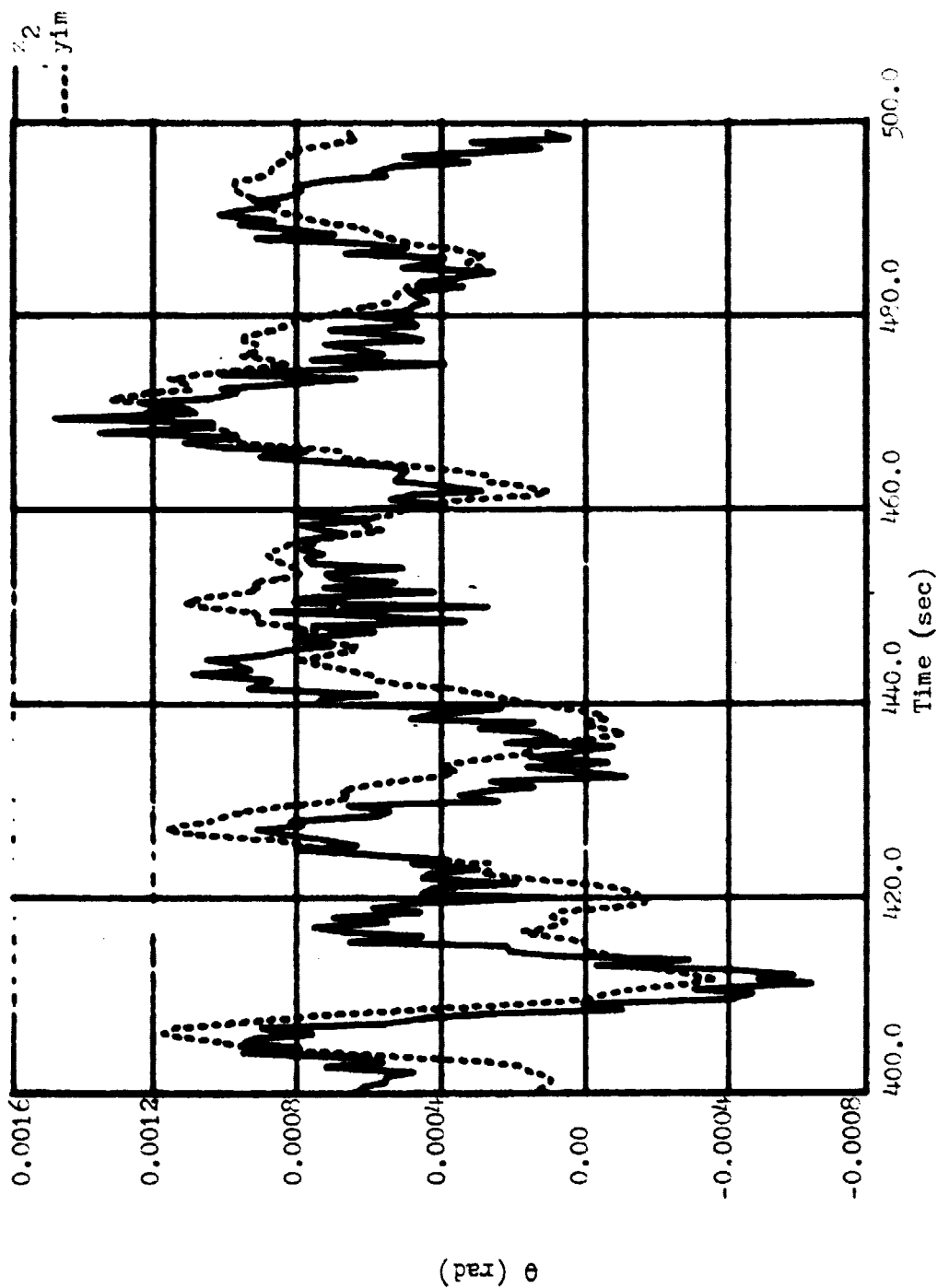


Fig. (4.4-24) Actual Results For angular Displacement

(5th Order Observer, $u=a_1$, $\lambda=-0.7$)

ORIGINAL PAGE IS
OF PCOR QUALITY

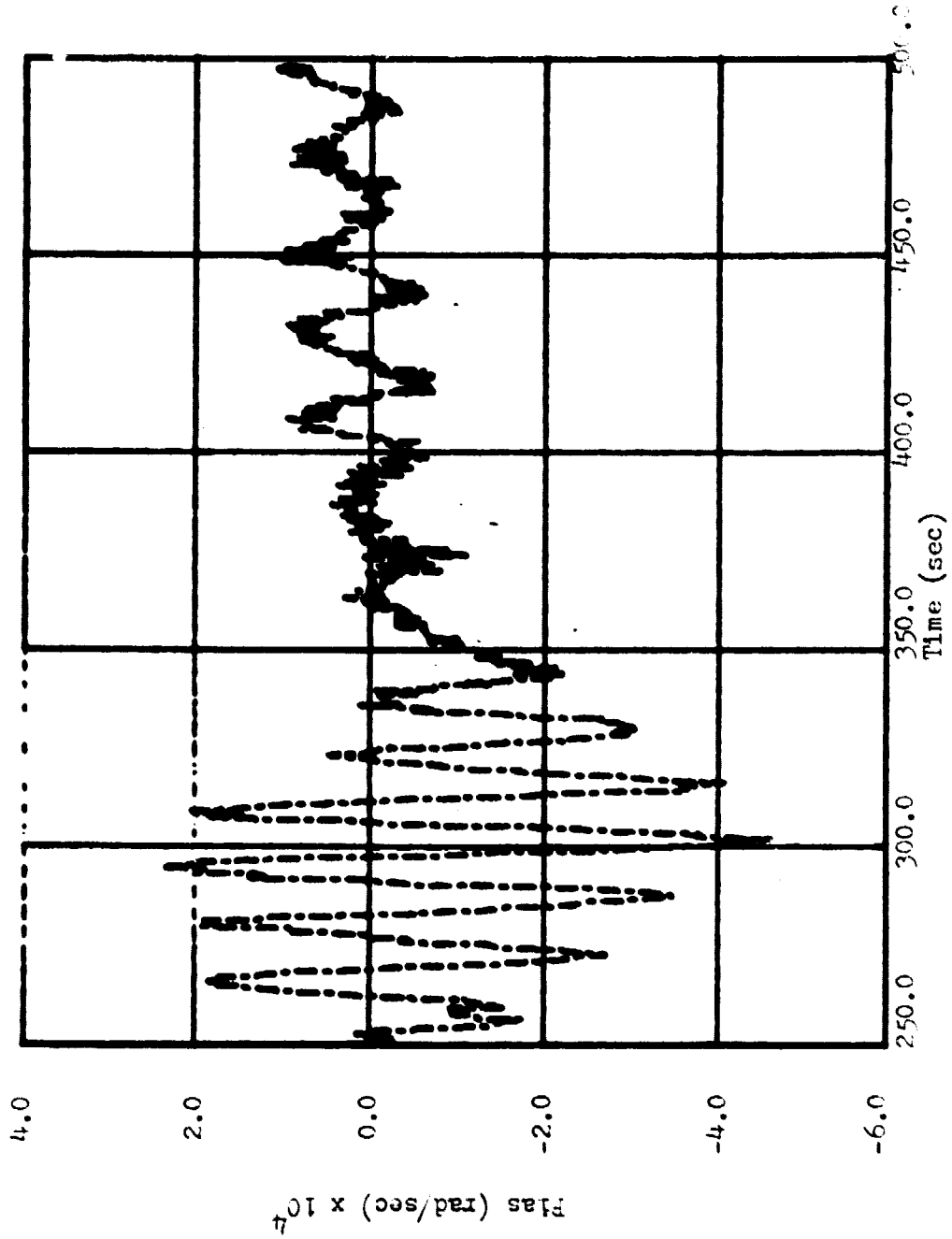


Fig. (4.4-25) Actual Results For Plas
(5th Order Observer, $u=a_1$, $\lambda=-0.7$)

4.5 Discussion of Balloon Observer Results

Figs.(4.4-2) and (4.4-4) indicate that the angular velocity results predicted by the fourth order observer differ significantly from those obtained from the gyroscope. The actual angular velocity of the balloon platform is different than that obtained from either the observer or gyroscope. Deficiencies in the ability of the gyroscope to reproduce the actual angular velocity are caused by mechanical insensitivity to sudden changes in angular velocity and bias. Errors in the angular velocity values predicted by the fourth order observer result from the form of the elements of the F and G matrices (see Sec. 4.3) and the magnitude of bias present in the output of the gyroscope.

Fig.(4.4-3) shows that the angular displacement predicted by the fourth order observer model without wind input differs significantly from that obtained by integrating the output from the gyroscope (y_1). The general trend of the angular displacement predicted by this model is similar to that obtained by integrating the output of the gyroscopes. However, the output of this model contains errors; e.g., the maximum difference between the two curves is 0.172° . This is significant in view of the fact that the maximum displacement predicted by the observer is 0.058° while that obtained by integrating the output from the gyroscope is 0.23° . These errors can be attributed to the fact that:

1. The effect of the wind acceleration is neglected.
2. Bias is present in the plant output.

Fig.(4.4-5) shows that the angular displacements obtained from the fourth order observer including wind acceleration compare less favorably (with the integrated gyroscope output) than those obtained from the previous model. The magnitude of the maximum angular displacement

predicted by this model is approximately 0.5° , while the maximum deviation is of the order 0.6° .

Figs.(4.4-6), (4.4-10), (4.4-14), (4.4-18), and (4.4-22) show that the angular velocity results obtained from the fifth order observer model differ significantly from the results (biased) obtained from the gyroscope. This is true regardless of whether the effect of wind acceleration is included. However, as the magnitude of the repeated eigenvalue (λ_1) increases, the differences between the two curves decrease.

Figs. (4.4-7), (4.4-8), (4.4-11), and (4.4-12) show that the angular displacements predicted by the fifth order observer model which was developed by excluding the affect of wind acceleration, are in good agreement with those obtained by integrating the modified output from the gyroscope (y_{im}). The latter was obtained by subtracting the bias predicted by this model from the actual gyroscope output. These figures indicate that the difference between the two curves increases with increasing time. Moreover, this difference decreases with increasing magnitude of λ_1 . The maximum displacement with $\lambda_1 = -0.2$ and -0.5 is of the order 0.05° ; while the maximum error is 0.08° and 0.02° respectively.

Figs.(4.4-15), (4.4-16), (4.4-19), (4.4-20), (4.4-23), and (4.4-24) indicate that the angular displacements predicted by the fifth order observer which includes the affect of wind acceleration are in good agreement with the values obtained by integrating the modified output from the gyroscope. The difference between these two curves remains constant over the entire observed time period. Moreover, this difference decreases with increasing magnitudes of λ_1 . The magnitude of the maximum error and displacement for all three cases is approximately

0.25° and 0.5° respectively.

Figs. (4.4-5), (4.4-15), (4.4-16), (4.4-19), (4.4-20), (4.4-23), and (4.4-24) show that the angular displacements predicted by the fourth and fifth order observer models compare favorably regardless of the value of λ_1 . This indicates that the predicted angular displacement is unchanged regardless which observer model is used. Thus, the fourth order observer model can be used to predict the angular displacement of the balloon platform.

Figs. (4.4-3), (4.4-7), (4.4-8), (4.4-11), and (4.4-12) show that the angular displacements predicted by the observer models without wind input differ significantly from those results predicted by the models which include wind input. This indicates that knowledge of wind acceleration is necessary in order to obtain accurate results for the attitude of the platform.

4.6 Conclusions

This study has shown that, for a completely observable balloon system, observer models can be constructed to accurately determine the angular displacement of the observational platform. Any errors in the predicted platform state are due mainly to errors in the balloon flight data (i.e., acceleration and angular velocity data) as opposed to deficiency in the observer model. Although the results for the angular velocity are in poor agreement with those obtained from the gyroscopes, these deviations can be decreased considerably by proper choice of the eigenvalues.

This study has also shown that the angular displacements predicted

by the observer models do not vary significantly with either the order of the model or the magnitude of the repeated eigenvalue. However, the results do vary significantly depending on whether the affect of wind acceleration is included.

APPENDIX A

Balloon Translational Acceleration Components

In the case of the LACATE experiment, the balloon's position was tracked by radar; the translational components were obtained with respect to the earth fixed axis shown in Fig. (A-1). The corresponding body axis for the balloon platform system is shown in Fig. (A-2). The angle α measured between these two coordinate systems (Fig. A-2) is given as follows; i.e.,

$$\alpha = \int_0^t \omega_3 dt - t\Omega s(\lambda) + \alpha_0, \quad (A-1)$$

where

ω_3 = spin component of angular velocity obtained from gyroscope,

Ω = magnitude of earth spin,

$$(7.2722 \times 10^{-5} \text{ (rad} \cdot \text{s}^{-1}\text{)}),$$

λ = latitude angle (0.5724(rad)), and

α_0 = initial value of α as measured by magnetometer.

The velocity components of the balloon were obtained by numerically differentiating the (radar tracked) translational components. The velocity components of the balloon (V_x , V_y) measured along the balloon's body axis are given as follows; i.e.,

$$V_1 = -V_x S(\alpha) + V_y C(\alpha), \quad V_2 = V_x C(\alpha) + V_y S(\alpha), \quad (A-2)$$

where

V_1 = balloon velocity component
along the e_2''' body axis,

V_2 = balloon velocity component along the e_1''' body axis,

V_x = balloon velocity component along the e_1 earth fixed axis,

V_y = balloon velocity component along the e_2 earth fixed axis,

and α is as defined in Eq. (A-1).

The balloon's translational acceleration components along the body axis can be obtained by differentiating Eq. (A-2) with respect to time.

The resulting equations are given as following; i.e.,

$$\begin{aligned} a_1 &= -\dot{V}_x S(\alpha) + \dot{V}_y C(\alpha) + \alpha(-V_x C(\alpha) - V_y S(\alpha)), \\ a_2 &= \dot{V}_x C(\alpha) + \dot{V}_y S(\alpha) + \alpha(-V_x S(\alpha) + V_y C(\alpha)), \end{aligned} \quad (A-3)$$

where

a_1 = translational acceleration component along the e_2''' body axis,

a_2 = translational acceleration component along the e_1''' body axis,

\dot{V}_x = translational acceleration component along the e_1 earth fixed axis,

\dot{V}_y = translational acceleration component along the e_2 earth fixed axis,

$\alpha = W_3 - \Omega S(\lambda)$, and

V_x , V_y and α are as defined previously. It should be noted that, in the above development, the earth's rotational effects are neglected.

ORIGINAL PAGE IS
OF POOR QUALITY

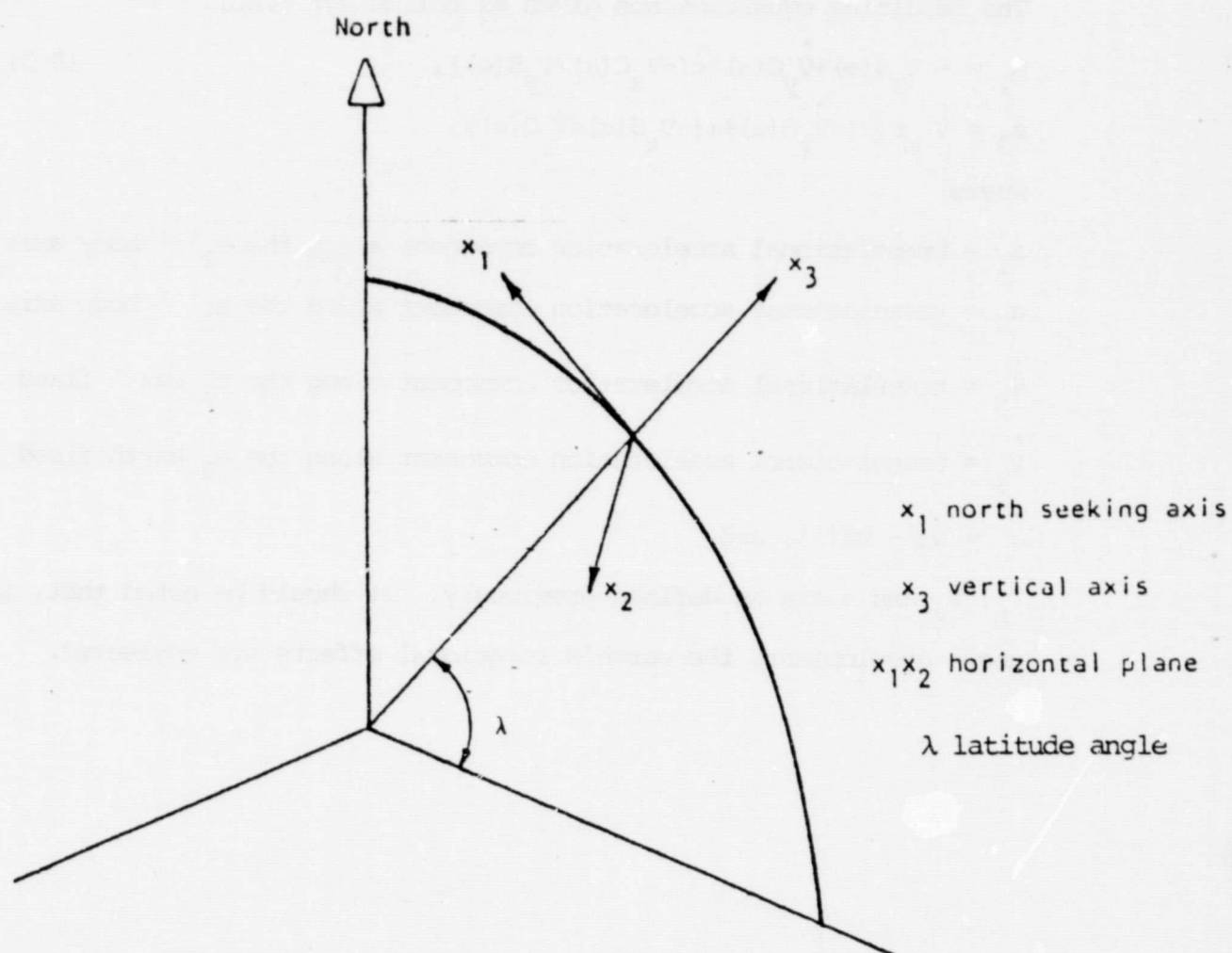


Fig.(A-1) Earth Fixed Axis

ORIGINAL PAGE IS
OF POOR QUALITY

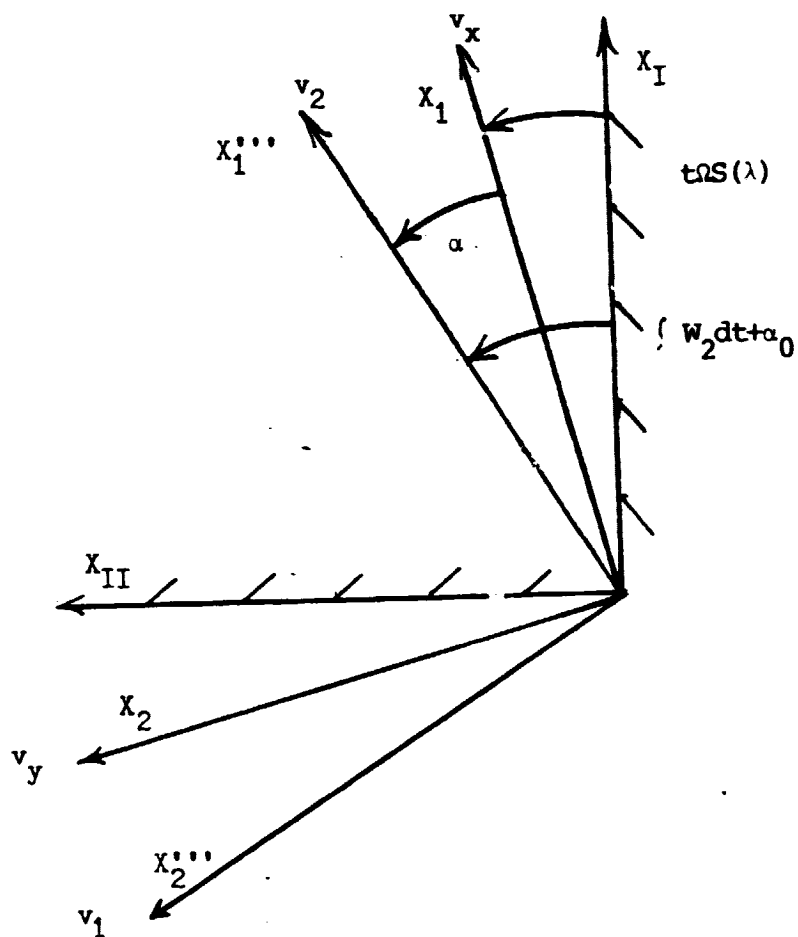


Fig.(A-2) Body and Earth Fixed Coordinate Axes

ORIGINAL PAGE IS
OF POOR QUALITY

APPENDIX B

Fortran Coding1. Body Axis Accelerations

```
1.000 C    PROGRAM TO OBTAIN BODY ACCEL. FROM
2.000 C    SENSITIVITY ANALYSIS
3.000      OUTPUT 'INPUT N'
4.000      INPUT N
5.000      DO 1 I=1,N
6.000      READ(103,2) T,P
7.000 2    FORMAT(2G)
8.000      READ(109,2)T,PD
9.000      READ(104,3) TO,XX,VX,AX
10.000 3   FORMAT(4G)
11.000      READ(107,5) T1,YY,VY,AY
12.000 5   FORMAT(4G)
13.000      A1=AX*COS(P)+AY*SIN(P)+(-VX*SIN(P)+VY*COS(P))*PD
14.000      A2=AX*(-SIN(P))+AY*COS(P)+(-VX*COS(P)-VY*SIN(P))*PD
15.000      WRITE(106,4) T,A1,A2
16.000 4   FORMAT(3E14.6)
17.000 1   CONTINUE
18.000      STOP
19.000      END
```

ORIGINAL PAGE IS
OF POOR QUALITY

2. Balloon Fourth Order Observer

```

1.000 C      BALLOON 4TH ORDER OBSERVER SYSTEM
2.000      COMMON/FCTT/A31,A32,A41,A42,G1,G2,G3,G4,B32
3.000      EXTERNAL FCT,OUTP
4.000      DIMENSION Y(5),DERY(5),PRMT(5),AUX(16,8)
5.000 9      OUTPUT 'INPUT Y10,Y20'
6.000      DATA (Y(I), I=1,4)/0.,0.,0.,0./
7.000      OUTPUT 'INPUT PRMT(I),I=1,4'
8.000      INPUT, (PRMT(I),I=1,4)
9.000      OUTPUT 'INPUT EIG'
10.000     INPUT EIG
11.000     A31=-1.622
12.000     A32=1.1926
13.000     A41=8.1096
14.000     A42=-8.1096
15.000     B32=.0437
16.000     G4=-4*EIG
17.000     G3=(G4*A31-4*EIG**3)/A41
18.000     G2=(-EIG**4-A32*A41+A42*A31)/(-A32*A41+A42*A31)
19.000     G1=(-6*EIG**2-A31-A42+A42*G2)/(-A41)
20.000     OUTPUT G1,G2,G3,G4
21.000     NDIM=4
22.000     OUTPUT 'INPUT 1 TO RUN'
23.000     INPUT J
24.000     IF (J.NE. 1) GO TO 9
25.000     DO 1 I=1,4
26.000 1     DERY(I)=0.25
27.000     CALL HPCG(PRMT,Y,DERY,NDIM,IHLF,FCT,OUTP,AUX)
28.000     STOP
29.000     END
30.000     SUBROUTINE FCT(X,Y,DERY,INO)
31.000     DIMENSION Y(1),DERY(1)
32.000     COMMON/FCTT/A31,A32,A41,A42,G1,G2,G3,G4,B32
33.000     COMMON/DAB/T1,THTD
34.000     IF(INO.EQ. 0) GO TO 2
35.000 4     FORMAT (2G)
36.000 5     FORMAT (3G)
37.000     READ(104,4)T1,THTD
38.000     READ(103,5)T2,A1,A2
39.000 2     DERY(1)=G1*(-Y(4)+THTD)+Y(3)
40.000     DERY(2)=G2*(-Y(4)+THTD)+Y(4)
41.000     DERY(3)=G3*(-Y(4)+THTD)+A31*Y(1)+A32*Y(2)-B32*A2
42.000     DERY(4)=G4*(-Y(4)+THTD)+A41*Y(1)+A42*Y(2)
43.000     RETURN
44.000     END
45.000     SUBROUTINE OUTP(X,Y,DERY,IHLF,NDIM,PRMT)
46.000     COMMON/DAB/T1,THTD
47.000     DIMENSION Y(1),DERY(1),PRMT(1)
48.000     WRITE(106,10)X,Y(2),Y(4),THTD
49.000 10    FORMAT(4E13.5)
50.000     RETURN
51.000     END

```

3. Balloon Fifth Order Observer

```
1.000 C      PROGRAM TO TEST 5TH ORDER OBSERVER SYSTEM WITH INPUT BIAS
2.000      COMMON/FCTT/A31,A32,A41,A42,G1,G2,G3,G4,G5,B32
3.000      EXTERNAL FCT,OUTP
4.000      DIMENSION Y(5),DERY(5),PRMT(5),AUX(16,8)
5.000 9      OUTPUT 'INPUT Y10,Y20,Y30'
6.000      DATA (Y(I), I=1,5)/0.,0.,0.,0.,0./
7.000      OUTPUT 'INPUT PRMT(I), I=1,4'
8.000      INPUT, (PRMT(I), I=1,4)
9.000      OUTPUT 'INPUT EIG'
10.000     INPUT EIG
11.000     A31=-1.622
12.000     A32=1.1926
13.000     A41=8.1096
14.000     A42=-8.1096
15.000     B32=.0437
16.000     G2=(5*EIG**4-A42*A31+A41*A32)/(-A42*A31+A41*A32)
17.000     G1=(10*EIG**2-A42*G2+A31+A42)/A41
18.000     G5=-EIG**5/(A42*A31-A41*A32)
19.000     G4=-5*EIG-G5
20.000     G3=(-10*EIG**3+A31*G4+(A31+A42)*G5)/A41
21.000     OUTPUT G1,G2,G3,G4,G5
22.000     NDIM=5
23.000     OUTPUT 'INPUT 1 TO RUN'
24.000     INPUT J
25.000     IF (J .NE. 1) GO TO 9
26.000     DO 1 I=1,5
27.000 1     DERY(I)=0.2
28.000     CALL HPCG(PRMT,Y,DERY,NDIM,IHLF,FCT,OUTP,AUX)
29.000     STOP
30.000     END
31.000     SUBROUTINE FCT(X,Y,DERY,INO)
32.000     DIMENSION Y(1),DERY(1)
33.000     COMMON/FCTT/A31,A32,A41,A42,G1,G2,G3,G4,G5,B32
34.000     COMMON/DAB/T1,THTD
35.000     IF(INO .EQ. 0) GO TO 2
36.000 4     FORMAT (2G)
37.000 5     FORMAT (3G)
38.000     READ(104,4)T1,THTD
39.000     READ(103,5)T2,A1,A2
40.000 2     DERY(1)=Y(3)+G1*(-Y(4)-Y(5)+THTD)
41.000     DERY(2)=Y(4)+G2*(-Y(4)-Y(5)+THTD)
42.000     DERY(3)=A31*Y(1)+A32*Y(2)+G3*(-Y(4)-Y(5)+THTD)-B32*A2
43.000     DERY(4)=A41*Y(1)+A42*Y(2)+G4*(-Y(4)-Y(5)+THTD)
44.000     DERY(5)=G5*(-Y(4)-Y(5)+THTD)
45.000     RETURN
46.000     END
47.000     SUBROUTINE OUTP(X,Y,DERY,IHLF,NDIM,PRMT)
48.000     COMMON/DAB/T1,THTD
49.000     DIMENSION Y(1),DERY(1),PRMT(1)
50.000     WRITE(106,10)X,Y(2),Y(4),Y(5),THTD
51.000 10     FORMAT(5E13.5)
52.000     RETURN
53.000     END
```


4. Hamming-Predictor Corrector

```
1.000 C .....
2.000 C
3.000 SUBROUTINE HPCG(PRMT,Y,DERY,NDIM,IHLF,FCT,OUTP,AUX)
4.000 C
5.000 C
6.000 DIMENSION PRMT(1),Y(1),DERY(1),AUX(16,1)
7.000 N=1
8.000 IHLF=0
9.000 X=PRMT(1)
10.000 H=PRMT(3)
11.000 PRMT(5)=0
12.000 DO 1 I=1,NDIM
13.000 AUX(16,I)=0.
14.000 AUX(15,I)=DERY(I)
15.000 1 AUX(1,I)=Y(I)
16.000 IF(H*(PRMT(2)-X))3,2,4
17.000 C
18.000 C ERROR RETURNS
19.000 2 IHLF=12
20.000 GOTO 4
21.000 3 IHLF=13
22.000 C
23.000 C COMPUTATION OF DERY FOR STARTING VALUES
24.000 4 INO=1
25.000 CALL FCT(X,Y,DERY,INO)
26.000 C
27.000 C RECORDING OF STARTING VALUES
28.000 CALL OUTP(X,Y,DERY,IHLF,NDIM,PRMT)
29.000 IF(PRMT(5))6,5,6
30.000 5 IF(IHLF)7,7,6
31.000 6 RETURN
32.000 7 DO 8 I=1,NDIM
33.000 8 AUX(8,I)=DERY(I)
34.000 C
35.000 C COMPUTATION OF AUX(2,I)
36.000 ISW=1
37.000 GOTO 100
38.000 C
39.000 9 X=X+H
40.000 DO 10 I=1,NDIM
41.000 10 AUX(2,I)=Y(I)
42.000 C
43.000 C INCREMENT H IS TESTED BY MEANS OF BISECTION
44.000 11 IHLF=IHLF+1
45.000 X=X-H
46.000 DO 12 I=1,NDIM
47.000 12 AUX(4,I)=AUX(2,I)
48.000 H=H
49.000 N=1
50.000 ISW=2
51.000 GOTO 100
52.000 C
```

```

53.000      13 X=X+H
54.000          INC=0
55.000          CALL FCT(X,Y,DERY,INO)
56.000          N=2
57.000          DO 14 I=1,NDIM
58.000          AUX(2,I)=Y(I)
59.000      14 AUX(9,I)=DERY(I)
60.000          ISW=3
61.000          GOTO 100
62.000 C
63.000 C      COMPUTATION OF TEST VALUE DELT
64.000      15 DELT=0.
65.000          DO 16 I=1,NDIM
66.000      16 DELT=DELT+AUX(15,I)*ABS(Y(I)-AUX(4,I))
67.000          DELT=.06666667*DELT
68.000          GO TO 19
69.000      17 IF(IHLF-10)11,18,18
70.000 C
71.000 C      NO SATISFACTORY ACCURACY AFTER 10 BISECTIONS. ERROR MESSAGE.
72.000      18 IHLF=11
73.000          X=X+H
74.000          GOTO 4
75.000 C
76.000 C      THERE IS SATISFACTORY ACCURACY AFTER LESS THAN 11 BISECTIONS.
77.000      19 X=X+H
78.000          INC=0
79.000          CALL FCT(X,Y,DERY,INO)
80.000          DO 20 I=1,NDIM
81.000          AUX(3,I)=Y(I)
82.000      20 AUX(10,I)=DERY(I)
83.000          N=3
84.000          ISW=4
85.000          GOTO 100
86.000 C
87.000      21 N=1
88.000          X=X+H
89.000          INC=0
90.000          CALL FCT(X,Y,DERY,INO)
91.000          X=PRMT(1)
92.000          DO 22 I=1,NDIM
93.000          AUX(11,I)=DERY(I)
94.000      22 OY(I)=AUX(1,I)+H*(.375*AUX(8,I)+.7916667*AUX(9,I)
95.000          1-.2083333*AUX(10,I)+.0416667*DERY(I))
96.000      23 X=X+H
97.000          N=N+1
98.000          INC=1
99.000          CALL FCT(X,Y,DERY,INO)
100.000          CALL OUTP(X,Y,DERY,IHLF,NDIM,PRMT)
101.000          IF(PRMT(5))6,24,6
102.000      24 IF(N-4)25,200,200
103.000      25 DO 26 I=1,NDIM
104.000          AUX(N,I)=Y(I)
105.000      26 AUX(N+7,I)=DERY(I)
106.000          IF(N-3)27,29,200

```

```

107.000 C
108.000 27 DO 28 I=1,NDIM
109.000      DELT=AUX(9,I)+AUX(9,I)
110.000      DELT=DELT+DELT
111.000 28 Y(I)=AUX(1,I)+.3333333*H*(AUX(8,I)+DELT+AUX(10,I))
112.000      GOTO 23
113.000 C
114.000 29 DO 30 I=1,NDIM
115.000      DFIT=AUX(9,I)+AUX(10,I)
116.000      DFIT=DFIT+DFIT+DFIT
117.000 30 Y(I)=AUX(1,I)+.375*H*(AUX(8,I)+DFIT+AUX(11,I))
118.000      GOTO 23
119.000 C
120.000 C      THE FOLLOWING PART OF SUBROUTINE HPCG COMPUTES BY MEANS OF
121.000 C      RUNGE-KUTTA METHOD STARTING VALUES FOR THE NOT SELF-STARTING
122.000 C      PREDICTOR-CORRECTOR METHOD.
123.000 100 DO 101 I=1,NDIM
124.000      Z=H*AUX(N+7,I)
125.000      AUX(5,I)=Z
126.000 101 Y(I)=AUX(N,I)+.4*Z
127.000 C      Z IS AN AUXILIARY STORAGE LOCATION
128.000 C
129.000      Z=X+.4*H
130.000      INO=C
131.000      CALL FCT(Z,Y,DFRY,INO)
132.000      DO 102 I=1,NDIM
133.000      Z=H*DFRY(I)
134.000      AUX(6,I)=Z
135.000 102 Y(I)=AUX(N,I)+.2969776*AUX(5,I)+.1587596*Z
136.000 C
137.000      Z=X+.4557372*H
138.000      INO=0
139.000      CALL FCT(Z,Y,DFRY,INO)
140.000      DO 103 I=1,NDIM
141.000      Z=H*DFRY(I)
142.000      AUX(7,I)=Z
143.000 103 Y(I)=AUX(N,I)+.2181004*AUX(5,I)-3.050965*AUX(6,I)+3.832865*Z
144.000 C
145.000      Z=X+H
146.000      INO=0
147.000      CALL FCT(Z,Y,DFRY,INO)
148.000      DO 104 I=1,NDIM
149.000 1040 Y(I)=AUX(N,I)+.1747603*AUX(5,I)-.5514807*AUX(6,I)
150.000      +1.205536*AUX(7,I)+.1711848*H*DFRY(I)
151.000      GOTO(9,13,15,21).ISW
152.000 C
153.000 C      POSSIBLE BREAK-POINT FOR LINKAGE
154.000 C
155.000 C      STARTING VALUES ARE COMPUTED.
156.000 C      NOW START HAMMINGS MODIFIED PREDICTOR-CORRECTOR METHOD.
157.000 200 ISTE=3
158.000 201 IF(N-8)204,202,204
159.000 C
160.000 C      N=8 CAUSES THE ROWS OF AUX TO CHANGE THEIR STORAGE LOCATIONS

```

```

161.000 202 DO 203 N=2,7
162.000      DO 203 I=1,NDIM
163.000      AUX(N-1,I)=AUX(N,I)
164.000 203 AUX(N+6,I)=AUX(N+7,I)
165.000      N=7
166.000 C
167.000 C      N LESS THAN 8 CAUSES N+1 TO GET N
168.000 204 N=N+1
169.000 C
170.000 C      COMPUTATION OF NEXT VECTOR Y
171.000      DO 205 I=1,NDIM
172.000      AUX(N-1,I)=Y(I)
173.000 205 AUX(N+6,I)=DERY(I)
174.000      X=X+H
175.000 206 ISTEP=ISTEP+1
176.000      DO 207 I=1,NDIM
177.000      ODELTA=AUX(N-4,I)+1.3333333*H*(AUX(N+6,I)+AUX(N+6,I)-AUX(N+5,I)
178.000      1AUX(N+4,I)+AUX(N+4,I))
179.000      Y(I)=DELTA-.9256198*AUX(16,I)
180.000 207 AUX(16,I)=DELTA
181.000 C      PREDICTOR IS NOW GENERATED IN ROW 16 OF AUX, MODIFIED PREDIC
182.000 C      IS GENERATED IN Y. DELTA MEANS AN AUXILIARY STORAGE.
183.000 C
184.000      INO=0
185.000      CALL FCT(X,Y,DERY,INO)
186.000 C      DERIVATIVE OF MODIFIED PREDICTOR IS GENERATED IN DERY
187.000 C
188.000      DO 208 I=1,NDIM
189.000      ODELTA=.125*(9.*AUX(N-1,I)-AUX(N-3,I)+3.*H*(DERY(I)+AUX(N+6,I)
190.000      1AUX(N+6,I)-AUX(N+5,I)))
191.000      AUX(16,I)=AUX(16,I)-DELTA
192.000 208 Y(I)=DELTA+.07438017*AUX(16,I)
193.000 C
194.000 C      TEST WHETHER H MUST BE HALVED OR DOUBLED
195.000      DELTA=0.
196.000      DO 209 I=1,NDIM
197.000 209 DELTA=DELTA+AUX(15,I)*ABS(AUX(16,I))
198.000      GO TO 210
199.000 C
200.000 C      H MUST NOT BE HALVED. THAT MEANS Y(I) ARE GOOD.
201.000 210 INO=1
202.000      CALL FCT(X,Y,DERY,INO)
203.000      CALL OUTF(X,Y,DERY,IHLF,NDIM,FRMT)
204.000      IF(PRMT(5))212,211,212
205.000 211 IF(IHLF-11)213,212,212
206.000 212 RETURN
207.000 213 IF(H*(X-PRMT(2)))214,212,212
208.000 214 IF(ABS(X-PRMT(2))-.1*ABS(H))212,215,215
209.000 215 GO TO 201
210.000 C
211.000 C
212.000 C      H COULD BE DOUBLED IF ALL NECESSARY PRECEDING VALUES ARE
213.000 C      AVAILABLE
214.000 216 IF(IHLF)201,201,217

```

ORIGINAL PAGE IS
OF POOR QUALITY

```

215.000 217 IF(N-7)201.218.218
216.000 218 IF(ISTFF-4)201.219.219
217.000 219 IMCT=ISTFP/2
218.000 IF(ISTFP-IMCT-IMCT)201.220.201
219.000 220 H=H
220.000 IHLF=IHLF-1
221.000 ISTFF=0
222.000 DO 221 I=1,NDIM
223.000 AUX(N-1,I)=AUX(N-2,I)
224.000 AUX(N-2,I)=AUX(N-3,I)
225.000 AUX(N-3,I)=AUX(N-4,I)
226.000 AUX(N+6,I)=AUX(N+5,I)
227.000 AUX(N+5,I)=AUX(N+4,I)
228.000 AUX(N+4,I)=AUX(N+3,I)
229.000 DELT=AUX(N+6,I)+AUX(N+5,I)
230.000 DELT=DELT+DELT+DELT
231.000 221 O AUX(16,I)=8.962963*(Y(I)-AUX(N-3,I))-3.361111*H*(DERY(I)+DELT
232.000 1+AUX(N+4,I))
233.000 GOTO 201
234.000 C
235.000 C
236.000 C H MUST BE HALVED
237.000 222 IHLF=IHLF+1
238.000 IF(IHLF-10)223,223,210
239.000 223 H=H
240.000 ISTFP=0
241.000 DO 224 I=1,NDIM
242.000 OY(I)=.00390625*(80.*AUX(N-1,I)+135.*AUX(N-2,I)+40.*AUX(N-3,I)+
243.000 1AUX(N-4,I))-1171875*(AUX(N+6,I)-6.*AUX(N+5,I)-AUX(N+4,I))*H
244.000 O AUX(N-4,I)=.00390625*(12.*AUX(N-1,I)+135.*AUX(N-2,I)+
245.000 1108.*AUX(N-3,I)+AUX(N-4,I)).0234375*(AUX(N+6,I)+18.*AUX(N+5,I)-
246.000 20.*AUX(N+4,I))*H
247.000 AUX(N-3,I)=AUX(N-2,I)
248.000 224 AUX(N+4,I)=AUX(N+5,I)
249.000 X=X-H
250.000 DELT=X-(H+H)
251.000 INO=0
252.000 CALL FCT(DELT,Y,DERY,INO)
253.000 DO 225 I=1,NDIM
254.000 AUX(N-2,I)=Y(I)
255.000 AUX(N+5,I)=DERY(I)
256.000 225 Y(I)=AUX(N-4,I)
257.000 DELT=DELT-(H+H)
258.000 INO=0
259.000 CALL FCT(DELT,Y,DERY,INO)
260.000 DO 226 I=1,NDIM
261.000 DELT=AUX(N+5,I)+AUX(N+4,I)
262.000 DELT=DELT+DELT+DELT
263.000 O AUX(16,I)=8.962963*(AUX(N-1,I)-Y(I))-3.361111*H*(AUX(N+6,I)+DEL
264.000 1+DERY(I))
265.000 226 AUX(N+3,I)=DERY(I)
266.000 GOTO 206
267.000 END

```


BIBLIOGRAPHY

1. Haser, L.N., "Dynamics and Attitude Control of the IM IR-Telescope Balloon Gondola," Proc., Ninth AFGL Scientific Balloon Symposium, 20:263-274.
2. Nigro, N.J., and Elkouh, A.F., "Attitude Determination of the LACATE Balloon System," Proc., Ninth AFGL Scientific Balloon Symposium, 20:239-262.
3. Luenberger, David G., "An Introduction to Observers," IEEE Transactions on Automatic Control, AC-16 (December 1971): 596-602.
4. Perkins, W.R., and Cruz, Jr., J.B., Engineering of Dynamic Systems, New York: John Wiley and Sons, 1969.
5. Swisher, G.M., Introduction to Linear Systems Analysis, Champaign: Matrix Publishers, 1976.
6. Miaou, Shao-Lun, "Motion of a Balloon Observational Platform," M.S. Essay, Marquette University, 1981.